View metadata, citation and similar papers at core.ac.uk
brought to you by CORE
provided by Technische Universität Dresden: Qucosa

Institut für Theoretische Physik
Fakultät Mathematik und Naturwissenschaften
Technische Universität Dresden

Aspects of Quantum Fluctuations under Time-dependent External Influences

Dissertation
zur Erlangung des akademischen Grades
Doctor rerum naturalium

vorgelegt von
Michael Uhlmann
geboren am 10. Oktober 1978 in Dresden

Dresden 2007

Eingereicht am 23. Mai 2007

1. Gutachter: Prof. Dr. Jan-Michael Rost

2. Gutachter: Dr. Ralf Schützhold

3. Gutachter: Prof. Dr. Grigory E. Volovik

Verteidigt am 1. Oktober 2007

Abstract

The vacuum of quantum field theory is not empty space but filled with quantum vacuum fluctuations, which give rise to many intriguing effects. The first part of this Thesis addresses cosmic inflation, where the quantum fluctuations of the inflaton field freeze and get amplified in the expanding universe. Afterwards, we turn our attention towards Bose-Einstein condensates, a laboratory system. Since most of our calculations are performed using a mean-field expansion, we will study the accuracy of a finite-range interaction potential onto such an expansion. Exploiting the universality of quantum fluctuations, several aspects of cosmic inflation will be identified in ballistically expanding Bose-Einstein condensates. The effective action technique for calculating the quantum backreaction will be scrutinized.

Finally, we consider dynamic quantum phase transitions in the last part of this Thesis. To this end two specific scenarios will be investigated: firstly, the structure formation during the superfluid to Mott-insulator transition in the Bose-Hubbard model; and secondly, the formation of spin domains as a two-dimensional spin-one Bose gas is quenched from the (polar) paramagnetic to the (planar) ferromagnetic phase. During this quench, the symmetry of the ground state is spontaneously broken and vortices (topological defects) form.

Contents

1 Introduction **9**
- 1.1 Motivation 9
- 1.2 Outline 11
  - 1.2.1 Cosmic inflation 11
  - 1.2.2 Cosmic analogues in Bose-Einstein condensates 13
  - 1.2.3 Quantum phase transitions 15
- 1.3 Notation 18

2 Traces of new physics in the cosmic microwave background? **19**
- 2.1 Introduction 19
  - 2.1.1 Definition of inflation 20
  - 2.1.2 Horizons 21
  - 2.1.3 Quantum fluctuations during inflation 22
  - 2.1.4 Modifications at highest energy 24
- 2.2 Generic modifications at high energies 24
  - 2.2.1 Initial state 26
  - 2.2.2 Final state 27
  - 2.2.3 Three-point function 27
- 2.3 Discussion 29
  - 2.3.1 Generalizations 29
  - 2.3.2 Lorentz invariance 30
  - 2.3.3 Comparison with previous calculations 30

3 On Quantum Effects in Bose-Einstein Condensates **35**
- 3.1 Bose-Einstein condensates 36
- 3.2 Finite-range interactions 38
  - 3.2.1 Number-conserving mean-field expansion 39
  - 3.2.2 Consistency of mean-field expansion 42
  - 3.2.3 Dipole-dipole interaction 45
- 3.3 Dimensional reduction 46

3.4 Effective Geometry . . . 48
  3.4.1 Hydrodynamics and effective space-time metric . . . 48
  3.4.2 Comoving Coordinates and Scaling . . . 50
3.5 Expanding Bose-Einstein condensates . . . 52
  3.5.1 Horizon Analogues . . . 53
  3.5.2 Density-Density Correlations in quasi-2D . . . 55
  3.5.3 Density-Density Correlations in 3D . . . 57
  3.5.4 Comparison with experiments . . . 60
3.6 On the backreaction problem . . . 61
  3.6.1 Backreaction . . . 63
  3.6.2 Comparison with effective action technique . . . 64
  3.6.3 Choice of classical background . . . 65
  3.6.4 Problems of Effective-Action Technique . . . 67
  3.6.5 Cut-off Dependence . . . 69
  3.6.6 Simple Example . . . 70
3.7 Discussion . . . 71

4 On quantum phase transitions . . . 77
4.1 Superfluid to Mott transition in the Bose-Hubbard model . . . 79
  4.1.1 Bose-Hubbard model . . . 79
  4.1.2 Linearization and effective horizon . . . 81
  4.1.3 Exponential sweep . . . 83
  4.1.4 Ring lattice . . . 85
4.2 Vortex creation and winding number scaling in quenched spinor Bose gas . . . 86
  4.2.1 Introduction . . . 86
  4.2.2 Hamiltonian and ground state properties . . . 87
  4.2.3 Domain formation in a $SO(D)$-symmetry breaking quench . . . 89
  4.2.4 Defect creation in a $SO(D)$-symmetry breaking quench . . . 90
  4.2.5 Vortex number scaling in two spatial dimensions . . . 92
4.3 Conclusions . . . 94

5 Conclusions . . . 97

6 Outlook . . . 99

Appendix AAdiabatic expansion . . . 101

Appendix BBackreaction for a Toy Model . . . 103

Appendix COn mean-field splits . . . 105

Appendix DEffective Hamiltonian for magnetization operator 107

Bibliography 111

1 Introduction

1.1 Motivation

The vacuum[1] of quantum field theory possesses a rich and complex structure. Space is not empty, but filled with quantum fluctuations – particles popping into existence only to disappear again almost immediately after their creation. This process is permitted by quantum mechanics since energy-time uncertainty, $\Delta E \Delta t \gtrsim \hbar/2$, places a bound on the determinability of energy in a time interval Δt. Quantum fluctuations are universal, they occur for all kinds of particles and on all energy scales (though the time a virtual particle can exist depends on its energy). The energy-time uncertainty indicates that vacuum fluctuations are small. They are almost not perceivable in everyday life. Nevertheless, some intriguing manifestations of this non-trivial vacuum structure can be observed even in the macroscopic world. One of the most illustrious examples is the static Casimir effect [1–3]: two perfectly-conducting plates placed in the vacuum experience a force. Due to the boundary conditions at the mirrors, less modes fit in between than are permitted outside; the vacuum structure is distorted. The different pressure exerted by the vacuum fluctuations on either side of the plates results in a net force pushing the two plates either together or apart (depending on the specific boundary conditions). The statical Casimir effect has been verified experimentally for many different geometries [4–7].

The dynamic situation is even more interesting [3, 8]: by moving one of the mirrors, it is possible to amplify the quantum vacuum fluctuations. The virtual particles will be squeezed out of the vacuum and converted into real particles. Again, this process is universal. In many situations, quantum fields are exposed to some classical external time-dependent influences. The quantum fluctuations respond to temporal variations of those external influences. If the response time is much shorter than the typical variation time, the fluctuation evolve adiabatically, i.e., they will stay in the ground state. Otherwise, non-equilibrium processes will create real particles, i.e., deviations from the ground state, see, e.g., [9–12].

Dynamic quantum phase transitions represent a particular example for the non-adiabatic evolution of vacuum fluctuations [13, 14]: consider a system containing two competing interactions, whose relative strength can be tuned by virtue of an external parameter g. This parameter could be the magnetic field or the pressure applied to a sample. Depending on the value of g, different ground-state manifolds may become energetically favorable and the system might develop different phases. In contrast to thermal phase transitions, quantum phase transitions are driven by quantum rather than thermal fluctuations and thus might occur at zero temperature as well. Quantum phase transitions are a genuine quantum effect.

---

[1] Throughout this Thesis, we will employ the notion of vacuum as synonym for the ground state of the considered systems, in particular also for condensed-matter systems.

For instance, first-order transitions are associated with a level crossing between two competing ground states at a critical value g_c of the external parameter, see Fig. 1.1. On either side of g_c, different states constitute the ground state of the system, e.g., the system might develop a paramagnetic phase on one side of g_c and a ferromagnetic phase on the other. The ground state becomes degenerate at the critical point g_c (which is the phase-separating point at zero temperature). Consequently, the energy gap ΔE between these two states (i.e., the two crossing levels) narrows and finally vanishes when approaching g_c. In view of the energy-time uncertainty, $\Delta E \Delta t \gtrsim \hbar/2$, the typical (response) time Δt of the quantum fluctuations diverges for $\Delta E \to 0$. Hence, adiabaticity will be violated when sweeping through the transition with a finite velocity $|\partial g/\partial t| > 0$. Non-equilibrium processes will lead to the freezing and amplification of the vacuum fluctuations. Similarly, a diverging response time (of the quantum fluctuations) will also occur in dynamic higher-order quantum phase transitions.

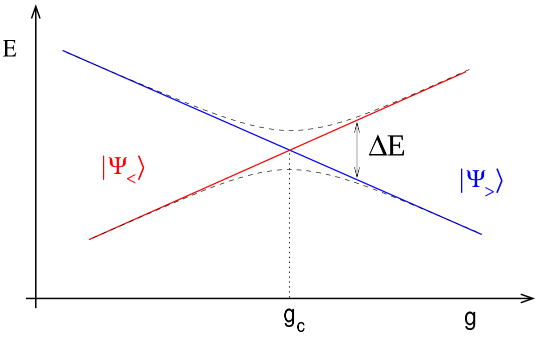

Figure 1.1: Sketch of a level-crossing (red and blue lines) and of an avoided crossing (dashed).

Quantum fluctuations are a generic property of quantum field theory. Dynamic as well as static effects associated with them occur at all scales and for all possible (quantum) fields. In the aforementioned examples, we mainly focused on low energies, but it is believed that quantum effects were also important in the early universe. According to our present standard model of cosmology, the vacuum fluctuations of the inflaton field were amplified and frozen during cosmic inflation[2] thus creating small inhomogeneities [15–20]. It is believed that these small inhomogeneities, generated at energies of order 10^{15} GeV, acted as seeds for the later structure formation in the universe; i.e., the large-scale structures in the universe, e.g., galaxy clusters, (presumably) originate from small quantum fluctuations.

---

[2] A postulated period of accelerated expansion in the very early stages of cosmic evolution, which lead to non-equilibrium effects. During cosmic inflation, the size of the universe increased by a huge factor. Since such an accelerated expansion can only be sustained for equations of state with negative pressure, cosmic inflation must be driven by non-ordinary matter, e.g., a quantum field – the inflaton field.

Coming back to laboratory systems, the common technique of time-of-flight images used in experiments on Bose-Einstein condensates shows parallels to cosmic inflation: when the confining trap potential of the condensate is switched off, the gas cloud starts to expand freely. Any spatial details of the condensate are scaled up. During the ballistic expansion of the condensate, the quantum fluctuations (phonons) freeze and get amplified in the expanding background; a small density contrast is generated. Though this laboratory effect bears strong similarities to cosmic inflation, it occurs at energies of order 10^{-12} eV – a typical scale which is 36 orders of magnitude smaller than that of cosmic inflation – and thus reveals the universal character of the quantum fluctuations.

Quantum fluctuations are a generic property of quantum theory. By studying different systems at different energies, system-specific effects might be identified and distinguished from universal features. Thus, a better understanding of quantum fluctuations in general could be attained. In view of the universal features of different quantum effects, it would become possible to gain new insight into condensed matter systems as well as into physics at ultrahigh energies (e.g., quantum gravity).

1.2 Outline

In this thesis, we will consider quantum fluctuations in various setups with particular emphasis on trapped quantum gases. In view of the rapid progress in the experimental capabilities and the theoretically well-understood microscopic physics, quantum gases are particularly well-suited for the study of quantum effects and thus offer many prospects for theoretical and also experimental investigations. On the other hand, due to the universal character of vacuum fluctuations, it is also believed that they were important during different stages of early cosmic evolution, *inter alia* during cosmic inflation.

1.2.1 Cosmic inflation

It is believed that the size of the universe grew by a large factor (at least e^{60}) during a phase of accelerated expansion, cosmic inflation[3], see Fig. 1.2. It was driven by a quantum field, the inflaton, slowly decaying from an excited state (e.g., a false vacuum) into its true vacuum. The small quantum fluctuations of the inflaton were frozen and amplified by the expanding background. Neighboring points, which were in thermal equilibrium prior to inflation, were dragged apart (during inflation) and soon lost causal contact. No signal emitted at either

---

[3] Cosmic inflation was introduced by A. Guth [19] in order to resolve the flatness and horizon problems of cosmology. Without the enormous enlargement of the universe, the observed flatness and homogeneity can (within the Friedman models of cosmology, e.g., [22, 23]) only be explained by fine-tuning the initial values at big bang, e.g., the curvature or the energy content, to extremely high accuracy. In inflationary theories, however, both problems are solved naturally: due to the immense growth, any initial curvature is smoothed out and the entire (visible) universe could have originated from a small region in equilibrium.

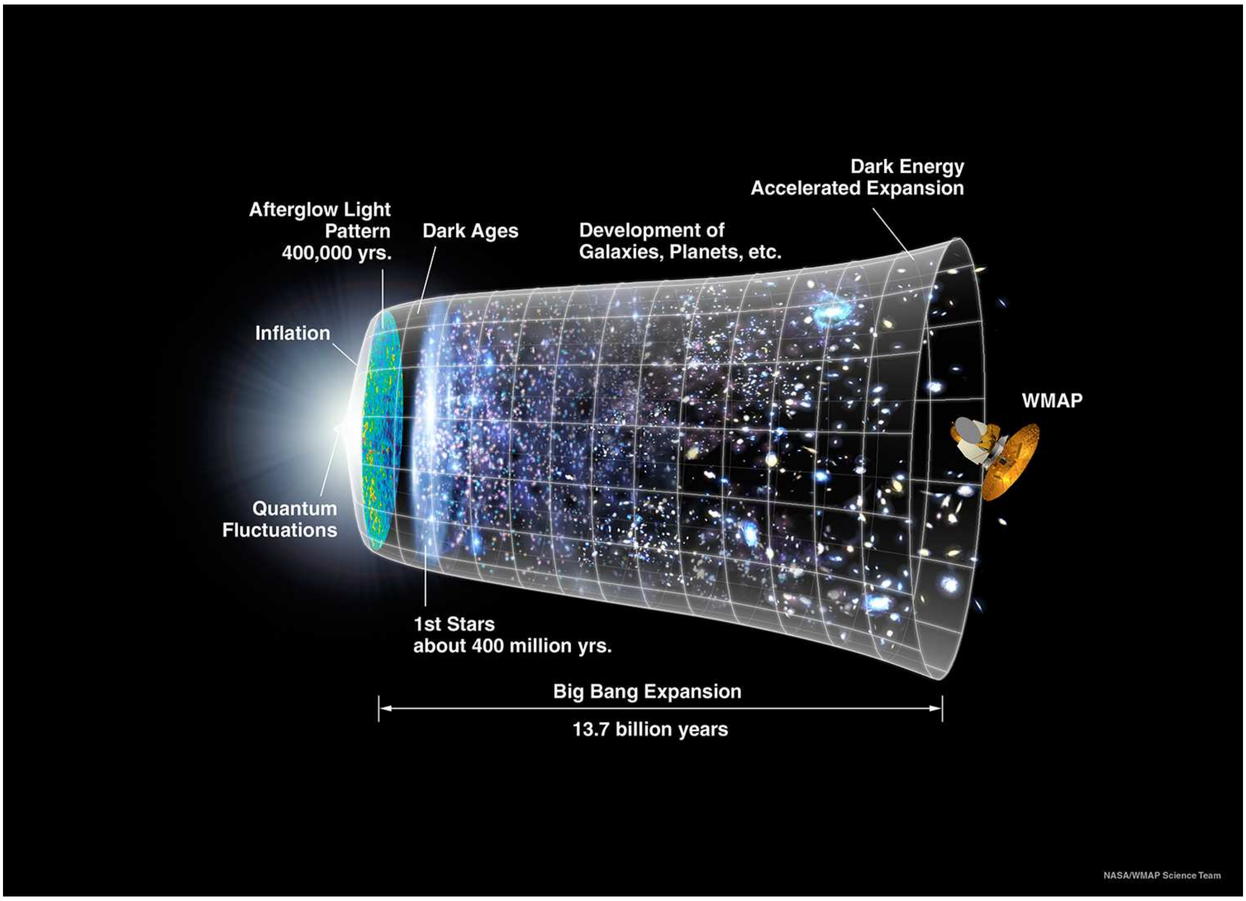
Dark Energy
Accelerated Expansion
Afterglow Light
Pattern
400,000 yrs.
Dark Ages
Development of
Galaxies, Planets, etc.
Inflation
WMAP
Quantum
Fluctuations
1st Stars
about 400 million yrs.
Big Bang Expansion
13.7 billion years
NASA/WMAP Science Team

Figure 1.2: Schematic timeline of the cosmic evolution [21].

of them could reach the other one; they were concealed behind a particle horizon. As the universe expanded, the wavelengths of vacuum fluctuations were continuously stretched from microscopic (e.g., sub-Planck length[4]) to cosmological sizes.

The quantum fluctuations were amplified and frozen when causal contact between neighboring nodes was lost [15–18, 20]. After inflation, the inflaton decayed into ordinary matter and (p)reheated the universe. The cosmos has become flat and contained almost homogeneously-distributed energy, an imprint of which is still visible in the cosmic microwave background radiation as measured by the WMAP [21] satellite and, with higher accuracy, by the future PLANCK [25] mission. The small anisotropies of order 10^{-5} in the microwave radiation presumably arose from the amplified and frozen quantum vacuum fluctuations of the inflation. Though originating from physics at highest energies ($10^{15}\,\mathrm{GeV}$), this small density contrast can be observed at much lower energies (10^{-4} eV).

---

[4] By using algebraic combinations of the speed of light c, the Planck constant $\hbar$, and the gravitational constant G, a fundamental scale, the Planck scale, can be defined, see, e.g., [24]. The Planck mass is defined as $m_{\mathrm{Planck}} = \sqrt{\hbar c/G} \approx 1.221\times10^{19}\,\mathrm{GeV}/c^2$. It corresponds to a length $l_{\mathrm{Planck}} = \sqrt{\hbar G/c^3} \approx 1.616\times10^{-33}\,\mathrm{cm}$ and a time $T_{\mathrm{Planck}} = \sqrt{\hbar G/c^5} \approx 5.39\times10^{-44}\,\mathrm{s}$. Since the Planck scale combines the fundamental constants of quantum theory ($\hbar$) and gravity (G), it is believed that the Planck scale plays an important role in a (still not completely known) theory of quantum gravity.

With cosmic inflation acting as a huge magnifying glass, the microwave background, see Fig. 1.2, might reveal some traces of physics at high energies [$\gtrsim \mathcal{O}(10^{15}\,\text{GeV})$]. At those scales, which are far beyond the capabilities of present and near-future ground-based experiments like the LHC [26], new physics beyond the present standard model of particle physics can be expected (see also Footnote 4 on Page 12). Since the amplification and freezing of the quantum fluctuations occur at energies of order 10^{15} GeV, new physics at such high energies $\gtrsim 10^{15}$ GeV might influence the (non-adiabatic) evolution of those fluctuations and thus leave a distinct signature in the microwave background. We will consider a generic modification of the inflaton field at high energies (Planck scale) in Chapter 2. The three-point function of the quantum fluctuations will be calculated; a signal which should be detectable (and discriminable) with the PLANCK satellite [25]. We will also address the possibility of Lorentz violation in Chapter 2.

The experimental study of quantum effects at ultrahigh energies seems impossible with present-day technology. Even in the case of (postulated) cosmic inflation and its traces in the microwave background, we only observe the outcome of processes in the early universe. For the investigation of quantum effects, this situation is not very convenient. On the other hand, quantum fluctuations are universal and occur on all scales. Hence, by scrutinizing laboratory systems which exhibit some similarities to the (anticipated) high-energy physics (*cosmic analogues*), generic features of the quantum effects might be deduced. The theoretical and experimental study of analogue systems may facilitate a better understanding of the physics at ultrahigh energies.

1.2.2 Cosmic analogues in Bose-Einstein condensates

In 1981, W. G. Unruh [27] discovered the kinematical analogy between phonons (quantized sound waves) propagating in an irrotational, inviscid fluid and a massless Klein-Gordon field in the Painlevé-Gullstrand-Lemaître metric [28–30]. He thus opened new perspectives for the study of quantum fields in curved space-times by means of model systems, e.g., sonic analogues of the Hawking radiation [27]. An effective space-time description for phonons, where the curvature is generated by the (superfluid) background flow, emerges as low-energy limit of the well-known microscopic behavior. The influence of the full microscopic physics on the quantum effects can be studied in theory and (in principle) also in experiment, see, e.g., [31–34] for review. (We can thus study possible consequences of quantum gravity by means of model systems.)

After the first experimental realization of Bose-Einstein condensation in dilute atomic gases in 1995 [35, 36] and the rapid progress in this field since then, a suitable analogue system with widely tunable parameters is available. Due to the rarefied state of atomic Bose-Einstein condensates, the time-scale on which the equilibrium state is restored becomes long compared to typical response times of dense systems (such as superfluid He), so that out-of-equilibrium phenomena become accessible within the typical time span of an experiment. Thus the tightly controlled study of such phenomena, e.g., the amplification and freezing of fluctuations and the generation of defects, becomes possible. We will discuss some aspects of *analogue gravity* based on Bose-Einstein condensates in Chapter 3.

Bose-Einstein condensation occurs in a metastable phase, which can only be preserved for dilute vapors, where the effective interaction range (the s-wave scattering length a_s) is much shorter than the typical inter-particle separation. The stable phase would be solid. It is therefore in general customary to approximate the two-particle interaction by a contact potential $V_{\text{int}}(\boldsymbol{r}-\boldsymbol{r}') \propto a_s\delta(\boldsymbol{r}-\boldsymbol{r}')$. For the classical background (the condensate fraction) and low-energy excitations (quasi-particles), this description works sufficiently well. In the high-energy limit, however, it can be expected to fail. For excitations with short wavelengths (e.g., of order a_s), the finite range of the interaction potential becomes important. We will investigate this aspect in Section 3.2 and also study the influence of the interaction potential on the mean-field expansion (classical background plus linearized quantum fluctuations).

By placing a Bose-Einstein condensate in a highly-anisotropic trap, the motion in one or two spatial directions can be frozen to the ground state. The condensate becomes effectively lower dimensional. A derivation of the effective, lower-dimensional action will be presented in Section 3.3. After linearization, the (lower-dimensional) action of the phonons can be identified with that of a massless Klein-Gordon field in a curved space-time, where the curvature is generated by the superfluid background flow. The derivation will be sketched in Sec. 3.4. In view of this formalism, we can employ the methods and tools known from general relativity in order to discuss the evolution of phonons in (strongly-confined) Bose-Einstein condensates.

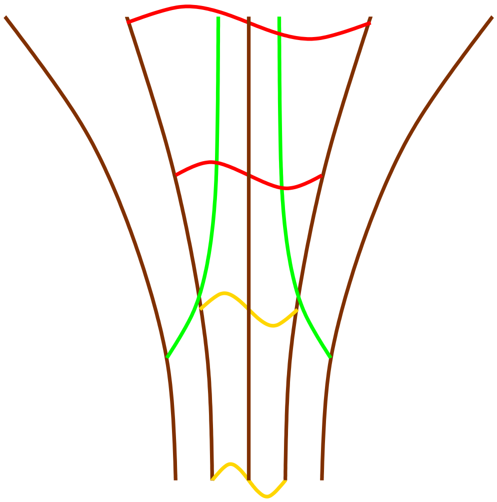

Figure 1.3: Sketch of comoving worldlines (brown) in an expanding Bose-Einstein condensate. An effective sound horizon for the (low-energy) phonons closes in from infinity after the condensate is released from the trap. The initially free quantum fluctuations (yellow) freeze and get amplified (red) when they are stretched.

In particular, we will consider in Sec. 3.5 the ballistic expansion of quasi-two- and three-dimensional condensates after they are released from the trap, see Fig. 1.3. In experiments, the free expansion of a condensate after switching off the confining potential is often employed in time-of-flight images to magnify any spatial details. This process resembles various aspects of cosmic inflation: in both cases, quantum fluctuations evolve above a classical, expanding background and any contained spatial structures are scaled up. In particular, the quantum fluctuations freeze and get amplified. We calculated the (frozen) density-density correlation spectrum for quasi-two-dimensional and three-dimensional setups in Sec. 3.5 and make estimates of the effect for realistic experimental values.

Finally, we address the backreaction problem[5] for Bose-Einstein condensates (i.e., the influence of the quantum fluctuations onto the classical background) in Sec. 3.6. We will derive an expression for the backreaction of the linearized quantum fluctuations onto the classical background (e.g., the condensate part) *ab initio*, i.e., from the full field equations. In view of the effective space-time approach introduced in Section 3.4, methods and techniques known from general relativity can also be applied to Bose-Einstein condensates. The results may be compared to those obtained in the *ab initio* calculation. In particular, we critically examine the effective-action technique (see, e.g., [10]) in Section 3.6. Lacking a unique and complete theory of quantum gravity, quantum fluctuations in general relativity are treated as small perturbations above a classical background. Some implications, e.g., concerning the validity of effective-action technique, might be deduced from the consideration of this laboratory systems (analogue systems).

A discussion of our results closes Chapter 3.

1.2.3 Quantum phase transitions

In systems where the energy spectrum of the Hamiltonian can be varied by means of an external parameter g, a quantum phase transition may occur [13, 14]. For instance, in first-order quantum phase transitions, two competing ground states cross at a point g_c. On either side of the level crossing, different phases form the ground state. The energy gap between these two states diminishes when approaching the critical point, $\Delta E \to 0$ as $g - g_c \to 0$. Hence, the response time of the quantum fluctuations diverges (due to energy-time uncertainty $\Delta E \Delta t \gtrsim \hbar/2$). They cannot follow the changing spectrum when sweeping through the transition with a finite velocity $|\partial g/\partial t| > 0$, i.e., they evolve non-adiabatically and thus freeze and get amplified. A complex correlation pattern, similar to that observed in the cosmic microwave background radiation, might develop during a (dynamic) quantum phase transition. It has even been suggested that the idea of cosmic inflation itself is only our distorted view of a quantum phase transition [37].

---

[5] Similarly to the two parallel plates, which experience the Casimir force owing to the vacuum fluctuations, any inhomogeneous background will distort the vacuum structure of a quantum field $\hat{\Phi}$ as well, see, e.g., [9–11]. For example, a curved space-time $\mathcal{M}$ might imply a spatially varying energy-momentum tensor $\langle \hat{T}_{\mu\nu} \rangle$ of $\hat{\Phi}$, which, by virtue of the Einstein equation of general relativity $G_{\mu\nu} = \kappa T_{\mu\nu}$, might react back on the space-time $\mathcal{M}$ and thus change its curvature.

Apart from the creation of small inhomogeneities, a second interesting issue concerning quantum phase transitions regards the possible creation of topological defects via the quantum analogue of the Kibble-Zurek mechanism: if the ground states on either side of the transition possess different non-trivial symmetries, spontaneous symmetry breaking may occur when sweeping through the critical point [38–40].

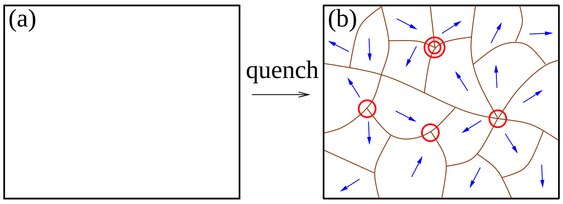

Figure 1.4: An initially homogeneous polar state (a) decays into a ferromagnetic phase (b), where each domain possesses a distinct magnetization (blue arrows) and vortices may form (red circles).

For example, consider a two-dimensional system, which is initially prepared in a polar (rotationally symmetric) state and which decays into a ferromagnetic state [broken $SO(2)$ symmetry], see Fig. 1.4. When the transition sets in, the quantum fluctuations of the magnetization are amplified into different directions at different spatial points. A complex ferromagnetic domain structure develops in the successive evolution. The direction of the magnetization in each domain is distinct. During the domain formation, stable topological defects (i.e., vortices), with the magnetization pointing either away from or towards an unmagnetized vortex core, might be created. Note that the interplay of spatial dimensionality and the broken symmetry is crucial for the occurrence of those defects. For instance, if we considered the same $SO(2)$-breaking process in three spatial dimensions, no stable (point-like) vortices would form.

By means of condensed matter systems (in particular superfluids and ultracold atomic gases), we are able to study some aspects of dynamic quantum phase transitions and the possible defect creation via the quantum analogue of the Kibble-Zurek mechanism during symmetry-breaking transitions [38–40]. Again, the study of these specific situations might facilitate a better understanding of quantum phase transitions in general. In contrast to the effective space-time analogy in (super)fluids, which is based on similar equations of motion for the linearized fields, the analogy of quantum phase transitions extends beyond the linearized action. In the vicinity of the critical point (where the non-equilibrium processes occur), the (effective) action for the full field operators may assume an analogous form in various systems, e.g., the potential in a laboratory condensed-matter system might resemble the well-known "Mexican hat" known from the Higgs mechanism of quantum field theory.

Two particular cases of quantum phase transitions in quantum gases will be considered in Chapter 4. Section 4.1 treats the amplification and freezing of quantum fluctuations in the Bose-Hubbard model, which describes a relatively simple setup of bosons being placed in a lattice, see Fig. 1.5. They repel each other if at the same site and might tunnel to neighboring sites. The Hamiltonian consists of two contributions: firstly, the repulsion per lattice site, which is proportional to the filling squared, $\hat{n}_a^2$, and has a strength U. And secondly, a kinetic term which is proportional to the filling $\hat{n}_a$ and describes the hopping between different lattice sites with a tunneling rate J. If the repulsion is small compared to the tunneling, the ground state of the system is a superfluid with long-ranged correlations and gapless excitations. In the other extremal case of negligible hopping, the Mott insulator phase becomes the ground state in systems with commensurate filling, $\langle \hat{n}_a \rangle \in \mathbb{N}$ (fixed chemical potential, $\mu = \text{const}$). The bosons are pinned to the lattice sites (which have integer filling numbers) and adjacent sites are almost uncorrelated (i.e., only very short-ranged correlations exist). For incommensurate fillings, a small superfluid fraction is retained even when the tunneling probability is small [41].

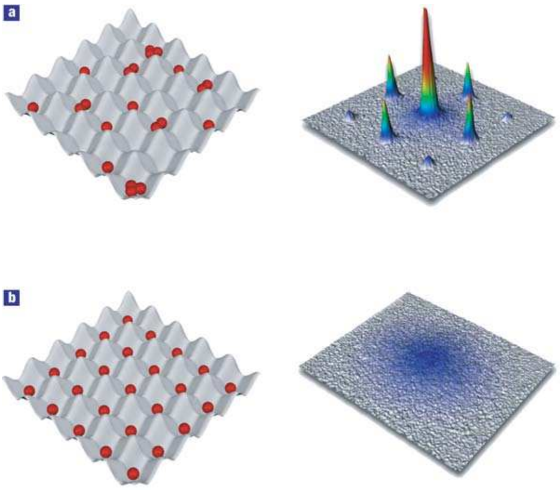

Figure 1.5: If the hopping term dominates in the Bose-Hubbard Hamiltonian, the atoms are delocalized and the system becomes superfluid with long-range phase correlation (a, left) A sharp peak appears in time-of-flight images (a, right). In the tunneling between different sites is negligible, a Mott insulator develops for commensurate filling, where the atoms are pinned to the lattice sites (b, left). The phase correlations decay and the sharp peak vanishes (b, right) [42].

In Sec. 4.1, we study the initial amplification and freezing of the quantum fluctuations when sweeping from the superfluid to the Mott insulator via a time-dependent tunneling strength $J(t) \propto e^{-\gamma t}$ with a finite velocity γ. The on-site number variations and the decaying off-site correlations depending on the sweep rate γ will be derived. The long-ranged order characteristic for the superfluid phase also decays during the quantum phase transition, see Fig. 1.5. As a further experimental signature of the decaying condensate part, we propose the sweep-rate dependent temporal shrinkage of the superfluid fraction in a ring-shaped persistent-current setup.

In the second example, we address in Sec. 4.2 the defect (vortex) creation in symmetry breaking quantum phase transitions, see Figures 1.4. Inspired by a recent experiment [43], we investigate an effectively two-dimensional spinor Bose condensate. Initially, it is prepared in the polar (paramagnetic) state. At high external magnetic fields, this state is energetically favorable due to the quadratic Zeeman shift. When lowering the field strength, the condensate undergoes a phase transition and develops a complex ferromagnetic domain structure. We derive the typical domain size and establish a scaling law for the standard deviation of the winding number (i.e., the excess defect number) with the system size. The generalization to $SO(D)$-breaking transitions in D-dimensional spaces will be discussed.

Conclusions and outlook in Chapters 5 and 6 close this Thesis.

1.3 Notation

Throughout this Thesis, we will use natural units with $\hbar = c = 1$. The speed of light c should not be confused with the speed of sound c_s, which we will not set to 1. We will also employ the sum convention throughout this work; whenever tensor indices occur twice (one covariant and one contravariant), they will be summed over. Lowercase Greek indices μ, ν etc. will label space-time components and run from 0 (time) to 3 (space). The spatial components shall be denoted by lowercase Latin letters starting from i, i.e., i, j etc. In contrast, the lowercase Latin letters from the first part of the alphabet describe more general indices, e.g., a, $b \in \mathbb{Z}$ or $a, b \in \{0, \pm 1\}$.

2 Traces of new physics in the cosmic microwave background?

2.1 Introduction

According to our present standard model of cosmology, the small anisotropies observed in the cosmic microwave background originate from small quantum fluctuations at very high energies. These quantum fluctuations were amplified and stretched during cosmic inflation, a phase of accelerated expansion in the very early universe [15, 17–19], see also Fig. 1.2. It was suggested by A. Guth in 1981 [19] as an add-on to big bang models in order to resolve the flatness and horizon problems of cosmology. Tiny regions of space are blown up to cosmological scales.

The expansion is, in the simplest models, driven by the homogeneous inflaton field, which slowly decays into its proper vacuum state. At the end of inflation, the inflaton field rapidly decays into ordinary matter and thus pre- and reheats the universe – with an uniform energy distribution over domains larger than the visible universe. The homogeneity displays itself in the cosmic microwave background radiation, a remnant from the time of decoupling of matter and radiation roughly 300,000 years after the big bang. The thermal photons did not interact any more with the matter and their temperature diminished due to the expanding background. The microwave background was discovered coincidentally by A. A. Penzias and R. W. Wilson in 1964, and showed the anticipated homogeneity and isotropy with the same black-body spectrum in all directions. The recent WMAP mission [21, 44] measures its temperature to 2.725 K with anisotropies of order 10^{-5}, see also Figure 2.1. These small anisotropies can be traced back in time, thereby undoing the red-shift through the expanding background, eventually to the quantum fluctuations of the inflaton at extremely short length scales, i.e., ultrahigh energies of order 10^{15} GeV [15,17,18,20]. Hence, the cosmic expansion acts as a huge microscope and physics at ultrahigh energies becomes accessible to observation. In particular, the new physics, which is believed to occur at the Planck scale of 10^{19} GeV, see also Footnote 4 on Page 12, might leave observable traces. Inspired by superfluid analogues (e.g., Bose-Einstein condensates, cf. Chapter 3), we will introduce a phenomenological modification to the action of the inflaton field and study its influence on the cosmic background radiation. Such a modification may arise generically from nonlinear Lorentz-preserving physics at ultrahigh energies (Planck scale). We will also address the possibility of Lorentz violation.

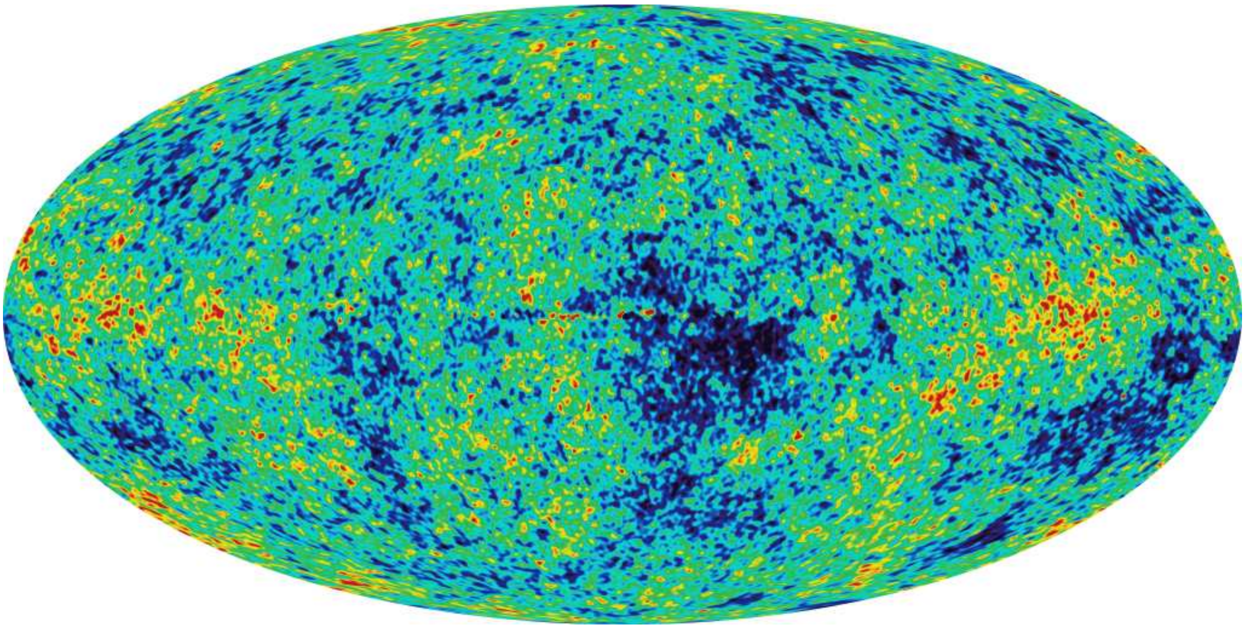

Figure 2.1: Anisotropies (of order 10^{-5}) in the cosmic microwave background radiation measured by the WMAP [21] satellite.

2.1.1 Definition of inflation

A homogeneous and isotropic space-time – like the observable universe – is most conveniently described in terms of the Friedman-Robertson-Walker-Lemaître metric, see, e.g., [15, 22, 23]

$$\mathrm{d}s^2 = \mathrm{d}t^2 - a^2(t)\left[\frac{\mathrm{d}\rho^2}{1-K\rho^2} + \rho^2(\mathrm{d}\theta^2 + \sin^2\theta\,\mathrm{d}\phi^2)\right], \tag{2.1}$$

where t is the physical time, ρ the comoving radial coordinate, and $a(t)$ the scale factor, i.e., the size of the universe. After a suitable redefinition of the radius ρ, the curvature K can assume the values $K = -1$ for open (hyperboloid), $K = 0$ for flat and $K = +1$ for closed (3-sphere) spaces. Due to the tremendous increase of the scale factor $a(t)$ by many orders of magnitude during inflation, any physical length $r = a(t)\rho$ will be stretched by a huge factor. The universe eventually becomes nearly flat, regardless of its initial curvature. Hence, we will consider only $K = 0$ from now on. Cosmic inflation is defined as a phase of accelerated expansion [15], in terms of the scale factor $a(t)$, this condition reads

$$\text{Inflation} \quad \Longleftrightarrow \quad \ddot{a} > 0\,, \tag{2.2}$$

where a dot means differentiation with respect to physical time t. Adopting the usual definition for the Hubble parameter $\mathfrak{H} = \dot{a}/a$, as characteristic scale of the expanding universe, this condition can be rewritten as

$$\frac{\mathrm{d}}{\mathrm{d}t}\frac{1}{\mathfrak{H}a} < 0\,, \tag{2.3}$$

i.e., the comoving Hubble length decreases with time during inflation.

2.1.2 Horizons

Aside from the well-known event horizons of static black holes, which mark the boundary from which nothing can escape the gravitational pull of the black hole, other horizon concepts are more important in cosmology [15,22–24,45,46]. For instance, the *particle horizon* refers to a chosen space-time trajectory $x^\mu(t) = (t, \boldsymbol{r} = \text{const})$. The future particle horizon is the boundary of a space-time region, which can be reached by signals emitted on the trajectory at a time t, see Fig. 2.2. For the highly-symmetry metric (2.1), we can calculate the (comoving) distance a photon emitted at a time t can travel

$$\Delta\rho^{\text{future}}_{\text{horizon}}(t) = \int\limits_t^\infty \frac{\mathrm{d}t'}{a(t')}\,. \tag{2.4}$$

If the above integral converges to a finite value, a particle horizon occurs. It is then given by a 3-sphere with comoving radius $\Delta\rho^{\text{future}}_{\text{horizon}}$ around the trajectory $x^\mu(t)$.

Similarly, the past particle horizon can be defined as the border of a space-time region, from which no signals can reach an observer at time t. Assuming that the big bang occurred at $t = 0$, the comoving horizon radius follows (for homogeneous and isotropic geometries)

$$\Delta\rho^{\text{past}}_{\text{horizon}}(t) = \int\limits_0^t \frac{\mathrm{d}t'}{a(t')}\,. \tag{2.5}$$

The past particle horizon with radius $\Delta\rho^{\text{past}}_{\text{horizon}}$ occurs when the integral (2.5) is finite. However, a main inconvenience of the concept of a particle horizon is that we need to know the space-time metric at all times in the past/future.

In contrast to a particle horizon, the notion of an *apparent horizon* requires the knowledge of the space-time at one instant of time only. It is closely related to trapped surfaces. Consider a space-like two-surface and two null-geodesics (light) orthogonal to it: if any two null-geodesics can (at least initially) only travel in one direction, the surface is said to be trapped. The apparent horizon is the boundary of a trapped region (i.e., on one side of the horizon all space-like two-surfaces are trapped, whereas those on the other side are not). However, one should be aware that this definition depends on the specific choice of coordinates (time-slicing). Furthermore, a trapped surface need not stay trapped forever.

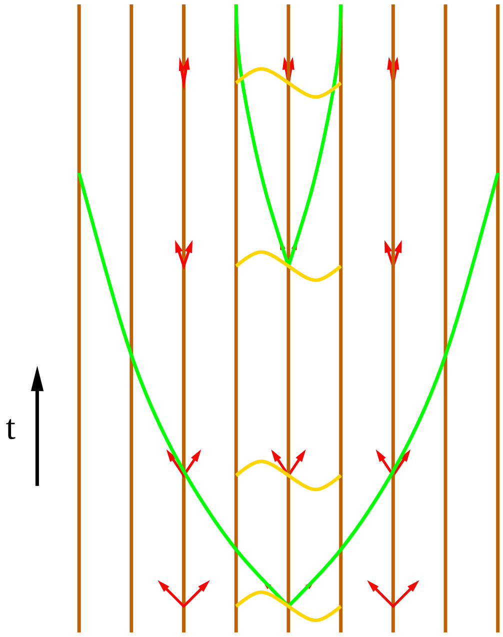

Figure 2.2: Lightcones (red) and comoving worldlines (brown) in the Friedman-Robertson-Walker-Lemaître space-time (2.1) during cosmic inflation. As the universe expands, the comoving lightcones (red) narrow (in physical time t). Hence, the distance a ray of light can travel in a time interval $(t, t+\Delta t)$ diminishes, see also Eq. (2.4). If this distance is finite for $\Delta t \uparrow \infty$, i.e., the interval (t, ∞), a (future) particle horizon occurs. Due to the temporal shrinkage of this horizon during inflation, initially freely oscillating fluctuations (yellow) might freeze and get amplified.

(The apparent horizon is only defined with respect to one instant of time and does not cover the evolution of the space-time. Conversely, the definition of the particle horizon includes and requires the knowledge of the full dynamics of the space-time.)

Let us apply the concept of an apparent horizon to an expanding Friedman-Robertson-Walker-Lemaître space-time (with physical distance r and proper time t). Due to homogeneity and isotropy, the velocity field of local freely-falling frames is given by $\boldsymbol{v}_0(t, \boldsymbol{r}) = \dot{a}(t)\boldsymbol{\rho}$. Since any particle contained inside these frames can at most travel at the speed of light $c = 1$, all particles will be dragged away from the origin, i.e., the observer, if the expansion velocity exceeds the speed of light $v_0(t, \boldsymbol{r}) > 1$. Hence, for the apparent horizon follows

$$r_{\text{horizon}} = \frac{1}{\mathfrak{H}}, \tag{2.6}$$

i.e., it is just given by the Hubble length. In the following, we will use both terms, Hubble length and horizon, synonymously.

2.1.3 Quantum fluctuations during inflation

According to our present standard model of cosmology, the small anisotropies observed in the cosmic microwave background originate from the quantum fluctuations of the inflaton field during inflation [15,17,18,20], which is characterized by a shrinking (comoving) Hubble length $1/\mathfrak{H}a$, cf. Figure 2.3. The comoving wavelength λ of a given quantum fluctuation remains constant. Hence, both quantities, $1/\mathfrak{H}a$ and λ, will eventually be equal at some time. Neighboring nodes of this mode λ will lose causal contact and cannot interact any more; they are concealed behind an apparent horizon. The quantum fluctuations freeze in and get amplified. With the decay of the inflaton field at the end of inflation, the amplified and frozen vacuum fluctuations with wavelength λ are transformed into a small density contrast with the same typical scale λ in the energy distribution. After inflation, the comoving Hubble radius, and thus the region in causal contact, grows again. Since the scale of the inhomogeneities generated by a fluctuations with wavelength λ remains constant, it eventually equals the horizon size once again, cf. Figure 2.3. The increasing horizon reveals the inhomogeneities and an imprint of them becomes visible in the cosmic microwave radiation.

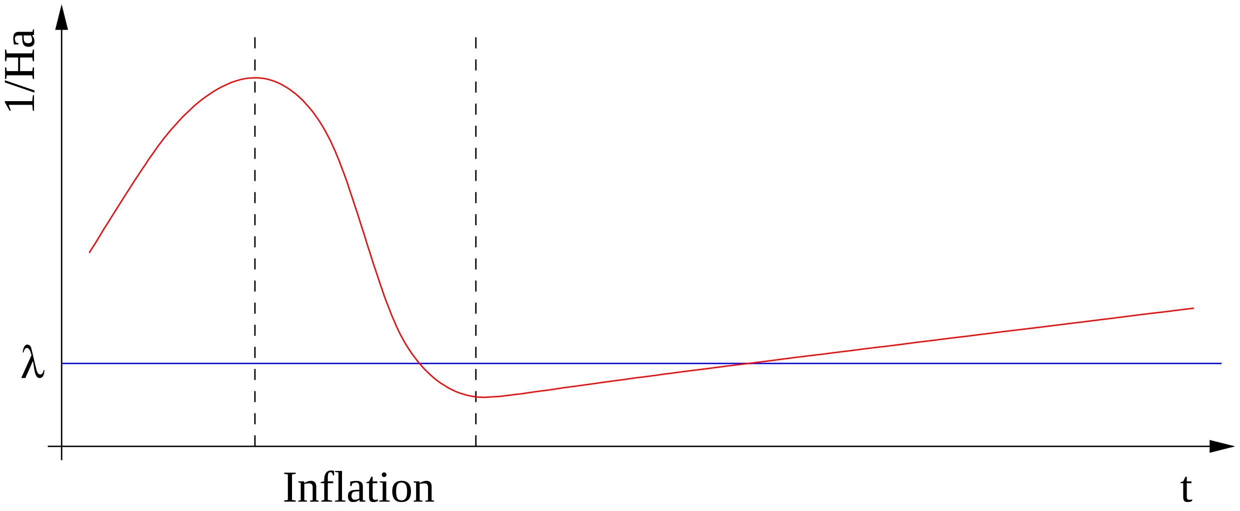

Figure 2.3: Schematic evolution of a mode with comoving wavelength λ (blue line) and of the comoving Hubble length $1/\mathfrak{H}a$ (red line) during different stages of cosmic evolution. Inflation is characterized by a decreasing comoving Hubble length (apparent horizon), whereas it increases before and afterwards. Consequently, λ equals the horizon size twice: firstly, during inflation, when the mode leaves the horizon and its fluctuations freeze and get amplified; and, secondly, when the growing horizon after inflation releases the mode again. The frozen and amplified quantum vacuum fluctuations are revealed (see Fig. 2.1). Similarly, λ could also be interpreted as size of a space-time region, which is homogeneous and in causal contact prior to inflation, but loses contact at some time during inflation. At the second horizon crossing, this homogeneous region becomes visible again.

In view of the tremendous enlargement of the scale factor $a(t)$ during cosmic inflation, the proper (physical) wavelength $a(t)\lambda$ is stretched by a huge factor as well; inflation acts as a cosmic microscope and the modes are red-shifted. By undoing this enormous red-shift, we can trace the anisotropies observed in the cosmic microwave radiation back in time to ultrahigh energies (such as the Planck energy and beyond). Energies which are inaccessible with present or (near) future terrestrial experiments, e.g., particle accelerators such as the Large Hadron Collider [26]. This observation entices the question of whether one might detect signatures of new interactions (such as quantum gravity) beyond the standard model of particle physics in the anisotropies.

2.1.4 Modifications at highest energy

Several different approaches for such expected deviations from our known laws of physics at highest energies have been investigated already. One possibility to change the physics at small distances is a modification of the dispersion relation of the inflaton field, implying a breakdown of the Lorentz invariance (which would then be just a low-energy symmetry), see, e.g., [47–53]. It was also shown that an explicit short-distance cut-off has a potentially measurable effect on the spectrum [54]. Possible backreaction effects resulting from ultraviolet modifications have been considered in [55] and a possible change of the propagator for the inflaton while preserving the local Lorentz invariance has been studied in [56]. Several authors have investigated different effects that result from a modification of the commutation relations at high energies such as $[\hat{x}_a, \hat{p}_b] = i\hbar\delta_{ab}(1 + \eta\hat{\boldsymbol{p}}^2)$, see, e.g., [57–63]. Finally, the impact of different choices of the initial vacuum state has been considered in [64–68], for example.

These references [64–68] already illustrate the importance of considering the correct initial state. One could obtain basically arbitrary results by changing the initial state correspondingly. Furthermore, the aforementioned investigations were mainly devoted to *linear* fields, whereas one would expect new physics such as quantum gravity to impose *nonlinear* corrections, i.e., interactions, as well. Therefore, a rather general nonlinear low-energy effective action for the inflaton field (interacting quantum fields in classical curved space-times) will be considered in this Chapter and the corrections due to new physics at ultrahigh energies in the anisotropies of the cosmic microwave background will be calculated. For simplicity, we assume the Planck scale to be the characteristic scale for new physics from now on, but our results can easily be generalized.

2.2 Generic modifications at high energies

During the relevant phase of inflation, the space-time can be approximated by the de Sitter metric, which is a flat Friedman-Robertson-Walker-Lemaître metric (2.1) with an exponentially growing scale factor $a(t) = e^{\mathfrak{H}t}$, where $\mathfrak{H}$ is Hubble's constant

$$\mathrm{d}s^2 \,=\, \mathrm{d}t^2 - e^{2\mathfrak{H}t}\mathrm{d}\boldsymbol{\rho}^2 \,=\, a^2(t)[\mathrm{d}\tau^2 - \mathrm{d}\boldsymbol{\rho}^2]\,. \tag{2.7}$$

Here, t and τ denote proper and conformal time, respectively. Assuming locality and covariance (non-covariant terms will be discussed later), the most general low-energy effective action for a scalar field can be represented in a gradient expansion and reads

$$\mathcal{L} \,=\, A(\varphi) + (\partial\varphi)^2 B(\varphi) + (\partial\varphi)^4 C(\varphi) + \mathcal{O}[(\partial\varphi)^6]\,, \tag{2.8}$$

with $(\partial\varphi)^2 = (\partial_\mu\varphi)(\partial^\mu\varphi)$ and arbitrary coefficient functions $A(\varphi)$, $B(\varphi)$, and $C(\varphi)$. Assuming low-energy stability $B(\varphi) > 0$ and adopting the usual field redefinition $d\phi = \sqrt{2B(\varphi)}\,d\varphi$, we get[1]

$$\mathcal{L} = \frac{1}{2}\left[(\partial\phi)^2 - V(\phi) + (\partial\phi)^4 W(\phi)\right] + \mathcal{O}[(\partial\phi)^6]\,. \tag{2.9}$$

The first two terms correspond to the usual scalar field theory whereas the third contribution of this low-energy effective action is a remnant of new physics (e.g., the interaction with massive gravitons) at ultrahigh energies. Identifying the scalar field ϕ with the inflaton field and using the slow-roll approximation (the inflaton field rolls down the potential slowly, see, e.g., [15]), we assume the two-point potential of chaotic inflation $V(\phi) = m^2\phi^2$ and a constant four-potential $W(\phi) = W$, but our main results can be easily generalized to other potentials (terms like $\lambda\phi^3$ will be discussed below in Section 2.3). Adopting a mean-field ansatz for the inflaton field, it can be split into a classical background field ϕ_0 plus its quantum fluctuations $\phi(\tau, \boldsymbol{\rho}) = \phi_0(\tau) + \Phi(\tau, \boldsymbol{\rho})$. In the usual slow-roll approximation $m \ll \mathfrak{H}$, the slowly decaying classical background solution reads $\phi_0(t) \propto \exp(-m^2 t/3\mathfrak{H})$, and the Lagrangian for the fluctuations is given by

$$\begin{aligned} L = &\int d^3\rho \left\{ \frac{a^2}{2}\left[(\partial_\tau\Phi)^2 - (\boldsymbol{\nabla}_{\boldsymbol{\rho}}\Phi)^2\right] - ag\left[(\partial_\tau\Phi)^3 - (\partial_\tau\Phi)(\boldsymbol{\nabla}_{\boldsymbol{\rho}}\Phi)^2\right]\right\} \\ &+ \mathcal{O}[(\partial\phi)^6] + \mathcal{O}[\Phi^4] + \mathcal{O}[g^2]\,, \end{aligned} \tag{2.10}$$

with $g = 2W\partial\phi_0/\partial t \approx -2\phi_0 W m^2/(3\mathfrak{H})$ denoting a roughly constant effective coupling strength. Note that the interaction term $(\partial\phi)^4$ in the Lagrangian (2.9) also implies small corrections such as $\dot{\Phi}^2$ and thus a small redefinition of the propagation speed c_{eff} and the amplitude of the inflaton field Φ etc. As usual during inflation, the mass term $m^2\Phi^2$ can be neglected for the fluctuations Φ due to $m \ll \mathfrak{H}$. With the main interest lying on the three-point function, higher-order terms $\mathcal{O}[\Phi^4]$ will not be considered, but the associated four-point contribution can be calculated via the same formalism (see discussion in Subsection 2.3.1). For the sake of brevity, stating the higher-order corrections $\mathcal{O}[(\partial\phi)^6] + \mathcal{O}[\Phi^4] + \mathcal{O}[g^2]$ will be omitted from now on.

After a Legendre transformation and subsequent quantization, the low-energy effective Hamiltonian density is obtained

$$\hat{\mathcal{H}} = \frac{1}{2}\left[\frac{\hat{\Pi}^2}{a^2} + a^2(\boldsymbol{\nabla}_{\boldsymbol{\rho}}\hat{\Phi})^2\right] + g\left[\frac{\hat{\Pi}^3}{a^5} - \frac{\hat{\Pi}}{2a}(\boldsymbol{\nabla}_{\boldsymbol{\rho}}\hat{\Phi})^2 - (\boldsymbol{\nabla}_{\boldsymbol{\rho}}\hat{\Phi})^2\frac{\hat{\Pi}}{2a}\right]\,. \tag{2.11}$$

The explicit time-dependence of this Hamiltonian can partly be removed via the (time-dependent) canonical transformation $\hat{\Pi} \to a\hat{\Pi}$ and $\hat{\Phi} \to \hat{\Phi}/a$ generated by the squeezing operator $\hat{S}$, giving rise to an additional term to the Hamiltonian: in the squeezed representation with the Schrödinger equation $i\,\mathrm{d}(\hat{S}|\Psi\rangle)/\mathrm{d}\tau = \hat{H}_S(\hat{S}|\Psi\rangle)$, the Hamilton density reads

---

[1] To first order (in W or g), which is the desired accuracy, we can eliminate terms containing $\Box\varphi$ (which would complicate the Hamiltonian analysis) after an integration by parts as well as by using the equation of motion for φ. The same applies to contributions of the type $\varphi^2(\partial_\mu\partial_\nu\varphi)(\partial^\mu\partial^\nu\varphi)$ etc.

$$\begin{aligned} \hat{\mathcal{H}}_S &= \frac{1}{2}\left[\hat{\Pi}^2 + (\boldsymbol{\nabla}_{\boldsymbol{\rho}}\hat{\Phi})^2\right] - \frac{a\mathfrak{H}}{2}\left[\hat{\Phi}\hat{\Pi} + \hat{\Pi}\hat{\Phi}\right] + \frac{g}{a^2}\left[\hat{\Pi}^3 - \frac{1}{2}\hat{\Pi}(\boldsymbol{\nabla}_{\boldsymbol{\rho}}\hat{\Phi})^2 - (\boldsymbol{\nabla}_{\boldsymbol{\rho}}\hat{\Phi})^2\frac{1}{2}\hat{\Pi}\right] \\ &= \hat{\mathcal{H}}_0 + \hat{\mathcal{H}}_{\mathfrak{H}} + \hat{\mathcal{H}}_g\,. \end{aligned} \tag{2.12}$$

This form allows for an intuitive physical interpretation: due to the cosmic expansion $a = e^{\mathfrak{H}t}$, the modes are being continuously stretched and hence the effects of the interactions $\hat{\mathcal{H}}_g \propto 1/a^2$ decrease with time whereas the influence of the expansion $\hat{\mathcal{H}}_{\mathfrak{H}} \propto a$ increases.

2.2.1 Initial state

Since the interactions are strong at early times, the derivation of the correct initial state requires the treatment of strongly interacting quantum fields in curved space-times, which is a non-trivial task, cf. [10]. Let us consider the evolution of the modes in more detail: due to spatial homogeneity, the comoving wavenumber $\boldsymbol{\kappa}$ corresponding to a spatial dependence of $e^{i\boldsymbol{\kappa}\cdot\boldsymbol{\rho}}$ remains constant – but the physical wavenumber $\boldsymbol{k} = \boldsymbol{\kappa}/a$ decreases (stretching). Hence modes with different κ leave the Planck scale at different times, i.e., when $\kappa/a = \mathcal{O}[M_{\text{Pl}}]$. Assuming that the rate of the cosmic expansion given by the Hubble parameter $\mathfrak{H}$ is much slower than the internal evolution rate of these Planckian modes (scale separation $\mathfrak{H} \ll M_{\text{Pl}}$), the most natural initial state is the adiabatic vacuum state, cf. [10]. During the further expansion, the wavelength increases until $\kappa/a \ll M_{\text{Pl}}$ holds and the low-energy effective action (2.9) becomes valid[2]. In view of the adiabatic theorem, the modes evolve adiabatically and hence stay in the adiabatic vacuum as long as the external time-dependence due to the cosmic expansion is slow compared to the internal dynamics. If now an intermediate time τ_0 was chosen such that $\mathfrak{H} \ll k/a(\tau_0) \ll M_{\text{Pl}}$, the effects of both, the cosmic expansion $\hat{\mathcal{H}}_{\mathfrak{H}}$ and the interaction $\hat{\mathcal{H}}_g$, are small and can be treated as perturbations. As a result, the quantum state (adiabatic vacuum) of these modes at that time τ_0 can be derived via the adiabatic expansion, see Appendix A

$$|\text{in}(\tau_0)\rangle = N_0|\Psi_0\rangle - i\sum_{n>0}|\Psi_n\rangle\left(\frac{\langle\Psi_n|(\partial_\tau\hat{H}_S)|\Psi_0\rangle}{\Delta E_n^2} + \frac{i}{\Delta E_n}\frac{\mathrm{d}}{\mathrm{d}\tau}\frac{\langle\Psi_n|(\partial_\tau\hat{H}_S)|\Psi_0\rangle}{\Delta E_n^2}\right) + \mathcal{O}[\mathfrak{H}^3]\,, \tag{2.13}$$

where $|\Psi_n\rangle$ are the instantaneous eigenvectors of the Hamiltonian $\hat{H}_S = \int \mathrm{d}^3\rho\,\hat{\mathcal{H}}_S$ with appropriate phases and $N_0 = 1 + \mathcal{O}[\mathfrak{H}^2]$ is a normalization. For $g = 0$, the Hamiltonian $\hat{H}_0 + \hat{H}_{\mathfrak{H}}$ can be diagonalized exactly (i.e., to all orders in $\mathfrak{H}$) via a Bogoliubov transformation

---

[2] Here, it is assumed $g = \mathcal{O}(1/M_{\text{Pl}}^2)$, but it would be sufficient to demand $g\mathfrak{H}^2 \ll 1$ and to replace M_{Pl} by $1/\sqrt{g}$, i.e., $\mathfrak{H} \ll \kappa/a(\tau_0) \ll 1/\sqrt{g}$.

$\hat{a}_{\boldsymbol{\kappa}} = \alpha_{\boldsymbol{\kappa}} \hat{b}_{\boldsymbol{\kappa}} + \beta_{\boldsymbol{\kappa}} \hat{b}^\dagger_{-\boldsymbol{\kappa}}$ (where $\hat{b}^\dagger_{\boldsymbol{\kappa}}$, $\hat{b}_{\boldsymbol{\kappa}}$ are the creation and annihilation operators diagonalizing $\hat{H}_0$ and $\hat{a}_{\boldsymbol{\kappa}}$, $\hat{a}^\dagger_{\boldsymbol{\kappa}}$ are those for $\hat{H}_0 + \hat{H}_{\mathfrak{H}}$). Up to second order in $\mathfrak{H}$ (the desired accuracy), the Bogoliubov coefficients $\alpha_{\boldsymbol{\kappa}}$ and $\beta_{\boldsymbol{\kappa}}$ read $\alpha_{\boldsymbol{k}} = 1 + ia\mathfrak{H}/2\kappa$ and $\beta_{\boldsymbol{k}} = ia\mathfrak{H}/2\kappa - a^2\mathfrak{H}^2/4\kappa^2$. The remaining corrections can be calculated with stationary perturbation theory

$$|\Psi_n\rangle \;=\; |\Psi^0_n\rangle + \sum_{m\neq n} |\Psi^0_m\rangle \frac{\langle\Psi^0_m|\hat{H}_g|\Psi^0_n\rangle}{E^0_n - E^0_m} + \mathcal{O}[g^2]\,, \tag{2.14}$$

where $(\hat{H}_0 + \hat{H}_{\mathfrak{H}})|\Psi^0_n\rangle = E^0_n|\Psi^0_n\rangle$ are the unperturbed eigenstates obtained via the aforementioned Bogoliubov transformation.

2.2.2 Final state

The impact of the cosmic expansion $\hat{H}_{\mathfrak{H}}$ on the modes increases with time and their evolution finally becomes non-adiabatic when $\kappa/a = \mathcal{O}[\mathfrak{H}]$, i.e., when they cross the horizon and freeze. Therefore, in order to calculate the final state, it is advantageous to switch from the Schrödinger representation (thereby undoing the canonical transformation $\hat{S}$ etc.) to the interaction picture: the Heisenberg operators carry full dynamics for the unperturbed problem $\hat{H}_0 + \hat{H}_{\mathfrak{H}}$ to all orders in $\mathfrak{H}$ (cf. [15, 17])

$$\hat{\Phi} \;=\; \int \frac{\mathrm{d}^3\kappa}{\sqrt{2\kappa(2\pi)^3}} \left(\frac{1}{a} + i\frac{\mathfrak{H}}{\kappa}\right) e^{i\boldsymbol{\kappa}\cdot\boldsymbol{\rho} + i\kappa/(\mathfrak{H}a)}\hat{a}_{\boldsymbol{\kappa}} + \text{H.c.} \tag{2.15}$$

Note that $\hat{a}_{\boldsymbol{k}}$ annihilates the adiabatic vacuum (2.13) for vanishing g, which can be used as a consistency check. The remaining small interaction Hamiltonian $\hat{H}_g$ acts on the quantum state, which enables us to calculate the final state via time-dependent perturbation theory

$$|\text{out}(\tau)\rangle \;=\; \left(1 - i\int\limits_{\tau_0}^{\tau} \mathrm{d}\tau'\,\hat{H}_g(\tau)\right)|\text{in}(\tau_0)\rangle + \mathcal{O}[g^2]\,. \tag{2.16}$$

As another test of the consistency of the used formalism, one may check that the resulting final state $|\text{out}(\tau)\rangle$ is indeed independent of τ_0 as it should be. Since the imprint of the modes observed today in the microwave background radiation froze well before the end of inflation, one may approximately extend the integration to infinite proper time $t = \infty$, which corresponds to vanishing conformal time $\tau = 0$.

2.2.3 Three-point function

With the final state obtained after performing the integration, we can calculate the three-point function of the frozen fluctuations (which then generate the anisotropies of the cosmic microwave background radiation) and obtain (after some algebra) the following spectrum

$$\begin{aligned}
&\langle\hat{\Phi}(\boldsymbol{\rho}_1)\hat{\Phi}(\boldsymbol{\rho}_2)\hat{\Phi}(\boldsymbol{\rho}_2)\rangle \\
&\quad= -g\mathfrak{H}^5\int\frac{\mathrm{d}^3\kappa_1\,\mathrm{d}^3\kappa_2\,\mathrm{d}^3\kappa_3}{(2\pi)^6}\,\frac{\delta(\boldsymbol{\kappa}_1+\boldsymbol{\kappa}_2+\boldsymbol{\kappa}_3)}{\kappa_1\kappa_2\kappa_3}\,\exp\{i(\boldsymbol{\kappa}_1\cdot\boldsymbol{\rho}_1+\boldsymbol{\kappa}_2\cdot\boldsymbol{\rho}_2+\boldsymbol{\kappa}_3\cdot\boldsymbol{\rho}_3)\} \\
&\quad\times\left(\frac{3}{\kappa_+^3}-\left\{\frac{\boldsymbol{e}_2\cdot\boldsymbol{e}_3}{\kappa_+^3}+\frac{1}{\kappa_+}\frac{\boldsymbol{e}_2\cdot\boldsymbol{e}_3}{2\kappa_2\kappa_3}+\frac{\boldsymbol{e}_2\cdot\boldsymbol{e}_3}{2\kappa_+^2}\left(\frac{1}{\kappa_2}+\frac{1}{\kappa_3}\right)+\text{perm.}\right\}\right) \\
&\quad\times\left(1+\mathcal{O}[\mathfrak{H}]+\mathcal{O}[g]\right)\,, \qquad (2.17)
\end{aligned}$$

with the abbreviations $\kappa_+ = \kappa_1+\kappa_2+\kappa_3$ and $\boldsymbol{e}_j = \boldsymbol{\kappa}_j/\kappa_j$. The remaining permutations (denoted by "perm.", i.e. $\kappa_1 \to \kappa_2$, $\kappa_2 \to \kappa_3$, and $\kappa_3 \to \kappa_1$ etc.) have to be included as well. The spectrum is scale invariant as one would expect since the sequence: leaving of Planck scale and stretching → horizon crossing and freezing occurs on all scales (just at different times). The first contribution $3/\kappa_+^3$ on the second line results from the $\hat{\Pi}^3$-term whereas the remaining ones appear because of the $\hat{\Pi}(\boldsymbol{\nabla}_{\boldsymbol{\rho}}\hat{\Phi})^2$-term in the interaction Hamiltonian $\hat{H}_g$ [see Eq. (2.12)].

An estimate of the relative size of this non-Gaussian contribution $\langle\hat{\Phi}\hat{\Phi}\hat{\Phi}\rangle$ can be obtained by comparison to the (Gaussian) two-point function $\langle\hat{\Phi}\hat{\Phi}\rangle$

$$\frac{\langle\hat{\Phi}\hat{\Phi}\hat{\Phi}\rangle}{\sqrt{\langle\hat{\Phi}\hat{\Phi}\rangle^3}} = \mathcal{O}[g\mathfrak{H}^2] = \mathcal{O}[\phi_0 W(\phi_0)m^2\mathfrak{H}] \ll 1\,. \qquad (2.18)$$

Note that m can be eliminated with the classical equations of motion and the Friedman equation (see, e.g., [22, 23]), i.e., $g\mathfrak{H}^2 = \mathcal{O}[\phi_0 W m^2\mathfrak{H}] = \mathcal{O}[W\mathfrak{H}^3 M_{\mathrm{Pl}}^2/\phi_0]$. Usually the typical scale of new physics such as quantum gravity is expected to be the Planck scale. Therefore, one would naturally assume that the coupling behaves according to $W \sim 1/M_{\mathrm{Pl}}^4$ if W did not depend on ϕ_0. In this case, the relative size of the effect would be suppressed with $\mathfrak{H}^3/M_{\mathrm{Pl}}^3$ and thus probably hard to measure.

However, one should also bear in mind that the usual picture of inflation involves a large value of the inflaton field $\phi_0 \gg M_{\mathrm{Pl}}$ and hence $W(\phi_0)$ could be much bigger than $1/M_{\mathrm{Pl}}^4$. Similarly, the inflaton potential $V(\phi)$ could differ from $m^2\phi^2$ or the scale for new physics might differ from the Planck scale. In all these cases, the effect could be far stronger than $\mathfrak{H}^3/M_{\mathrm{Pl}}^3$. As another, more speculative option, Ref. [37] mentions the idea that our picture of cosmic inflation might only provide a distorted view on a quantum phase transition (see also Chapter 4) in the early universe – in which case $\mathfrak{H}/M_{\mathrm{Pl}}$ needs not to be very small.

On the other hand, the employed formalism only works if $g\mathfrak{H}^2 \ll 1$ holds, i.e., if the relative size of the effect (2.18) is small compared to one (which is consistent with the observations [21]). Given these two extremal cases, the possible range of the f_{NL} parameter (see, e.g., [69]) frequently used as a measure of the nonlinearity is very wide and covers values from $f_{\mathrm{NL}} \ll 1$ to $f_{\mathrm{NL}} \gg 1$. Taking the wavenumbers of the modes κ_i to be equal[3], one obtains (see also [69–71]).

---

[3] Strictly speaking, the f_{NL} parameter depends on all κ-values since the spectrum does not factorize.

$$f_{\rm NL} = \mathcal{O}[W\dot{\phi}^2] = \mathcal{O}\left[g\mathfrak{H}^2\frac{M_{\rm PL}}{\phi}\frac{M_{\rm PL}}{\mathfrak{H}}\right] \tag{2.19}$$

Therefore even with $g\mathfrak{H}^2 \ll 1$ the parameter $f_{\rm NL}$ might be greater than one.

2.3 Discussion

Assuming locality and covariance, the most general low-energy effective action of the scalar inflaton field (including possible remnants from Planckian interactions) was derived via a gradient expansion. Based on this ansatz, a formalism for the treatment of this (strongly) interacting quantum field theory in a curved space-time and the derivation of the quantum state via the adiabaticity assumption was presented in this Chapter. The induced spectrum of the three-point function – which is quite robust against uncertainties in cosmic evolution – was predicted. The spectrum (2.17) can be clearly distinguished from other effects such as a $\lambda\hat{\Phi}^3$-term, see Subsection 2.3.1, making the three-point function a promising observable. This concrete prediction of the explicit spectrum facilitates a refined search in the present/future WMAP [21] and PLANCK [25] data with good statistics and hence high sensitivity. Abandoning covariance, it might even be possible to detect violations of the Lorentz invariance at the Planck scale, see Subsection 2.3.2.

2.3.1 Generalizations

Let us discuss the impact of momentum-independent interaction terms such as $\lambda\hat{\Phi}^3$ [in contrast to contributions like $(\partial\hat{\Phi})^4$], which occur if the potential V is not just given by the mass term $V(\phi) \neq m^2\phi^2$. In contrast to $\hat{\mathcal{H}}_g$, these momentum-independent interaction terms become important at late times. Hence the three-point spectrum generated by the $\lambda\hat{\Phi}^3$-term can be derived from time-dependent perturbation theory and behaves as $\kappa_+/(\kappa_1\kappa_2\kappa_3)^3$. This spectrum is dominated by large length scales and thus not scale invariant – which should make it easy to distinguish between the effects of the momentum-independent interaction $\lambda\hat{\Phi}^3$ and those generated by high-energy (Planckian) interactions such as the spectrum (2.17). A non-trivial ϕ-dependence of the four-point potential $W(\phi)$ does not affect the calculated three-point function significantly in the slow-roll regime, but could have consequences for the higher-order contributions.

The derivation of the four-point function can be accomplished by means of the same formalism – but necessitates higher orders in the adiabatic expansion etc. The relative size of the non-Gaussian contribution (compared to the Gaussian part of the four-point function, for example) can roughly be estimated via $\mathcal{O}[W\mathfrak{H}^4]$. Hence the comparison of the relative sizes of the non-Gaussian contributions of the three-point and the four-point functions, respectively, yields the unknown ratio $\mathfrak{H}\phi_0/M_{\rm Pl}^2$, which could be used to obtain additional information about inflation.

2.3.2 Lorentz invariance

So far, we assumed the Planckian interactions to respect local Lorentz invariance, and thus start with the covariant action (2.9). However, it may well be that the usual local Lorentz invariance is just a low-energy symmetry and broken at the Planck scale[4]. In this case, many more terms can occur in the low-energy effective action – even if, complying with the cosmological principle, spatial homogeneity and isotropy are still demanded: first of all, bilinear terms such as $(\partial^2\hat{\Phi}/\partial\tau^2)$ and $(\boldsymbol{\nabla}_{\boldsymbol{\rho}}^2\hat{\Phi})^2$ exactly correspond to a change in the dispersion relation mentioned in the introduction. Assuming adiabaticity (which will, however, not by valid for all dispersion relations), one may treat those corrections with the presented formalism: in de Sitter space-times, it turns out that they basically generate a global and constant shift of the scale-invariant two-point spectrum to lowest order, which is probably hard to measure. (But these bilinear terms do not contribute to the three-point function $\langle\hat{\Phi}\hat{\Phi}\hat{\Phi}\rangle$.) The next terms occurring in an expansion into powers of $\hat{\Phi}$ and the numbers of derivatives are exactly the combinations $\hat{\Pi}^3$ and $\hat{\Pi}(\boldsymbol{\nabla}_{\boldsymbol{\rho}}\hat{\Phi})^2$ discussed before[5]. However, without Lorentz invariance, the prefactors of these two terms are no longer necessarily equal. Therefore, measuring and comparing the relative strength of the two contributions in the above three-point spectrum (2.17) provides a possibility to detect possible violations of the Lorentz invariance at the Planck scale.

2.3.3 Comparison with previous calculations

Non-Gaussianities in the cosmic microwave background radiation have been considered before, see, e.g., [69–72]. In Ref. [72], non-Gaussianities due to higher-order terms of the usual action (scalar field plus gravity) are considered. The spectrum and the prefactor obtained there differ from our result in Eq. (2.17). Although both effects would be roughly of the same order of magnitude, provided one assumes $W \propto 1/M_{\rm Pl}^4$, the two spectra have a completely different shape. Hence, it should be possible to distinguish between the two effects in high-precision observations.

Furthermore, non-Gaussianities stemming from effective Lagrangians of the type (2.9) have already been considered in Refs. [69–71]. However, in these works, the final state was calculated by extrapolating the perturbative expression in Eqs. (2.15) and (2.16) to arbitrary times $\tau_0 \downarrow -\infty$ (supplemented with a shift into the imaginary direction $\tau \to \tau + i\epsilon|\tau|$). This procedure basically assumes the Bunch-Davies vacuum of the free field as the initial state. But since the interactions are strong at early times, this assumption is not justified. The authors of [69–71] provide some arguments based on adiabaticity and scattering theory in order to argue that their results are nevertheless correct, but – as we shall see below – these arguments are of limited applicability in general curved space-times and cannot substitute a careful analysis of the correct initial state. Therefore, it is rather surprising that the over-extrapolation of Eqs. (2.15) and (2.16) done in [69–71] indeed yields the correct result for the three-point function (2.17) in de Sitter space-times. But this coincidence can be traced back to the highly-symmetric (and scale-invariant) character of the de Sitter metric and does not imply that the method used in [69–71] works in general curved space-times.

---

[4] For example, the fluctuations (phonons) in Bose-Einstein condensates obey only an effective low-energy Lorentz invariance, which is broken below the healing length, see chapter 3.

[5] In case of multiple inflaton fields, many more combinations are possible. Furthermore, it is assumed here that the scale factors $a(t)$ occur with the same power as in the Lorentz invariant situation (minimal extension) which is not strictly necessary without demanding covariance.

Let us study some simple, but illustrative, counterexamples: first, we consider the frequently discussed case of a bouncing universe with scale factor $a(t) = \cosh(\mathfrak{H}_0 t)$ and hence $\mathfrak{H}(t) = \mathfrak{H}_0 \tanh(\mathfrak{H}_0 t)$. Instead of (2.15), the normal-mode expansion now reads

$$\hat{\Phi} = \int \frac{d^3\kappa}{(2\pi)^{3/2}} \frac{\mathfrak{H}_0^{1/2}}{\sqrt{2\kappa\sqrt{1+\kappa^2/\mathfrak{H}_0^2}}} \left(\frac{\sqrt{1+\kappa^2/\mathfrak{H}_0^2}}{\cosh(\mathfrak{H}_0)t} + i\tanh(\mathfrak{H}_0 t) \right) e^{i\boldsymbol{\kappa}\cdot\boldsymbol{\rho}+i\phi_\kappa(\tau)}\hat{a}_\kappa + \text{H.c.} \tag{2.20}$$

with the time-dependent phase

$$\phi_\kappa(t) = 2\sqrt{1+\kappa^2/\mathfrak{H}_0}\arcsin\sqrt{\frac{1-\tanh(\mathfrak{H}_0 t)}{2}}\,,$$

which reduces to the standard result (2.15) for $\mathfrak{H}_0 t \gg 1$ and $\kappa/\mathfrak{H}_0 \gg 1$. Following the procedure in [69–71], one would obtain an additional factor of $(1 - \exp\{-i\pi\kappa_+/\mathfrak{H}_0\})$ in the three-point spectrum in this situation. This spurious factor arises from contributions of the interaction Hamiltonian prior to the bounce, which occur due to the extrapolation of the perturbative expression (2.16) to early times. In contrast, the natural choice of the adiabatic vacuum as initial state gives a spectrum that does not depend on the pre-bounce fluctuations. This means, the extrapolation of the the initial state to arbitrarily early times $t \to -\infty$ generates an additional rapidly oscillating factor[6]. When taking the adiabatic (post-bounce) vacuum as initial state, this artificial factor does not occur, cf. Subsection 2.2.1.

A similar rapidly oscillating and unphysical factor would occur if one inserted a time-dependent coupling $g(\tau)$ such as $g(\tau) = g_0\Theta(\tau - \tau_0)$ into the integral in [69–71]. Apart from this step-function, even a smooth variation of $g(\tau)$ can reveal problems of the extrapolation used in [69–71]. Let us consider a coupling constant $g(\tau) = g_0 \exp\{-\tau^3/\tau_0^3\}$ in terms of the conformal time $\tau < 0$ together with a convergence factor $\exp\{\epsilon\tau^5/\tau_0^5\}$ in order to render

---

[6] An analogous spurious factor occurs in a bouncing universe described by power-law inflation with the scale factor $a = (a_0 t)^2$, where t runs from $-\infty$ to $+\infty$ and a_0 is a characteristic energy scale.

$g(\tau)$ finite for $t \to -\infty$, i.e., $g(\tau) = g_0 \exp\{-\tau^3/\tau_0^3 + \epsilon\tau^5/\tau_0^5\}$. The method in [69–71] yields integrals like

$$I = g_0 \int_{-\infty}^{0} \mathrm{d}\tau P_\kappa(\tau) e^{-i\kappa_+\tau - \tau^3 + \epsilon\tau^5} , \tag{2.21}$$

with $P_\kappa(\tau)$ being some polynomial in τ. The upper limit of the integration contour $\tau = 0$ gives rise to the usual contribution (2.17). In addition, the extrapolation of the integral to arbitrarily early times yields an exponentially large contribution from the saddle point $\propto \exp\{1/\epsilon^{3/2}\}$, which again shows the limited validity of the method used in [69–71].

Finally, let us study the scenario of a linearly expanding universe with scale factor $a = a_0 t = e^{a_0\tau}$ as a limiting case of power-law inflation (as $\partial^2 a/\partial_\tau^2 = 0$). In this situation, there is no particle horizon (just an apparent horizon). However, a critical slowing down $[\tau = \ln(a_0 t)/a_0]$ can be inferred from the mode decomposition of the scalar field

$$\hat{\Phi}(\boldsymbol{\rho}, \tau) = \int \frac{\mathrm{d}^3\kappa}{(2\pi)^{3/2}} \frac{\exp\{i\boldsymbol{\kappa}\cdot\boldsymbol{\rho} - (a + i\sqrt{\kappa^2 - a_0^2})t\}}{a_0\sqrt{2}(\kappa^2 - a_0^2)^{1/4}} \hat{a}_{\boldsymbol{\kappa}} + \mathrm{H.c.} \tag{2.22}$$

The above situation can be interpreted as the limiting case of weak power-law inflation scenarios $a \propto t^{1+\epsilon}$, which do possess a particle horizon (but are far more difficult to treat analytically). Insertion into the interaction Hamiltonian yields a first-order correction (in g) of the following form

$$|\mathrm{out}(\tau)\rangle = \left(1 - ig \sum_{\boldsymbol{\kappa}_1,\boldsymbol{\kappa}_2,\boldsymbol{\kappa}_3} F(\boldsymbol{\kappa}_1, \boldsymbol{\kappa}_2, \boldsymbol{\kappa}_3) \int\limits_{-\infty}^{\tau} \mathrm{d}\tau\, \exp\{-2a_0\tau + iE_{\sum}\tau\} \hat{a}^\dagger_{\boldsymbol{\kappa}_1} \hat{a}^\dagger_{\boldsymbol{\kappa}_2} \hat{a}^\dagger_{\boldsymbol{\kappa}_3}\right) |\mathrm{in}\rangle , \tag{2.23}$$

where $F(\boldsymbol{\kappa}_1, \boldsymbol{\kappa}_2, \boldsymbol{\kappa}_3)$ is some time-independent function, which can be specified by the mode decomposition of the interaction Hamiltonian, and $E_{\sum} = E_1 + E_2 + E_3 = \sqrt{\kappa_1^2 - a_0^2} + \sqrt{\kappa_2^2 - a_0^2} + \sqrt{\kappa_3^2 - a_0^2}$. Obviously, the shift $\tau \to \tau + i\epsilon|\tau|$ used in [69–71] is not sufficient to render the integral finite. Even a quadratic regulator $e^{-\epsilon^2\tau^2}$ (which is the usual procedure in Fourier analysis) does not work, since the integral is still divergent for $2a_0 > E_{\sum}$ (as can be observed after quadratic completition of the exponent). As one example, one could imagine that the regulator $e^{-\epsilon^2\tau^2}$ represents a weak time-dependence of the coupling $g(\tau)$ in which case this slow variation gives rise to huge corrections.

Of course, the above divergence is an artifact of the unphysical extrapolation to early times employed in Refs. [69–71]. The correct initial state can be obtained from the adiabatic expansion – but since the Hubble parameter is not constant in this situation, a re-summation up to arbitrarily high orders (in the adiabatic expansion, not in g) is necessary. Fortunately, this can be done analytically after the squeezing transformation, because $\hat{S}'$ is time-independent

$$|\mathrm{in}(\tau_0)\rangle = |\Psi_0\rangle - i \sum_{n>0} |\Psi_n\rangle \sum_{\alpha=0}^{\infty} \left(\frac{i}{\Delta E_n}\frac{\mathrm{d}}{\mathrm{d}\tau}\right)^{\alpha} \frac{\langle\Psi_n|\dot{\hat{H}}_S|\Psi_0\rangle}{\Delta E_n^3} . \tag{2.24}$$

Owing to the simple time-dependence of the interaction Hamiltonian $\hat{H}_I$, the sum is just a geometric series. After the transformation to the interaction picture and the integration of the Schrödinger equation, we obtain the following first-order correction from the Π^3-term

$$\begin{aligned}|\mathrm{out}(\tau)\rangle &= |0\rangle - \frac{ig}{a^2(\tau)}\int\frac{\mathrm{d}^3\kappa_1\mathrm{d}^3\kappa_2\mathrm{d}^3\kappa_3}{(4\pi)^{3/2}}\delta^{(3)}(\boldsymbol{\kappa}_1+\boldsymbol{\kappa}_2+\boldsymbol{\kappa}_3)\\ &\times\frac{\exp\{iE_{\sum}\tau\}}{\sqrt{E_1E_2E_3}}\frac{(a_0-iE_1)(a_0-iE_2)(a_0-iE_3)}{2a_0-i(E_1+E_2+E_3)}|\boldsymbol{\kappa}_1,\boldsymbol{\kappa}_2\boldsymbol{\kappa}_3\rangle\,. \qquad (2.25)\end{aligned}$$

Note that (in contrast to the de Sitter case) for late times with $a(\tau)\uparrow\infty$, the first-order correction vanishes. Clearly, the above result cannot be obtained with the method used in [69–71] – which demonstrates the advantage of deriving the correct initial state via the adiabatic expansion. In summary, while the simple method [69–71] of over-extrapolation to early times by means of the shift $\tau\to\tau+i\epsilon|\tau|$ seems to work in many cases, it is not guaranteed to work in all cases – as we have seen in the above counterexamples. (Of course, in order to decide whether such a simplified method works or not, one has to compare it to the correct calculation.)

3 On Quantum Effects in Bose-Einstein Condensates

Since the first experimental realization of Bose-Einstein condensation in trapped, dilute vapors of rubidium [35] and sodium atoms [36], tremendous progress in the experimental handling but also in the theoretical understanding of ultracold atomic gases has been made, see, e.g., [41, 73, 74]. It is now possible to produce Bose-Einstein condensates of many different atomic (or molecular) species, with atom numbers ranging from few hundred to several million [75, 76]. The dilute gases can be trapped in magnetic (Ioffe-Pritchard) as well as in optical traps [77]. Basically every parameter can be varied in experiments.

Bose-Einstein condensates provide a promising, finite-sized laboratory system for the study of quantum effects, in general, and for the construction of cosmic analogues, where the different aspects of quantum gravity are modeled in the laboratory, in particular, see, e.g., [32] for review. For instance, in Ref. [78], a quantum field in a time-dependent Friedman-Robertson-Walker-Lemaître space-time, cf. Eq. (2.1), is mimicked by phonons in a single-component Bose-Einstein condensate, where the time-dependence of the effective metric can be mediated by tuning the two-particle interaction strength through Feshbach resonance [79–85]. Two-component condensates (where, e.g., different hyperfine states of one atomic species are trapped) offer even more possibilities: for example, the authors of Ref. [86] simulate quantum aspects of cosmic inflation by tuning the inter-species interaction strength. Massive pseudo-particle modes in an effective space-time are constructed in Ref. [87].

In the following Section 3.1, a brief introduction to trapped, dilute Bose-Einstein condensates will be given. Due to their dilute character, the effective two-particle interaction length is much smaller than the typical inter-particle separation. Therefore, the interaction can be approximated by a contact potential, i.e., a δ-function, in many theoretical treatments. On the other hand, quantum fluctuations at all length scales – including those comparable to the effective interaction length – enter some of the expectation values (such as the quantum depletion). We address the influence of the finite range of the two-particle potential[1] and also scrutinize the accuracy of the mean-field expansion in Sec. 3.2.

---

[1] For instance, in Ref. [88], the inter-atomic potential for Rb-Rb scattering is reconstructed from experimental data.

By placing a Bose-Einstein condensate in a highly-anisotropic trap, the motion in one or two spatial directions can be confined to the lowest bound state. We will derive the resulting effectively lower-dimensional action in Sec. 3.3. In the subsequent Section 3.4, we introduce an effective space-time metric for the phonons (quantized low-energy sound-waves) in an arbitrary number of spatial dimensions. Using this formalism, we can adopt the methods and tools known from general relativity in order to discuss the evolution of the quantum fluctuations in Bose-Einstein condensates. In particular, we discuss the free, ballistic expansion of the gas cloud (after the confining potential has been turned off) in Sec. 3.5. This situation bears strong similarities to cosmic inflation. In both cases, quantum fluctuations evolve in an expanding background. They freeze and get amplified when an (effective) horizon forms. A distinct pattern in the (frozen) correlation function can be observed.

Another crucial point in quantum field theory concerns the backreaction of the quantum fluctuations onto the (classical inhomogeneous) background. Such a background might be a curved space-time or the condensate fraction of a trapped Bose-Einstein condensate. Starting from the field equations for the full field operator of the dilute bosonic gas, we will derive *ab initio* an expression for the backreaction. On the other hand, we can also adopt the effective space-time description of the phonons and employ the effective-action technique [10] known from quantum field theory in curved space-times. Both results may be compared. We are thus able to scrutinize a technique known from cosmology by means of an analogue system in Sec. 3.6.

A discussion in Sec. 3.7 closes this chapter.

3.1 Bose-Einstein condensates

Bose-Einstein condensation of confined gases, cf. Fig. 3.1, occurs in a metastable phase. At the conditions (e.g., temperature) required for the condensation, the equilibrium phase would be a solid. It is therefore necessary to dilute the gas such that the gaseous phase can be maintained, i.e., three-body interactions must be very rare events and thus negligible. (Note that the recombination through three-body interactions would also reduce the boson density in the original hyperfine state and thus hamper condensation.) Hence the condensate can be described by the many-body Hamiltonian of N interacting particles with mass m and two-body interaction potential $V_{\mathrm{int}}(\boldsymbol{r}-\boldsymbol{r}')$ in an external trap $V_{\mathrm{ext}}(\boldsymbol{r})$ (see, e.g., [41,73,74,76])

$$\begin{aligned}\hat{H} &= \int \mathrm{d}^3r\, \hat{\Psi}^\dagger(\boldsymbol{r}) \left[-\frac{\boldsymbol{\nabla}^2}{2m} + V_{\mathrm{ext}}(\boldsymbol{r})\right] \hat{\Psi}(\boldsymbol{r}) \\ &+ \frac{1}{2}\int \mathrm{d}^3r\mathrm{d}^3r'\, \hat{\Psi}^\dagger(\boldsymbol{r})\hat{\Psi}^\dagger(\boldsymbol{r}')V_{\mathrm{int}}(\boldsymbol{r}-\boldsymbol{r}')\hat{\Psi}(\boldsymbol{r}')\hat{\Psi}(\boldsymbol{r})\,, \end{aligned} \tag{3.1}$$

where $\hat{\Psi}(\boldsymbol{r})$ and $\hat{\Psi}^\dagger(\boldsymbol{r})$ are the bosonic field operators annihilating and creating an atom or molecule at position $\boldsymbol{r}$, respectively. They obey the usual bosonic equal-time commutation

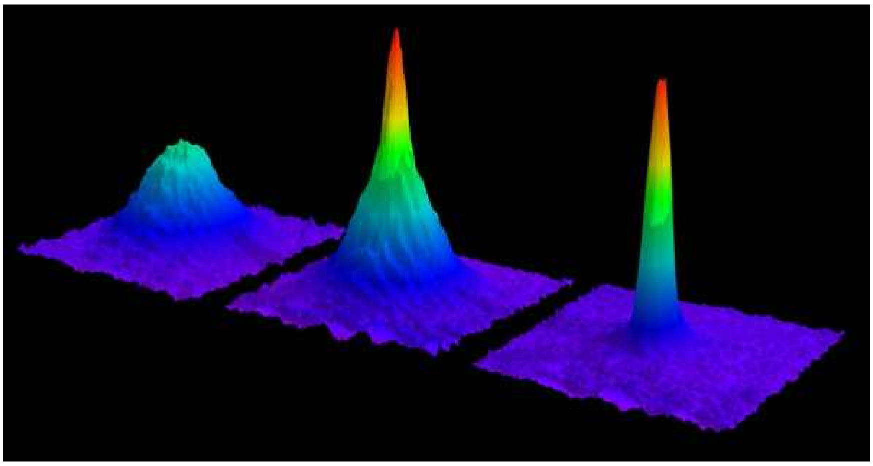

Figure 3.1: Absorption image of ballistically expanding clouds [89]. Most bosons from the initial thermal cloud (left) condense in the ground state of the trap as the vapor is cooled and form a narrow peak in the density distribution below the critical temperature (middle). By further cooling, the condensate fraction can be increased (right).

relation

$$\left[\hat{\Psi}(\boldsymbol{r},t),\hat{\Psi}^\dagger(\boldsymbol{r}',t)\right] \;=\; \delta(\boldsymbol{r}-\boldsymbol{r}')\,. \tag{3.2}$$

Furthermore the neglect of three-body collisions can only be achieved if the effective interaction length is much smaller than the average inter-particle separation. To lowest order, it is therefore possible to describe the two-body interactions as sole s-wave scattering, and to approximate them by a contact potential

$$V_{\mathrm{int}}(\boldsymbol{r}-\boldsymbol{r}') \;=\; g\delta(\boldsymbol{r}-\boldsymbol{r}')\,, \tag{3.3}$$

where $g = 4\pi a_s/m$ is the coupling constant and a_s is the s-wave scattering length. By virtue of Feshbach resonances, the interaction strength g can be tuned to a wide range of positive and negative values (and even to zero) [79–85]. One should bear in mind that Bose-Einstein condensation of atomic vapors occurs in a metastable phase, which can be preserved for dilute gases only. As soon as the diluteness parameter, $\varrho|a_s|^3$ in three dimensions, becomes of order 1, the condensate would become unstable, i.e., $\varrho_0|a_s|^3 \ll 1$ is crucial. (When increasing the diluteness parameter, three-body collisions would become more likely events and thus the life-time of the condensate diminishes.)

Characterized by a macroscopic ground-state population, cf. Fig. 3.1, a split of the field operator $\hat{\Psi}$ into the (classical) order parameter $\Phi = \langle\hat{\Psi}\rangle$ and small quantum fluctuations $\hat{\Psi}'$ [73, 76, 90] is in general advantageous[2]

$$\hat{\Psi}(\boldsymbol{r},t) \;=\; \Phi(\boldsymbol{r},t) + \hat{\Psi}'(\boldsymbol{r},t)\,. \tag{3.4}$$

---

[2] Note that this decomposition (3.4) does not conserve the atomic particle number, because the fluctua-

Therewith, the number density of the condensate follows

$$\varrho = \langle \hat{\Psi}^\dagger \hat{\Psi} \rangle = \varrho_0 + \langle \hat{\Psi}'^\dagger \hat{\Psi}' \rangle \,, \tag{3.5}$$

where $\varrho_0(\boldsymbol{r},t) = |\Phi(\boldsymbol{r},t)|^2$ is the condensate density and $\langle \hat{\Psi}'^\dagger \hat{\Psi}' \rangle$ accounts for the quantum depletion (the fraction of bosons not in the condensate). To a large extent (and often within experimental errors), experiments on Bose-Einstein condensates can be described by the behavior of the classical order parameter Φ only and quantum vacuum fluctuations are neglected in many theoretical calculations.

Several characteristic length scales occur in trapped Bose-Einstein condensates: the size of the condensate R is in general larger than the trap size $a_{\text{trap}} = 1/\sqrt{m\omega_{\text{trap}}}$, which is typically of order 1 to 10 μm. The healing length[3]

$$\xi = \frac{1}{\sqrt{g\varrho_0 m}} = \frac{1}{\sqrt{4\pi\varrho a_s}} \tag{3.6}$$

is the minimal distance over which the condensate can heal. For distances larger than ξ the interaction term in the Hamiltonian (3.1) dominates, whereas for scales smaller than ξ the kinetic term becomes important. The smallest characteristic scale is the interaction length, which is in the s-wave scattering approximation given by a_s. It is typically of order nanometers. Ideally, all scales are well-separated

$$R \gg a_{\text{trap}} \gg \xi \gg a_s \,, \tag{3.7}$$

which is also the typical situation in experiments. Note that the difference between R and a_{trap} arises because of the two-particle interactions. Although all bosons constituting the condensate are trapped in the lowest state (with size a_{trap}), the mutual repulsion leads to a particle-number-dependent broadening of the condensates.

3.2 Finite-range interactions

In most calculations concerning Bose-Einstein condensates, the two-particle interaction is approximated as s-wave scattering, where the true interaction potential $V_{\text{int}}(\boldsymbol{r}-\boldsymbol{r}')$ is replaced by the contact pseudo-potential (3.3) and any microscopic details beyond this are

---

tions are expressed in terms of the real atomic creation and annihilation operators. Furthermore, using (3.4), we have no real control over higher-orders, since, by construction, the operators $\hat{\Psi}'$ are linear and small. Higher-order terms enter the equations of motion for $\hat{\Psi}'$ via the nonlinear two-body interactions [the last line in the Hamiltonian (3.1)]. In particular, these contributions of higher order might become large due to mode summations. Therefore, we will employ a particle-number conserving mean-field ansatz (3.10) in the following sections. However, the split (3.4) serves our purpose in this Section to give a brief and illustrative introduction to some basic methods treating Bose-Einstein condensates.

[3] In the literature, two slightly different definitions of the healing length ξ are used: for example in Ref. [73], it is defined as $\xi = 1/\sqrt{8\pi\varrho a_s}$, whereas Ref. [91] uses the definition (3.6).

discarded. For the classical order parameter, this approximation is in general adequate. But since the quantum corrections contain mode sums owing to the nonlinearity of the Hamiltonian (3.1), the microscopic behavior of V_{int} might have a non-trivial impact on the corrections, e.g., through an effective cut-off wavenumber.

In the following, the size of the interacting atoms or molecules forming the dilute gas is assumed to be much smaller than all other involved length scales such as the s-wave scattering length a_s; typical energy scales associated with scattering processes are thus assumed to be well below the internal energy differences in this limit. The point-particle approximation may be adopted and the interacting objects can be treated as structureless entities described by the field operator $\hat{\Psi}$. The Heisenberg equation of motion for the field operator

$$i\frac{\partial\hat{\Psi}}{\partial t} = \left[-\frac{\boldsymbol{\nabla}^2}{2m} + V_{\mathrm{ext}}(\boldsymbol{r})\right]\hat{\Psi}(\boldsymbol{r}) + \int \mathrm{d}^3r'\,\hat{\Psi}^\dagger(\boldsymbol{r}')V_{\mathrm{int}}(\boldsymbol{r}-\boldsymbol{r}')\hat{\Psi}(\boldsymbol{r}')\hat{\Psi}(\boldsymbol{r}) \tag{3.8}$$

follows from the Hamiltonian (3.1). The finite-range two-particle interaction potential $V_{\mathrm{int}}(\boldsymbol{r}-\boldsymbol{r}')$ is assumed to be sufficiently "weak" in the sense that the Born approximation applies, e.g., $V_{\mathrm{int}}(\boldsymbol{r})$ is supposed to be integrable (i.e., to decay more rapidly with distance than $1/r^3$) such that its Fourier transform $\widetilde{V}_{\mathrm{int}}(\boldsymbol{k})$ is a well-defined function of $\boldsymbol{k}$. For large wavelengths, the finite-range two-particle interaction potential $V_{\mathrm{int}}(\boldsymbol{r}-\boldsymbol{r}')$ yields an effective coupling constant g determined by the s-wave scattering length a_s (see also [88]). In three spatial dimensions, it reads

$$g = \frac{4\pi a_s}{m} = \int \mathrm{d}^3r\,V_{\mathrm{int}}(\boldsymbol{r}) = \widetilde{V}_{\mathrm{int}}(\boldsymbol{k}=0)\,. \tag{3.9}$$

3.2.1 Number-conserving mean-field expansion

The Bogoliubov mean-field approximation [90], cf. Eq. (3.4), is based on the assumption that the fluctuations associated to excitations above the ground state are small (compared to the mean field) if the number N of particles is large. The derivation of the mean-field expansion of the system described in Eq. (3.8) in the large N limit, i.e., an expansion of $\hat{\Psi}$ into powers of N, is presented in the following. To this end, a particle-number-conserving mean-field ansatz (satisfying $\langle\hat{\Psi}\rangle = 0$) [92–95] is employed

$$\hat{\Psi} = \left(\psi_0 + \hat{\chi} + \hat{\zeta}\right)\frac{\hat{A}}{\sqrt{\hat{N}}}\,. \tag{3.10}$$

Here, the *order parameter* is ψ_0. The single-particle excitations are described by $\hat{\chi}$, where *single-particle* here means that the Fourier components of $\hat{\chi}$ are linear superpositions of annihilation and creation operators of quasi-particles $\hat{a}_{\boldsymbol{k}}$ and $\hat{a}_{\boldsymbol{k}}^\dagger$, cf. Eq. (3.15). The higher-order corrections $\hat{\zeta}$ are due to multi-particle excitations and correlations. Here $\hat{N} = \hat{A}^\dagger\hat{A}$ counts the total number of particles. [Apart from the operator $\hat{A}$, which was introduced to ensure total particle number conservation, the fluctuations $\hat{\Psi}'$ introduced in Eq. (3.4) would correspond to $\hat{\chi} + \hat{\zeta}$.]

The *dilute-gas limit* may formally be defined by placing a very large number $N \uparrow \infty$ of identical bosons into a finite trap with gN remaining constant [95, 96]. The diluteness parameter of the gas then scales as $(g^3 \varrho)^{1/2} \propto 1/N$, i.e., the gas becomes rapidly more dilute with increasing particle number in this limit. This limit should be compared and contrasted with the usual thermodynamic limit, in which the density and particle interaction remains constant, while the size of the (trapped) system increases with $N \uparrow \infty$, adjusting the trapping potential correspondingly. (In D spatial dimensions, the thermodynamic limit corresponds to keeping $N\omega^D$ constant for $N \uparrow \infty$, where ω is the geometric mean of the trapping frequencies [73]). In the presently used dilute-gas limit, on the other hand, the trapping potential remains constant, but the interaction and the density change. The advantage of the limit $N \uparrow \infty$ with gN constant is that in this limit one has a well-defined prescription for checking the mean-field approximation, keeping one power of g for each factor of N, cf. [97].

Given the dilute-gas limit, there arises a question which is central to the applicability of the mean-field expansion: do the supposedly small multi-particle corrections $\hat{\zeta}$ actually become small in this limit for a given behavior of the inter-particle potential $V_{\text{int}}(\boldsymbol{r} - \boldsymbol{r}')$? In order to tackle this question, let us consider the following scenario: initially, the interaction is completely switched off, $V_{\text{int}}(\boldsymbol{r} - \boldsymbol{r}') = 0$, and all N bosons occupy the same single-particle state (at zero temperature), described by the single-particle wave-function $\psi_0/\sqrt{N}$. In this case, Eq. (3.10) is trivially satisfied with $\psi_0 = \mathcal{O}(\sqrt{N})$, $\hat{\chi} = \mathcal{O}(N^0)$, $\hat{\zeta} = 0$, and $\hat{A} = \hat{a}_0 \hat{n}_0^{-1/2} \hat{N}^{1/2}$, where $\hat{n}_0 = \hat{a}_0^\dagger \hat{a}_0$ corresponds to the macroscopically occupied state, cf. [92–94]. If the interaction is now switched on slowly enough, the system stays in its ground state due to the adiabatic theorem (see Appendix A) and we may follow the evolution of the field operator $\hat{\Psi}$ and hence ψ_0, $\hat{\chi}$, and $\hat{\zeta}$ (with $\hat{A}$ remaining constant, i.e., the evolution at given particle number) via insertion of Eq. (3.10) into (3.8).

Assuming that the corrections $\hat{\zeta}$ indeed become small for $N \uparrow \infty$, the leading order ($\sqrt{N}$) yields, in the dilute-gas limit, the Gross-Pitaevskii equation for the order parameter ψ_0

$$i \frac{\partial \psi_0}{\partial t} = \left(-\frac{\boldsymbol{\nabla}^2}{2m} + V_{\text{ext}} + g|\psi_0|^2 \right) \psi_0 \,. \tag{3.11}$$

The next-to-leading order (N^0) terms govern the evolution of the fluctuations $\hat{\chi}$ via the nonlocal analogue of the Bogoliubov-de Gennes equations [90, 98]

$$i \frac{\partial \hat{\chi}}{\partial t} = \left(-\frac{\boldsymbol{\nabla}^2}{2m} + V_{\text{ext}} + g|\psi_0|^2 \right) \hat{\chi} + \int \mathrm{d}^3 r' \, V_{\text{int}}(\boldsymbol{r} - \boldsymbol{r}') \left[|\psi_0|^2 \hat{\chi}(\boldsymbol{r}') + \psi_0^2 \hat{\chi}^\dagger(\boldsymbol{r}') \right] \,. \tag{3.12}$$

The remaining equation of motion for $\hat{\zeta}$ takes for a general nonlocal potential the rather complicated form

$$i\frac{\partial\hat{\zeta}}{\partial t} = \left(-\frac{\boldsymbol{\nabla}^2}{2m} + V_{\text{ext}} + |\psi_0|^2\left[g + \widehat{V}_{\text{int}}*\right]\right)\hat{\zeta} + \psi_0^2\widehat{V}_{\text{int}} * \hat{\zeta}^\dagger$$
$$+ \psi_0^*\hat{\chi}\widehat{V}_{\text{int}} * \hat{\chi} + \psi_0(\widehat{V}_{\text{int}} * \hat{\chi}^\dagger)\hat{\chi} + \psi_0\widehat{V}_{\text{int}} * (\hat{\chi}^\dagger\hat{\chi}) + \left[\widehat{V}_{\text{int}} * (\hat{\chi}^\dagger\hat{\chi})\right]\hat{\chi}$$
$$+ \mathcal{O}\left(\frac{\hat{\zeta}}{\sqrt{N}}\right), \tag{3.13}$$

where $\widehat{V}_{\text{int}}*$ is an abbreviation for the convolution with the quantity right from the "$*$" as in Eq. (3.12), and $\mathcal{O}(\zeta/\sqrt{N})$ denote formally sub-leading terms containing $\hat{\zeta}$ or $\hat{\zeta}^\dagger$ or both. Observe that the commutation relations $[\hat{\chi}, \hat{A}\hat{N}^{-1/2}] = [\hat{\zeta}, \hat{A}\hat{N}^{-1/2}] = 0$ valid initially are preserved under the evolution given by the equations above, i.e., the excitations $\hat{\chi}$ and $\hat{\zeta}$ are always particle-number-conserving, cf. [92–95].

If one starts with free particles, and switches on the interaction by following the evolution in Eqs. (3.11), (3.12), and (3.13), the mixing of $\hat{\chi}$ and $\hat{\chi}^\dagger$ due to Eq. (3.12) can be observed. Furthermore, the nonlinear fluctuations $\hat{\zeta}$ do not vanish anymore due to the four source terms $\hat{\chi}\widehat{V}_{\text{int}} * \hat{\chi}$, $(\widehat{V}_{\text{int}} * \hat{\chi}^\dagger)\hat{\chi}$, $\widehat{V}_{\text{int}} * (\hat{\chi}^\dagger\hat{\chi})$, and $[\widehat{V}_{\text{int}} * (\hat{\chi}^\dagger\hat{\chi})]\hat{\chi}$. The viability of mean-field theory depends on the scaling of the induced terms in $\hat{\zeta}$ with particle number, i.e., if and to which extent they decrease for $N \uparrow \infty$. Naive power counting would imply $\hat{\zeta} = \mathcal{O}(1/\sqrt{N})$, but the nonlinearity due to the product of two or more field operators (such as in the above source terms) and the associated mode sum(s) may compensate the smallness of $1/\sqrt{N}$. As an example, let us consider the expectation values of the four source terms. The last term $[\widehat{V}_{\text{int}} * (\hat{\chi}^\dagger\hat{\chi})]\hat{\chi}$ is both sub-leading and odd so that its expectation value vanishes. However, the expectation values of the remaining terms do not vanish, and affect $\langle\hat{\zeta}(N)\rangle$.

For the sake of notational convenience, in what follows a homogeneous condensate $\psi_0 = \sqrt{\varrho_0} = \text{const}$ in a constant "trapping" potential $V_{\text{ext}} = -g\varrho_0$, so that the two last terms in the round brackets on the right-hand side of the Bogoliubov-de Gennes equation (3.12) cancel, will be considered. A normal-mode expansion for the fluctuation operators then yields in Fourier space[4]

$$i\frac{\partial\hat{\chi}_{\boldsymbol{k}}}{\partial t} = \left(\frac{\boldsymbol{k}^2}{2m} + \varrho_0\widetilde{V}_{\text{int}}(\boldsymbol{k})\right)\hat{\chi}_{\boldsymbol{k}} + \varrho_0\widetilde{V}_{\text{int}}(\boldsymbol{k})\hat{\chi}^\dagger_{\boldsymbol{k}}, \tag{3.14}$$

so that the annihilation operators $\hat{\chi}_{\boldsymbol{k}}$ of the original bosons have the following Bogoliubov transformation form in terms of the quasi-particle operators $\hat{a}_{\boldsymbol{k}}, \hat{a}^\dagger_{\boldsymbol{k}}$

$$\hat{\chi}_{\boldsymbol{k}} = \sqrt{\frac{\boldsymbol{k}^2}{2m\omega_{\boldsymbol{k}}}}\left[\left(\frac{1}{2} - \frac{m\omega_{\boldsymbol{k}}}{\boldsymbol{k}^2}\right)\hat{a}^\dagger_{\boldsymbol{k}} + \left(\frac{1}{2} + \frac{m\omega_{\boldsymbol{k}}}{\boldsymbol{k}^2}\right)\hat{a}_{\boldsymbol{k}}\right]. \tag{3.15}$$

The generalized Bogoliubov dispersion relation reads

$$\omega^2_{\boldsymbol{k}} = \varrho_0\widetilde{V}_{\text{int}}(\boldsymbol{k})\frac{\boldsymbol{k}^2}{m} + \frac{\boldsymbol{k}^4}{4m^2}. \tag{3.16}$$

---

[4] The interaction potential is assumed to be symmetric $V_{\text{int}}(\boldsymbol{r}) = V_{\text{int}}(-\boldsymbol{r})$.

For wavenumbers $\boldsymbol{k}^2\xi^2 \gg 1$ much larger than the inverse of the healing length $\xi = 1/\sqrt{g\varrho_0 m}$, we have $\hat{\chi}_{\boldsymbol{k}} \sim \hat{a}_{\boldsymbol{k}} - \hat{a}_{\boldsymbol{k}}^\dagger m\varrho_0 \widetilde{V}_{\text{int}}(\boldsymbol{k})/\boldsymbol{k}^2$, i.e., the quasi-particles become asymptotically equal to the original bosons. However, this $1/\boldsymbol{k}^2$ decrease alone is not sufficient for rendering the expectation value of $\langle\hat{\chi}\widehat{V}_{\text{int}} * \hat{\chi}\rangle$ finite (except in one spatial dimension).

A smooth (and integrable) interaction potential $V_{\text{int}}(\boldsymbol{r})$ implies a faster-than-polynomial decrease $\widetilde{V}_{\text{int}}(\boldsymbol{k}^2 \gg k_{\text{cut}}^2) = 0$ for large wavenumbers $\boldsymbol{k}^2 \gg k_{\text{cut}}^2$. The *cut-off wavenumber* k_{cut}, then, is determined by the first significant deviations of $\widetilde{V}_{\text{int}}$ from its long-wavelength behavior $\widetilde{V}_{\text{int}}(\boldsymbol{k}^2 \ll k_{\text{cut}}^2) = g$ and is assumed to be much larger than the inverse of the healing length. This faster-than-polynomial decrease renders all relevant expectation values finite. For example, the expectation value of the so-called "anomalous" term reads

$$\langle\hat{\chi}\widehat{V}_{\text{int}} * \hat{\chi}\rangle = -\frac{\psi_0^2}{2\pi^2}\int dk\, \frac{k^2\widetilde{V}_{\text{int}}^2(k)}{2\omega_k}\,, \tag{3.17}$$

where a spherically symmetric potential $V_{\text{int}}(r)$ and hence $\widetilde{V}_{\text{int}} = \widetilde{V}_{\text{int}}(k)$ is assumed. The expectation value is taken in the ground state of the quasi-particles (remember the adiabatic switching process) which is annihilated by $\hat{a}_{\boldsymbol{k}}$ (but not by $\hat{\chi}_{\boldsymbol{k}}$, of course). For a sufficiently regular $\widetilde{V}_{\text{int}}(k)$, an expansion into powers of $1/(\xi k_{\text{cut}})$ yields

$$\langle\hat{\chi}\widehat{V}_{\text{int}} * \hat{\chi}\rangle = -\frac{\psi_0^2}{2\pi^2}\int dk\, \widetilde{V}_{\text{int}}^2 + \frac{g^2\psi_0^2}{\xi\pi^2} + \mathcal{O}\left(\frac{g^3\varrho_0^2}{k_{\text{cut}}}\right). \tag{3.18}$$

The $1/(\xi k_{\text{cut}})$-corrections depend on the explicit form of $V_{\text{int}}(r)$ and hence $\widetilde{V}_{\text{int}}(k)$, e.g., for $\widetilde{V}_{\text{int}}(k) = g\Theta(k_{\text{cut}} - k)$, the integral in Eq. (3.17) yields $g^2(\sqrt{\xi^2k_{\text{cut}}^2 + 4} - 2)/\xi$.

In contrast to the so-called "anomalous" term $\langle\hat{\chi}\widehat{V}_{\text{int}} * \hat{\chi}\rangle$, the expectation value of the quantum depletion terms $\widehat{V}_{\text{int}} * \langle\hat{\chi}^\dagger\hat{\chi}\rangle$ and $\langle(\widehat{V}_{\text{int}} * \hat{\chi}^\dagger)\hat{\chi}\rangle$ occurring as source terms in Eq. (3.13) do not have a contribution linear in k_{cut}. Hence their (for $\xi k_{\text{cut}} \gg 1$) dominant terms are independent of k_{cut} and both give $g\langle\hat{\chi}^\dagger\hat{\chi}\rangle \approx \sqrt{g^5\varrho_0^3}/(3\pi^2)$. The higher-order $1/(\xi k_{\text{cut}})$-corrections, however, again depend on the shape of $\widetilde{V}_{\text{int}}(\boldsymbol{k})$ and can be calculated analogously.

3.2.2 Consistency of mean-field expansion

To explicitly address the principal question of whether the higher-order corrections $\hat{\zeta}$ in the mean-field expansion (3.10) indeed become small in the large-N limit (in which one would naively expect mean-field to become more and more accurate), three concrete examples for the formal scaling behavior of the interaction V_{int} with the number of particles N will be discussed in the following. To this end, the particle-number-dependent potential $V_{\text{int}}^{(N)}$ is always chosen such that it reproduces the $g \propto 1/N$ dilute-gas limit prescription for the behavior of the coupling constant in the large-N limit.

In the first example, the cut-off wavenumber k_{cut} is assumed to be formally independent of N

$$V_{\text{int}}^{(N)}(\boldsymbol{r}) = \frac{1}{N}V_{\text{int}}^{(1)}(\boldsymbol{r})\,. \tag{3.19}$$

Since k_{cut} remains constant for $N \uparrow \infty$, the mode sums due to the nonlinear terms in Eq. (3.13) cannot compensate the smallness of the prefactors such as $1/\sqrt{N}$ and thus one obtains

$$\hat{\zeta} = \mathcal{O}\left(\frac{1}{\sqrt{N}}\right) . \tag{3.20}$$

However, this decrease is not sufficient yet for ensuring the usual split of the total density

$$\varrho = \left\langle \hat{\Psi}^\dagger \hat{\Psi} \right\rangle = |\psi_0|^2 + \langle \hat{\chi}^\dagger \hat{\chi} \rangle + \mathcal{O}\left(\frac{1}{\sqrt{N}}\right) , \tag{3.21}$$

since $\psi_0 \langle \hat{\zeta} \rangle$ could be of the same order as $\langle \hat{\chi}^\dagger \hat{\chi} \rangle$. For the above split, one needs $\langle \hat{\zeta} \rangle = \mathcal{O}(1/N)$ instead of $\mathcal{O}(1/\sqrt{N})$, which requires absorbing the expectation values of the source terms into a *modified* GP equation

$$i\frac{\partial \psi_0}{\partial t} = \left(-\frac{\boldsymbol{\nabla}^2}{2m} + V_{\text{ext}} + g|\psi_0|^2 + g \left\langle \hat{\chi}^\dagger \hat{\chi} \right\rangle \right) \psi_0 + \langle \hat{\chi} \widehat{V}_{\text{int}} * \hat{\chi} \rangle \psi_0^* + \langle (\widehat{V}_{\text{int}} * \hat{\chi}^\dagger) \hat{\chi} \rangle \psi_0 . \tag{3.22}$$

Inserting Eq. (3.18), one sees that the dominant (for $\xi k_{\text{cut}} \gg 1$) and density-independent fluctuation contribution $\langle \hat{\chi} \widehat{V}_{\text{int}} * \hat{\chi} \rangle$ proportional to k_{cut} can be absorbed by a renormalization of the coupling constant

$$\begin{aligned} g_{\text{ren}} &= g - \frac{1}{2\pi^2} \int \mathrm{d}k\, \widetilde{V}_{\text{int}}^2 \\ &= g + \int \mathrm{d}^3 r\, V_{\text{int}} \boldsymbol{\nabla}^{-2} V_{\text{int}} , \end{aligned} \tag{3.23}$$

where the second line is due to Parseval's theorem, using the formal inverse of the Laplace operator $\boldsymbol{\nabla}^2$. Since $-\boldsymbol{\nabla}^{-2}/2$ and $V_{\text{int}}/2$ are the kernels of the Schrödinger Hamiltonian $\hat{H}_0$ (up to a factor $1/m$) and the interaction Hamiltonian $\hat{H}_1$, respectively, this just corresponds to the usual one-loop renormalization $\langle \hat{H}_1 \rangle - \langle \hat{H}_1 \hat{H}_0^{-1} \hat{H}_1 \rangle$ of the interaction potential. Note that in three spatial dimensions, sub-dominant contributions like $\langle \hat{\chi}^\dagger \hat{\chi} \rangle$ cannot be absorbed by such a ϱ-independent renormalization procedure.

The physical significance of the renormalized coupling g_{ren} can be demonstrated further by calculating the k_{cut}-corrections to the total energy of a homogeneous gas

$$E = \langle \hat{H} \rangle \approx N V_{\text{ext}} + \frac{N}{2} g \varrho - \frac{N}{4\pi^2} \varrho \int \mathrm{d}k\, \widetilde{V}_{\text{int}}^2 , \tag{3.24}$$

which gives $E = N V_{\text{ext}} + N g_{\text{ren}} \varrho / 2$ plus higher-order corrections (cf. [97]).

A potential complication which arises from the prescription (3.19) is that the range of the two-particle interaction potential in Eq. (3.19) will exceed the inter-particle distance d_i for large N since $\varrho_0 \sim N$ and thus $d_i \sim 1/N^{1/3}$ (in three spatial dimensions). If the two-particle interaction potential is mainly caused by direct collisions, this might lead to a conflict with the point-particle approximation used in writing down the starting point of the analysis, Eq. (3.8). Therefore, as a second example, consider the support of $V_{\text{int}}(\boldsymbol{r})$ to be decreasing in proportion to the inter-particle distance d_i,

$$V_{\text{int}}^{(N)}(\boldsymbol{r}) \,=\, V_{\text{int}}^{(1)}(N^{1/3}\boldsymbol{r})\,. \tag{3.25}$$

As a consequence, the cut-off scales as $k_{\text{cut}} \sim N^{1/3}$, and thus $\langle \hat{\chi}\widehat{V}_{\text{int}} * \hat{\chi}\rangle \sim N^{-2/3}$, which ensures that the remaining $\hat{\zeta}$ corrections are still small, though decreasing with a smaller power in N than in the first example, cf. Eq. (3.20):

$$\hat{\zeta} \,=\, \mathcal{O}\left(\frac{1}{N^{1/6}}\right)\,. \tag{3.26}$$

The above scaling with particle number is due to the fact that for each additional operator in Eq. (3.13), which might contribute a factor $k_{\text{cut}} \sim N^{1/3}$ after the mode summation, there is a prefactor of order $1/\sqrt{N}$. In this case, the split in Eq. (3.21) is still possible provided the modification of the GP equation (3.22) is employed, but the estimate of the accuracy is now the rather slow decrease of $\mathcal{O}(1/N^{1/6})$ instead of $\mathcal{O}(1/N^{1/2})$.

Finally, as a third example, a scaling employed by Lieb et al. [96,99] will be investigated. It is used in a proof for the asymptotic exactness of the Gross-Pitaevskii energy functional in three spatial dimensions, and in an analysis of one-dimensional systems of bosons in three-dimensional traps, respectively. This scaling reads

$$V_{\text{int}}^{(N)}(\boldsymbol{r}) \,=\, N^2 V_{\text{int}}^{(1)}(N\boldsymbol{r})\,, \tag{3.27}$$

and implies that the cut-off increases linearly with particle number, $k_{\text{cut}} \sim N$, and thus $\langle \hat{\chi}\widehat{V}_{\text{int}} * \hat{\chi}\rangle \sim N^0$, so that the anomalous term becomes of the same order as other terms in the Gross-Pitaevskii equation, for example as large as the mean-field interaction term $g|\psi_0|^2$. The "correction" operator then behaves as

$$\hat{\zeta} \,=\, \mathcal{O}\left(\sqrt{N}\right)\,, \tag{3.28}$$

and one has no true control over the corrections in the mean-field expansion which ought to be negligible. The mean-field approximation can only be consistent (if at all) with a modified Gross-Pitaevskii equation (3.22) inducing a renormalization of the coupling according to Eq. (3.23). However, even given these modifications, the applicability of the mean-field expansion is not obvious since higher-order operator products can yield $\mathcal{O}(N)$ contributions after the k-summation/integration and thus the hierarchy $\hat{\zeta} \ll \hat{\chi}$ is not evident. Similarly, the first-order correction in Eq. (3.23) is comparable to the zeroth order (i.e., of the same order in N), which hints at the fact that all orders must be taken into account in a suitable way.

It might be illuminating to compare the employed dilute-gas limit ($N \uparrow \infty$ particles in a fixed volume with gN remaining constant) with the thermodynamic limit ($N \uparrow \infty$ particles in an increasing volume $\mathcal{V}$ with g and $N/\mathcal{V}$ remaining constant): translation of the scaling in Eq. (3.19) to the thermodynamic limit yields an interaction potential whose range increases proportional to the system size $\mathcal{V}$ whereas its strength decreases accordingly. It is not very surprising that the mean-field expansion is very good in this case. The analogue of Eq. (3.25) in the thermodynamic limit is an interaction potential with constant strength and range (where the applicability of the mean-field expansion is less obvious). Finally, Eq. (3.27) corresponds to a potential with decreasing range and increasing strength (in the thermodynamic limit). Again, it is not very surprising that such a scaling might generate difficulties in the ordinary mean-field expansion and requires taking into account all orders in a suitable way.

3.2.3 Dipole-dipole interaction

As an example for interactions with a finite range, consider a dipole-dipole force $\propto g_{\mathrm{d}}$ in addition to the usual contact repulsion $\propto g$. Dipole-dipole interactions between atoms [100] can either be induced by an external electric field or be due to an intrinsic magnetic dipole moment. For example, $g_{\mathrm{d}} = \mu_0 d_{\mathrm{m}}^2/3$ for magnetic dipoles; Bose-Einstein condensation of chromium, which has a ground state moment of $d_{\mathrm{m}} = 6\mu_{\mathrm{B}}$, has been achieved recently [101].

If the dipole moments of all atoms/molecules are aligned along the z-axis, the dipole-dipole interaction potential reads (in three spatial dimensions)

$$V_{\mathrm{dd}}(\boldsymbol{r}) = \frac{3g_{\mathrm{d}}}{4\pi}\frac{1-3z^2/|\boldsymbol{r}|^2}{|\boldsymbol{r}|^3}\,. \tag{3.29}$$

In addition to this long-range interaction, the particles are subject to a short-range repulsion whose impact can be represented by a contact potential $\propto \delta(\boldsymbol{r}-\boldsymbol{r}')$. Consequently, the Fourier transformed potential reads for intermediate momenta

$$\widetilde{V}_{\mathrm{int}}(\boldsymbol{k}) = g + g_{\mathrm{d}}\left(\frac{3k_z^2}{\boldsymbol{k}^2}-1\right). \tag{3.30}$$

The (ideal) dipole-dipole interaction potential behaves as $1/r^3$ which is not integrable and, strictly speaking, is therefore just at the limit of applicability of the analysis presented in this Section – for example, $\widetilde{V}_{\mathrm{int}}$ is not well-defined at $\boldsymbol{k}=0$, which complicates the introduction of an effective coupling g (finite-size effects etc.). Nevertheless, the nonintegrable dipole-dipole interaction potential can be regarded as a limit of integrable potentials and one may calculate the corresponding corrections beyond the s-wave scattering approximation. For example, the quantum depletion is modified from the pure contact case via

$$\begin{aligned}\langle\hat{\chi}^\dagger\hat{\chi}\rangle &= \frac{(m\varrho_0)^{3/2}}{24\pi^2}\sqrt{2g_{\mathrm{d}}+g}\,(g_{\mathrm{d}}+5g) - \frac{(m\varrho_0)^{3/2}}{16\pi^2}\frac{(g-g_{\mathrm{d}})^2}{\sqrt{3g_{\mathrm{d}}}}\ln\left[\frac{g-g_{\mathrm{d}}}{(\sqrt{3g_{\mathrm{d}}}+\sqrt{2g_{\mathrm{d}}+g}\,)^2}\right]\\ &= \frac{(gm\varrho_0)^{3/2}}{3\pi^2}\left[1+\frac{3}{10}\frac{g_{\mathrm{d}}^2}{g^2}+\mathcal{O}\left(\frac{g_{\mathrm{d}}^3}{g^3}\right)\right].\end{aligned} \tag{3.31}$$

This expression is valid for $g \geq g_\mathrm{d}$ only, since otherwise the excitation spectrum (for a homogeneous condensate) and hence also $\langle \hat{\chi}^\dagger \hat{\chi} \rangle$ contain imaginary parts indicating an instability, cf. [102]. Further expectation values such as the total energy $E = \langle \hat{H} \rangle$ can be calculated analogously.

3.3 Dimensional reduction

One advantage of using confined Bose-Einstein condensates for the simulation of various quantum effects is the possibility to achieve effectively lower-dimensional systems by applying highly-anisotropic trap potentials and thus confining the motion in one or two directions to the ground state. To this end, highly-anisotropic traps will be considered in this section and the Lagrangian density for effectively lower-dimensional condensates will be derived. In three spatial dimensions, Bose-Einstein condensates can be described by the Lagrange density [103]

$$\mathcal{L} \,=\, \frac{i}{2}(\Psi^* \dot{\Psi} - \dot{\Psi}^* \Psi) - \frac{|\boldsymbol{\nabla}\Psi|^2}{2m} - V_\mathrm{ext}(\boldsymbol{r}, t)|\Psi|^2 - \frac{g}{2}\,|\Psi|^4\,, \tag{3.32}$$

where the s-wave approximation (3.3) for the interaction potential V_int is employed and the external one-particle trapping potential V_ext may possess arbitrary space-time dependence. If the external one-particle trapping potential can be split up into a parallel and a static transversal part via

$$V_\mathrm{ext}(\boldsymbol{r}, t) \,=\, V^\parallel_\mathrm{ext}(\boldsymbol{r}_\parallel, t) \,+\, V^\perp_\mathrm{ext}(\boldsymbol{r}_\perp)\,, \tag{3.33}$$

it is useful to decompose the order parameter Ψ (and its quantum fluctuations $\hat{\Psi}'$) into a complete set of real and time-independent functions $\phi_a(\boldsymbol{r}_\perp)$ governing the transversal dependence (cf. [104] where the density of an elongated condensate is decomposed in a similar manner)

$$\Psi(\boldsymbol{r}, t) \,=\, \sum_a \phi_a(\boldsymbol{r}_\perp)\psi_a(\boldsymbol{r}_\parallel, t)\,. \tag{3.34}$$

The time evolution of the coefficient functions $\psi_a(\boldsymbol{r}_\parallel, t)$ is determined by the reduced Lagrangian density

$$\begin{aligned}
\mathcal{L}_\parallel \,&=\, \int \mathrm{d}\mathcal{V}^{3-D}_\perp\, \mathcal{L} \\
&=\, \sum_{ab} \left[\frac{i}{2}(\psi^*_a \dot{\psi}_b - \dot{\psi}^*_a \psi_b) - \frac{1}{2m}(\boldsymbol{\nabla}\psi^*_a)\cdot(\boldsymbol{\nabla}\psi_b) - V^\parallel_\mathrm{ext}\psi^*_a\psi_b\right] \int \mathrm{d}\mathcal{V}^{3-D}_\perp\, \phi_a\phi_b \\
&\quad - \sum_{ab} \psi^*_a\psi_b \int \mathrm{d}\mathcal{V}^{3-D}_\perp\, \phi_a \left[-\frac{\boldsymbol{\nabla}^2_\perp}{2m} + V^\perp_\mathrm{ext}\right]\phi_b - \frac{g}{2}\sum_{abcd} \psi^*_a\psi_b\psi^*_c\psi_d \int \mathrm{d}\mathcal{V}^{3-D}_\perp\, \phi^*_a\phi_b\phi^*_c\phi_d\,.
\end{aligned} \tag{3.35}$$

If the functions $\phi_a(\boldsymbol{r}_\perp)$ are now chosen to be orthonormal eigenfunctions of the self-adjoint operator $\mathcal{K}$ with eigenvalues Ω_a

$$\mathcal{K}\phi_a \;=\; \left(-\frac{\boldsymbol{\nabla}_\perp^2}{2m} + V_{\text{ext}}^\perp\right)\phi_a \;=\; \Omega_a\phi_a\,, \tag{3.36}$$

the reduced Lagrangian density simplifies to

$$\begin{aligned}\mathcal{L}_\parallel \;=& \sum_a \left[\frac{i}{2}(\psi_a^*\dot{\psi}_a - \dot{\psi}_a^*\psi_a) - \frac{1}{2m}|\boldsymbol{\nabla}\psi_a|^2 - (V_{\text{ext}}^\parallel + \Omega_a)|\psi_a|^2\right] \\ & - \frac{g}{2}\sum_{abcd}\psi_a^*\psi_b\psi_c^*\psi_d \int \mathrm{d}\mathcal{V}_\perp^{3-D}\;\phi_a^*\phi_b\phi_c^*\phi_d\,. \end{aligned}\tag{3.37}$$

The last term induces a coupling of different modes, which complicates the solution. However, assuming that the coupling term is sufficiently small and the lowest mode $a = 0$ dominates $|\psi_0| \gg |\psi_{a>0}|$, we may estimate the population of the higher modes in analogy to stationary perturbation theory: the mixing between the lowest mode $a = 0$ and all higher modes $a > 0$ is small if the energy differences $\Delta\Omega_a = \Omega_a - \Omega_0$ are large compared to the transition matrix elements of the interaction Hamiltonian, i.e.,

$$\Delta\Omega_a \;\gg\; g|\psi_0|^2 \int \mathrm{d}\mathcal{V}_\perp^{3-D}\;\phi_a^*\phi_b\phi_c^*\phi_d\,. \tag{3.38}$$

Since the modes ϕ_a are normalized $\phi_a \sim 1/\sqrt{\mathcal{V}_\perp^{3-D}}$, this condition can be re-expressed in terms of the size of the transversal dimension $a_\perp$ and the healing length $\xi = 1/\sqrt{g|\psi_0|^2 m}$. Therefore, imposing the conditions

$$\xi \;\gg\; a_\perp \;\gg\; a_s\,, \tag{3.39}$$

where the latter requirement $a_\perp \gg a_s$ is necessary for the Gross-Pitaevskii Lagrangian density in Eq. (3.32) to be valid, we arrive at the reduced Lagrangian density for the lowest mode $\psi = \psi_0$

$$\mathcal{L}_\parallel \;=\; \frac{i}{2}(\psi^*\dot{\psi} - \dot{\psi}^*\psi) - \frac{1}{2m}|\boldsymbol{\nabla}\psi|^2 - V_{\text{ext}}^\parallel|\psi|^2 - \frac{g_\parallel}{2}\,|\psi|^4\,, \tag{3.40}$$

where Ω_0 has been absorbed into $V_{\text{ext}}^\parallel$ and

$$g_\parallel \;=\; g\int \mathrm{d}\mathcal{V}_\perp^{3-D}\,|\phi_0|^4 \;=\; \frac{4\pi a_s}{m}\int \mathrm{d}\mathcal{V}_\perp^{3-D}\,|\phi_0|^4 \propto \frac{a_s}{a_\perp^{3-D}}\,, \tag{3.41}$$

denotes the reduced (lower-dimensional) coupling constant. For example, the eigenfunctions $\phi_a(\boldsymbol{r}_\perp) = \phi_a(z)$ of a harmonic potential $V_\perp(z) = m\omega_z^2 z^2/2$ with the transversal length scale $a_\perp = 1/\sqrt{m\omega_z}$ are just the Legendre polynomials with an equidistant energy spectrum. In this case, the reduced coupling is given by $g_\parallel = g\sqrt{m\omega_z/2\pi}$. However, it should be emphasized that the method presented above is applicable to more general potentials satisfying the aforementioned conditions as well.

Note that if we relaxed condition (3.39) and the transverse size of the condensate, a_z, would be of comparable order with the scattering length, $\mathcal{O}(a_s/a_z) = 1$, we would obtain a lower-dimensional condensate with a different interaction term. The two-particle interaction could no longer be approximated by (free) three-dimensional scattering (with length a_s) but it would become necessary to account for finite-size effects as well [105–110].

3.4 Effective Geometry

After the discussion of dimensional reduction in highly-anisotropic traps in the previous section (and thus the realization of condensates in an arbitrary number of spatial dimensions D), we can now introduce an effective space-time metric for the phonons. To this end, we consider the Lagrangian (3.40) equipped with a more general self-coupling term $|\psi|^{2\mathcal{N}}$

$$\mathcal{L} = \frac{i}{2}(\psi^*\dot{\psi} - \dot{\psi}^*\psi) - \frac{1}{2m}|\boldsymbol{\nabla}\psi|^2 - V_{\text{ext}}|\psi|^2 - \frac{g}{2}\,|\psi|^{2\mathcal{N}}, \tag{3.42}$$

where the scripts $\|$ are omitted for brevity.

3.4.1 Hydrodynamics and effective space-time metric

By splitting the order parameter ψ into its modulus $\sqrt{\varrho}$ and a phase S

$$\psi = \sqrt{\varrho}\, e^{iS}\,, \tag{3.43}$$

we obtain the Lagrangian for density ϱ and phase S

$$\mathcal{L} = -\varrho\,\partial_t S - \frac{\varrho}{2m}(\boldsymbol{\nabla}S)^2 - \frac{(\boldsymbol{\nabla}\sqrt{\varrho})^2}{2m} - V_{\text{ext}}\,\varrho - \frac{g}{2}\,\varrho^{\mathcal{N}}. \tag{3.44}$$

As usual, variation with respect to S yields the equation of continuity

$$\frac{\partial\varrho}{\partial t} + \boldsymbol{\nabla}\cdot(\varrho\boldsymbol{v}) = 0\,, \tag{3.45}$$

where $\boldsymbol{v} = \boldsymbol{\nabla}S/m$ is the mean-field velocity, and variation with respect to ϱ yields the Bernoulli equation[5]

$$\frac{\partial S}{\partial t} + \frac{m}{2}\boldsymbol{v}^2 + V_{\text{ext}} - \frac{1}{2m}\frac{\boldsymbol{\nabla}^2\sqrt{\varrho}}{\sqrt{\varrho}} + \frac{g\mathcal{N}}{2}\varrho^{\mathcal{N}-1} = 0\,. \tag{3.46}$$

Assuming that the density profile is sufficiently smooth, i.e., that the relevant length scales are much larger than the healing length (Thomas-Fermi approximation), the quantum pressure term $(\boldsymbol{\nabla}\sqrt{\varrho})^2$ will be neglected in the following. Linearization $S = S_0 + \delta S$ and

---

[5] The gradient of Eq. (3.46) is the Euler equation of irrotational, inviscid fluids with external force $\boldsymbol{\nabla}V_{\text{ext}}$ and the specific pressure $p(\varrho, \boldsymbol{\nabla}^2\sqrt{\varrho})$.

$\varrho = \varrho_0 + \delta\varrho$ around a background solution S_0 and ϱ_0 yields the second-order Lagrange density (cf. [86, 111–114])

$$\mathcal{L}^{(2)} = -\delta\varrho\,\partial_t\delta S - \frac{\varrho_0}{2m}(\boldsymbol{\nabla}\delta S)^2 - \delta\varrho\,\boldsymbol{v}_0\cdot\boldsymbol{\nabla}\delta S - \frac{g_{\mathcal{N}}}{2}\,\delta\varrho^2\,, \tag{3.47}$$

where

$$g_{\mathcal{N}} = g\,\frac{\mathcal{N}(\mathcal{N}-1)}{2}\,\varrho_0^{\mathcal{N}-2} \tag{3.48}$$

is the effective coupling. It simplifies to the bare coupling $g_{\mathcal{N}} = g$ for the usual case $\mathcal{N} = 2$, but one should still bear in mind that an arbitrary number of spatial dimensions D is considered. Note that there are no sound waves at all for $\mathcal{N} = 1$, since the theory is non-interacting in that case.

In the Thomas-Fermi approximation, the linearized Bernoulli equation can be solved for the density fluctuations

$$\delta\varrho = -\frac{\partial_t + \boldsymbol{v}_0\cdot\boldsymbol{\nabla}}{g_{\mathcal{N}}}\,\delta S\,, \tag{3.49}$$

and inserting this result back into Eq. (3.47), we obtain the effective Lagrangian for the phase fluctuations $\phi = \delta S$ only

$$\mathcal{L}_{\text{eff}}^{(2)} = \frac{1}{2g_{\mathcal{N}}}\left(\dot{\phi} + \boldsymbol{v}_0\cdot\boldsymbol{\nabla}\phi\right)^2 - \frac{\varrho_0}{2m}(\boldsymbol{\nabla}\phi)^2\,. \tag{3.50}$$

Even in an arbitrary number of spatial dimensions D (the difficulties for $D = 1$ will be discussed below) and for general self-coupling $\mathcal{N} > 1$, this Lagrangian is completely equivalent to that of a free (minimally coupled) scalar field in a curved space-time (e.g., [10])

$$\mathcal{L}_{\text{eff}}^{(2)} = \frac{1}{2}\sqrt{|\mathrm{g}_{\text{eff}}|}\,(\partial_\mu\phi)\mathrm{g}_{\text{eff}}^{\mu\nu}(\partial_\nu\phi)\,, \tag{3.51}$$

provided that $\mathrm{g}_{\mu\nu}^{\text{eff}}$ is given by the Painlevé-Gullstrand-Lemaître metric [28–30]

$$\begin{aligned}
\mathrm{g}_{\mu\nu}^{\text{eff}} &= A_D^{(\mathcal{N})}\begin{pmatrix} c_{\mathcal{N}}^2 - \boldsymbol{v}_0^2 & \boldsymbol{v}_0 \\ \boldsymbol{v}_0 & -\mathbf{1}\end{pmatrix}, \\
\mathrm{g}_{\text{eff}}^{\mu\nu} &= \frac{1}{A_D^{(\mathcal{N})}c_{\mathcal{N}}^2}\begin{pmatrix} 1 & \boldsymbol{v}_0 \\ \boldsymbol{v}_0 & \boldsymbol{v}_0\otimes\boldsymbol{v}_0 - c_{\mathcal{N}}^2\mathbf{1}\end{pmatrix},
\end{aligned} \tag{3.52}$$

with the speed of sound $c_{\mathcal{N}}^2 = g_{\mathcal{N}}\varrho_0/m$ and the conformal factor

$$A_D^{(\mathcal{N})} = \left(\frac{c_{\mathcal{N}}}{g_{\mathcal{N}}}\right)^{2/(D-1)}\,. \tag{3.53}$$

This expression already indicates problems in one spatial dimension $D = 1$ due to conformal invariance of the scalar field action (3.51) in 1+1 dimensions. Without the introduction of an additional dilaton field, the identification of an effective metric is only possible if $c_{\mathcal{N}}/g_{\mathcal{N}} = \text{const}$, for example if the bare coupling g [cf. Eq. (3.42)] is time-independent and $\mathcal{N} = 3$, see also the next Subsection 3.4.2.

3.4.2 Comoving Coordinates and Scaling

Since phase fluctuations in Bose-Einstein condensates behave (in the Thomas-Fermi approximation) exactly as a scalar field in a specific curved space-time described by the effective metric in Eq. (3.52), it will be useful to investigate this metric with the tools known from general relativity. The effective line element reads

$$\mathrm{d}s_{\text{eff}}^2 = A_D^{(\mathcal{N})}\left([c_{\mathcal{N}}^2 - \boldsymbol{v}_0^2]\mathrm{d}t^2 + 2\boldsymbol{v}_0 \cdot \mathrm{d}\boldsymbol{r}\mathrm{d}t - \mathrm{d}\boldsymbol{r}^2\right) . \tag{3.54}$$

In analogy to cosmology, local isotropy and homogeneity will be assumed – which is a good approximation in the center of the gas cloud. Since the coupling g is supposed to be constant for simplicity, this assumption implies a spatially homogeneous but possibly time-dependent density $\varrho_0 = \varrho_0(t)$ and effective coupling $g_{\mathcal{N}} = g_{\mathcal{N}}(t)$. Furthermore, after a suitable re-definition of the origin of our coordinate system, we may set $\boldsymbol{v}_0 \propto \boldsymbol{r}$ due to the presumed local isotropy and homogeneity. Insertion of this *ansatz* into the equation of continuity yields [86, 113]

$$\varrho_0(t) = \frac{\varrho_0(t=0)}{b^D(t)} \quad \leftrightarrow \quad \boldsymbol{v}_0(t,\boldsymbol{r}) = \frac{\dot{b}}{b}\boldsymbol{r} , \tag{3.55}$$

which allows to describe $\varrho_0(t)$ and $\boldsymbol{v}_0(t,\boldsymbol{r})$ as well as $g_{\mathcal{N}}(t)$ by means of a single time-dependent scaling parameter $b(t)$ satisfying an appropriate initial condition. For example, one has $b(t=0) = 1$ and $\dot{b}(t=0) = 0$ for a freely expanding condensate released from the trap at $t = 0$.

As known from general relativity, an off-diagonal metric such as in Eq. (3.54) can be diagonalized by introducing comoving spatial coordinates via (cf. the scaling transformation for Bose-Einstein condensates in Refs. [115, 116])

$$\boldsymbol{\rho} = \frac{\boldsymbol{r}}{b(t)} \quad \to \quad \mathrm{d}\boldsymbol{\rho} = \frac{\mathrm{d}\boldsymbol{r} - \boldsymbol{v}_0\mathrm{d}t}{b(t)} \quad \to \quad \mathrm{d}s_{\text{eff}}^2 = A_D^{(\mathcal{N})}\left(c_{\mathcal{N}}^2\mathrm{d}t^2 - b^2\mathrm{d}\boldsymbol{\rho}^2\right) . \tag{3.56}$$

In addition, we may transform from the laboratory time t to the effective proper (comoving wrist-watch) time τ in order to eliminate the factor in front of $\mathrm{d}\tau^2$

$$\tau = \int \mathrm{d}t \sqrt{A_D^{(\mathcal{N})}}\, c_{\mathcal{N}} \quad \to \quad \mathrm{d}s_{\text{eff}}^2 = \mathrm{d}\tau^2 - A_D^{(\mathcal{N})}b^2\mathrm{d}\boldsymbol{\rho}^2 , \tag{3.57}$$

arriving at the standard Friedman-Robertson-Walker representation, see Eq. (2.1) and, e.g., Ref. [10, 22, 23]. The scaling behavior of the factors can be deduced as follows: with $\varrho_0(t) \propto b^{-D}(t)$ according to Eq. (3.55), we obtain from Eq. (3.48) for the effective coupling coefficient $g_{\mathcal{N}}(t) \propto b^{-D(\mathcal{N}-2)}(t)$ and for the speed of sound follows $c_{\mathcal{N}}(t) \propto b^{-D(\mathcal{N}-1)/2}(t)$. Hence the factor in front of $\mathrm{d}\boldsymbol{\rho}^2$ scales as

$$A_D^{(\mathcal{N})}b^2 \propto b^{2+D(\mathcal{N}-3)/(D-1)} , \tag{3.58}$$

according to Eq. (3.53). Interestingly, the exponent vanishes for

$$\mathcal{N} = \frac{2}{D} + 1\,, \tag{3.59}$$

e.g., for $D = 2$ and $\mathcal{N} = 2$, or $D = 3$ and $\mathcal{N} = 5/3$, or $D = 1$ and $\mathcal{N} = 3$. As was observed above, special care is required for the latter case $D = 1$, but for $\mathcal{N} = 3$ one can indeed introduce an effective metric and the conformal factor can be chosen at will since it does not enter the calculation.

If the condition in Eq. (3.59) is satisfied and thus the exponent in Eq. (3.58) vanishes, the transformed metric in Eq. (3.57) is flat and hence the wave equation for the phonon modes becomes trivial in terms of the coordinates τ and $\boldsymbol{\rho}$

$$\left(\frac{\partial^2}{\partial\tau^2} - \frac{1}{A_D^{(\mathcal{N})}(t=0)}\frac{\partial^2}{\partial\boldsymbol{\rho}^2}\right)\phi = 0\,, \tag{3.60}$$

i.e., a solution $\phi(\tau, \boldsymbol{\rho})$ is independent of the external time dependence mediated via the scaling parameter $b(t)$. It turns out that this perfect scaling is not only valid for the phonon modes, but can be extended to the full field operator: starting with the equation of motion in the Heisenberg picture (3.8) with general s-wave coupling ($\mathcal{N}$) and in D spatial dimensions[6]

$$i\frac{\partial}{\partial t}\hat{\Psi} = \left(-\frac{1}{2m}\frac{\partial^2}{\partial\boldsymbol{r}^2} + V_{\text{ext}}(t,\boldsymbol{r}) + g\,(\hat{\Psi}^\dagger)^{\mathcal{N}-1}\hat{\Psi}^{\mathcal{N}-1}\right)\hat{\Psi}\,, \tag{3.61}$$

one may account for an arbitrarily time-dependent external one-particle trapping potential $V_{\text{ext}}(t, \boldsymbol{r})$ as long as it is purely harmonic at all times

$$V_{\text{ext}}(t,\boldsymbol{r}) = \frac{m}{2}\,\omega_{\text{ext}}^2(t)\boldsymbol{r}^2\,, \tag{3.62}$$

by inserting the scaling ansatz derived above (cf. [116])

$$\hat{\Psi}(t,\boldsymbol{r}) = \frac{\exp\{im\boldsymbol{v}_0^2(t,\boldsymbol{r})/2\}}{\sqrt{b^D(t)}}\,\hat{\psi}(\tau,\boldsymbol{\rho})\,. \tag{3.63}$$

The numerator $\exp\{im\boldsymbol{v}_0^2(t,\boldsymbol{r})/2\}$ of the prefactor reproduces $\boldsymbol{v}_0$ and the denominator $\sqrt{b^D(t)}$ accounts for $\varrho_0(t) = \varrho_0(t=0)/b^D(t)$ and ensures the correct commutation relations for $\hat{\psi}(\tau, \boldsymbol{\rho})$, i.e.,

$$[\hat{\psi}(\tau,\boldsymbol{\rho}), \hat{\psi}^\dagger(\tau,\boldsymbol{\rho}')] = \delta(\boldsymbol{\rho}-\boldsymbol{\rho}')\,. \tag{3.64}$$

For a flat metric $\mathcal{N} = 1 + 2/D$, the proper time is (independently of D) determined as

$$\tau = \int\frac{\mathrm{d}t}{b^2(t)}\,, \tag{3.65}$$

---

[6] Note that the coupling g in Eqs. (3.42) and (3.61) differs by a factor $\mathcal{N}/2$.

and $\boldsymbol{\rho}$ is of course still given by $\boldsymbol{\rho} = \boldsymbol{r}/b(t)$. Finally, after arranging the scale parameter $b(t)$ according to

$$\ddot{b}(t) + \omega_{\text{ext}}^2(t)b(t) = \frac{\omega_{\text{ext}}^2(t=0)}{b^3(t)} = \frac{\omega_0^2}{b^3(t)}, \tag{3.66}$$

the equation of motion for $\hat{\psi}(\tau, \boldsymbol{\rho})$ becomes independent of $b(t)$

$$i\frac{\partial}{\partial\tau}\hat{\psi}(\tau, \boldsymbol{\rho}) = \left(-\frac{1}{2m}\frac{\partial^2}{\partial\boldsymbol{\rho}^2} + \frac{m}{2}\,\omega_0^2\boldsymbol{\rho}^2 + g\,(\hat{\psi}^\dagger)^{\mathcal{N}-1}\hat{\psi}^{\mathcal{N}-1}\right)\hat{\psi}(\tau, \boldsymbol{\rho}), \tag{3.67}$$

i.e., a perfect scaling solution of the full field operator $\hat{\Psi}$ is obtained exactly in those cases where the effective metric is flat. Note that the implications of this property of the full field operator go far beyond the scaling of the hydrodynamic solution – one also obtains a perfect scaling of the quantum fluctuations to arbitrary order and for large wavenumbers (provided that the s-wave approximation is still valid, of course), where hydrodynamic (Thomas-Fermi) solution breaks down. It is not even necessary to assume the mean-field expansion, i.e., the scaling also applies to non-condensed bosons.

Interestingly, all three examples of perfect scaling (from $D = 1$ to $D = 3$) are potentially relevant for real physical systems:

- $D = 1$ and $\mathcal{N} = 3$: in quasi-1D Bose-Einstein condensates, one may obtain an effective $|\psi|^6$ coupling if the perpendicular size a_z is comparable to the s-wave scattering length a_s, see, e.g., [106, 108–110].

- $D = 2$ and $\mathcal{N} = 2$: this is the usual quasi-2D Bose-Einstein condensate with quartic coupling, e.g., [73].

- $D = 3$ and $\mathcal{N} = 5/3$: even though the exponent $\mathcal{N} = 5/3$ may seem somewhat unnatural, it appears in an effective description of a weakly interacting two-component Fermi gas in the BCS state, where the equation of state is determined by the Fermi energy $E_{\text{F}} \propto \varrho^{5/3}$, and which therefore also shows scaling behavior, see, e.g., [113, 117].

3.5 Expanding Bose-Einstein condensates

In view of the effective space-time description for Bose-Einstein condensates in two and three dimensions, we can now employ the tools of general relativity, cf. Chapter 2, and discuss the evolution of the quantum fluctuations during the ballistic expansion, which sets in when the confining potential is switched off. The one-dimensional case, however, will not be considered, because of the aforementioned problems concerning the introduction of an effective space-time metric. With the obvious analogy of expanding condensates to the period of cosmic inflation – in both cases small quantum fluctuations evolve atop a classical expanding background – different horizon concepts known from general relativity are applied. The spectrum of the frozen quantum fluctuations will be calculated for quasi-two-dimensional and three-dimensional condensates in Subsections 3.5.2 and 3.5.3, respectively, where the usual quartic coupling ($\mathcal{N} = 2$) will be considered in both cases.

3.5.1 Horizon Analogues

Apart from the question of whether it can be cast into a flat space-time form by means of an appropriate coordinate transformation or not, the emergence of a non-trivial effective metric in Eq. (3.52) suggests the application of concepts known from general relativity, such as horizons [15, 23, 45], see also Subsection 2.1.2. Generally speaking, horizons correspond to a loss of causal connectivity, i.e., events beyond a horizon have no influence or cannot be influenced. The most prominent example is the event horizon of a (classical) black hole, beyond which everything is trapped forever (i.e., nothing can ever escape to infinity).

On the other hand, in cosmology, two slightly different horizon concepts play a more important role due to the large-scale homogeneity and isotropy – the particle horizon and the apparent horizon. The particle horizon always refers to a chosen trajectory and indicates the border to the space-time region, which cannot be reached by any signal starting from this trajectory or from where no signal can reach this trajectory. The apparent horizon depends on the chosen coordinates and is (roughly speaking) defined as the border, beyond which all closed two-surfaces can either only expand or only contract w.r.t. the chosen coordinates.

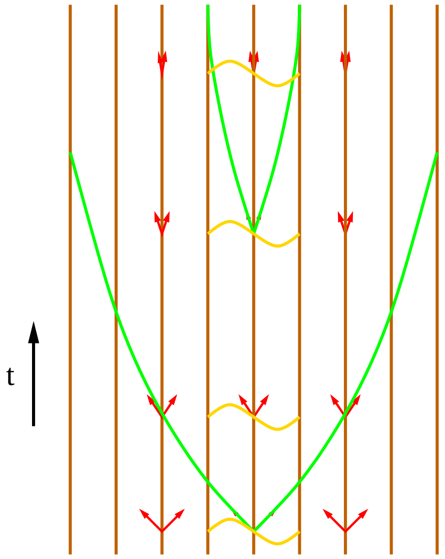

Figure 3.2: Comoving worldlines (brown), lightcones (red) and lightrays (green) in an expanding spacetime, see also Fig. 2.2.

As it turns out, the concepts of the particle and the apparent horizon can be applied to expanding Bose-Einstein condensates. Let us start with the particle horizon and choose the trajectory $\boldsymbol{r} = 0 \to \boldsymbol{\rho} = 0$, for which the particle horizon can conveniently be determined using the metric in Eq. (3.56). The question is: which values of the comoving coordinate $\boldsymbol{\rho}$ can a sound wave reach by starting at the origin $\boldsymbol{\rho} = 0$ at time t and being described by a null line $ds^2_{\text{eff}} = 0$, i.e., how far can it travel? According to Eq. (3.56), this length can be calculated via the following integral [cf. also [15] and Eq. (2.4)]

$$\Delta\rho_{\text{horizon}}(t) = \int\limits_t^\infty dt' \, \frac{c_{\mathcal{N}}(t')}{b(t')} = c_{\mathcal{N}}(t = 0) \int\limits_t^\infty \frac{dt'}{b^{1+D(\mathcal{N}-1)/2}(t')} \,. \tag{3.68}$$

If the above integral converges to a finite result $\Delta\rho_{\mathrm{horizon}}(t)$, this corresponds to a particle horizon since no point beyond this comoving coordinate can be reached by sound waves anymore. [Note that, in contrast to the speed of light $c = 1$, the speed of sound $c_{\mathcal{N}}$ in Bose-Einstein condensates is not constant but instead depends on density ϱ_0, coupling strength etc. and therefore enters Eq. (3.68).]

For a free expansion of the condensate $V_{\mathrm{ext}}(t \uparrow \infty) = 0$, one obtains $b(t \uparrow \infty) \propto t$ at late times according to Eq. (3.66) and thus a horizon exists for all $\mathcal{N} > 1$. The occurrence of a horizon might be puzzling if the metric in terms of the proper time τ in Eq. (3.57) is flat – but this puzzle can be resolved by the observation that the proper time τ reaches a finite value $\tau(t \uparrow \infty) < \infty$ in the limit of arbitrarily late laboratory times in that case, cf. Eq. (3.65).

In contrast to the particle horizon, which necessitates the knowledge of the full future (or past), the apparent horizon can be identified by means of the configuration at a certain instant of time only. Instead of a trajectory as for the particle horizon, one has to choose a specific coordinate system (time slices) in order to define the apparent horizon. The coordinates $(\tau, \boldsymbol{\rho})$ leading to a flat metric, for example, do of course not allow the introduction of an apparent horizon. On the other hand, since the expanding condensate is observed using the laboratory coordinate system $(t, \boldsymbol{r})$, one should choose these coordinates instead. For a spherically symmetric metric as in Eq. (3.52), the apparent horizon is determined by $g_{00}^{\mathrm{eff}} = 0$, i.e., where the velocity of the condensate $\boldsymbol{v}_0$ exceeds the speed of sound $c_{\mathcal{N}}$

$$\boldsymbol{v}_0^2(t, r_{\mathrm{horizon}}) = c_{\mathcal{N}}^2(t) \quad \to \quad r_{\mathrm{horizon}}(t) \propto \frac{b^{1-D(\mathcal{N}-1)/2}}{\dot{b}} \,. \tag{3.69}$$

The very intuitive interpretation is that no sound wave can enter the region $r < r_{\mathrm{horizon}}$ from the outside.

For perfect scaling $\mathcal{N} = 1 + 2/D$ and a freely expanding condensate, the apparent horizon settles down at late times (when $\dot{b}$ becomes constant) to a finite value $r_{\mathrm{horizon}}(t \uparrow \infty) = r_{\mathrm{horizon}}^{\infty} > 0$, otherwise it may increase or decrease forever (depending on D and $\mathcal{N}$). Note that both, the apparent and the particle horizon are never at rest with respect to the comoving coordinate $\boldsymbol{\rho}$ but always decreasing. As a result, the wavelength of all sound modes $\exp\{i\boldsymbol{\kappa} \cdot \boldsymbol{\rho}\}$ exceeds the horizon size at some instant of time (horizon crossing) in view of the permanent stretching of modes due to the expansion of the condensate, cf. also Subsection 2.1.3 and Fig. 2.3. After the wavelength exceeds the horizon size, the regions of higher and lower pressure cannot interact anymore and hence the modes stop oscillating (freezing of modes). As a result, comparing each mode with a harmonic oscillator, the momentum and its variance decrease drastically – and according to the Heisenberg uncertainty relation, the complementary variance must increase in order to compensate this. Ergo, the initial ground/vacuum state gets squeezed, which amplifies the quantum fluctuation in a certain direction. This admittedly rather intuitive picture (horizon crossing, freezing, and squeezing) applies to both, the expanding universe (provided a horizon exists, such as during cosmic inflation) as well as expanding Bose-Einstein condensates in a very similar way and must of course be further supported by explicit calculations, see Sections 3.5.2 and 3.5.3.

Note that analogue horizons (and perhaps horizons in real gravity as well) are only low-energy effective concepts since, for very small wavelengths (below the healing length), the quantum pressure term becomes important leading to group and phase velocities exceeding the usual speed of sound. Furthermore, as the healing length increases during the expansion, the late-time limit in the derivation of the particle horizon is not strictly valid. Nevertheless, the main effects such as the amplification of quantum fluctuations are not modified drastically, see the next subsections.

3.5.2 Density-Density Correlations in quasi-2D

According to the results of Section 3.4.2, the time-evolution of a quasi-two-dimensional condensate with the usual quartic coupling (i.e., $\mathcal{N} = D = 2$) is particularly simple to solve due to its perfect scaling behavior – which allows to derive its dynamics exactly (e.g., including the quantum-pressure corrections). If the initial trapping potential is considered to be harmonic, the free expansion after switching off the longitudinal trap $V_{\|}^{\rm ext}(t>0) = 0$ is fully described by the time-evolution of the scaling parameter according to Eq. (3.66)

$$b(t) = \sqrt{1 + \omega_0^2 t^2}\,. \tag{3.70}$$

The associated proper time τ can be calculated from Eq. (3.65)

$$\tau(t > 0) = \frac{\arctan \omega_0 t}{\omega_0}\,. \tag{3.71}$$

Since τ quickly approaches a finite value at late times $t \uparrow \infty$, the fluctuations freeze in and assume the value at proper time $\tau = \pi/(2\omega_0)$. In view of the perfect scaling discussed in Sec. 3.4.2, both, the background and the phonon modes – expressed in terms of $\boldsymbol{\rho}$ and τ – behave in the same way before and during the expansion, leaving the relative correlation function

$$C(\boldsymbol{\rho}, \boldsymbol{\rho}') = \frac{\langle \delta\hat{\varrho}(t,\boldsymbol{\rho})\delta\hat{\varrho}(t,\boldsymbol{\rho}')\rangle}{\varrho_0(t,\boldsymbol{\rho})\varrho_0(t,\boldsymbol{\rho}')} = \frac{\langle \delta\hat{\varrho}(\boldsymbol{\rho})\delta\hat{\varrho}(\boldsymbol{\rho}')\rangle}{\varrho_0(\boldsymbol{\rho})\varrho_0(\boldsymbol{\rho}')} \tag{3.72}$$

unchanged. Consequently, the spectrum of the relative density contrast in comoving coordinates after horizon crossing is given by the initial correlation spectrum. Besides the quasi-two-dimensional condensate with usual quartic coupling ($\mathcal{N} = D = 2$), this also holds for all other cases where perfect scaling occurs.

As discussed in Section 3.5.1, the apparent horizon depends on the chosen time-slicing, i.e., the set of coordinates. (The particle horizon is independent of the set of coordinates, but requires the knowledge of the whole future evolution.) comoving coordinates, albeit advantageous to describe the evolution of the modes, are not suitable for describing the appearance of an apparent horizon. On the other hand, all observations are performed in laboratory time t and coordinates $\boldsymbol{r}$ with the metric (3.52) showing the formation of an apparent horizon according to Eq. (3.69). For $\mathcal{N} = 1 + 2/D$, it follows

$$r_{\text{horizon}}(t) = \frac{c_{\mathcal{N}}(0)}{\dot{b}(t)} = c_{\mathcal{N}}(0)\frac{\sqrt{1+\omega_0^2 t^2}}{\omega_0^2 t}\,, \tag{3.73}$$

in the homogeneous case. While the trapping potential is still turned on ($t < 0$), the (apparent) horizon size r_{horizon} is infinite. Clearly, without any expansion, all points are causally connected via sound waves. After releasing the condensate, however, the horizon settles down very quickly ($\omega_0 t \gg 1$) at a finite position (in laboratory coordinates) $c_{\mathcal{N}}(0)/\omega_0$, given by the initial speed of sound $c_{\mathcal{N}}(0)$ and trapping frequency ω_0.

Since the (apparent) horizon quickly settles to a finite position in laboratory coordinates $(t, \boldsymbol{r})$ and every phonon mode with a given wavelength λ expands with the condensate cloud, each phonon mode will cross the horizon eventually. Equivalently, in terms of the comoving coordinates, the horizon size decreases for all times (as long as the condensate is expanding) and the (comoving) wavenumber $\boldsymbol{\kappa}$ remains constant. As mentioned before, the initial correlation function of a quasi-two-dimensional condensate translates directly into the frozen density contrast after horizon crossing.

In order to derive the density-density correlation function quantitatively, the phonon modes are quantized within the initial condensate $\boldsymbol{v}_0 = 0$ using the approximation (center of the gas cloud) of a constant background density $\varrho_0 = \text{const}$. After a normal mode expansion, the Lagrange function (3.44) reads

$$L = \int \mathrm{d}^2 r\,\mathcal{L} = \frac{\mathcal{V}_Q}{4}\sum_{\boldsymbol{k}}\left[\left(g_{2\mathrm{D}} + \frac{\boldsymbol{k}^2}{4m\varrho_0}\right)^{-1}(\delta\dot{S}_{\boldsymbol{k}})^2 - \frac{\varrho_0 \boldsymbol{k}^2}{m}(\delta S_{\boldsymbol{k}})^2\right]\,, \tag{3.74}$$

where $\mathcal{V}_Q$ denotes the quantization volume. Note that, in contrast to Eq. (3.47), we did not neglect the quantum pressure term. In a straightforward manner, the phase and density fluctuations can be quantized via the introduction of creation ($\hat{a}_{\boldsymbol{k}}^\dagger$) and annihilation operators ($\hat{a}_{\boldsymbol{k}}$) which diagonalize the Hamiltonian. The quantized phase and density fluctuations read

$$\delta\hat{S}_{\boldsymbol{k}} = \sqrt{\frac{1}{\mathcal{V}_Q\omega_{\boldsymbol{k}}}\left(g_{2\mathrm{D}} + \frac{\boldsymbol{k}^2}{4m\varrho_0}\right)}\left(\hat{a}_{\boldsymbol{k}} + \hat{a}_{\boldsymbol{k}}^\dagger\right)\,, \tag{3.75}$$

$$\delta\hat{\varrho}_{\boldsymbol{k}} = i\sqrt{\frac{\omega_{\boldsymbol{k}}}{\mathcal{V}_Q}\left(g_{2\mathrm{D}} + \frac{\boldsymbol{k}^2}{4m\varrho_0}\right)^{-1}}\left(\hat{a}_{\boldsymbol{k}} - \hat{a}_{\boldsymbol{k}}^\dagger\right)\,, \tag{3.76}$$

with the well-known Bogoliubov dispersion relation

$$\omega_{\boldsymbol{k}}^2 = \mu\frac{\boldsymbol{k}^2}{m} + \frac{\boldsymbol{k}^4}{4m^2}\,, \tag{3.77}$$

where $\mu = g_{2\mathrm{D}}\varrho_0^{2\mathrm{D}}$ is the (initial) chemical potential.

For a perfectly-scaling condensate, the two-point function in Eq. (3.72) yields the density-density correlations at all times, and in particular also the frozen correlations (the density contrast) after horizon crossing. We can thus calculate the Fourier components

$$C_{2\mathrm{D}}(\boldsymbol{\kappa}) = \int \mathrm{d}^2\rho \, \frac{\langle \delta\hat{\varrho}(t,\mathbf{0})\delta\hat{\varrho}(t,\boldsymbol{\rho})\rangle}{\varrho_0^2(t)} \, e^{i\boldsymbol{\kappa}\cdot\boldsymbol{\rho}} = \frac{g_{2\mathrm{D}}|\boldsymbol{\kappa}|}{\mu\sqrt{4m\mu+\boldsymbol{\kappa}^2}} \, . \tag{3.78}$$

in order to obtain the spectrum.

For large wavelengths, the spectrum is linear in the (comoving) momentum $\boldsymbol{\kappa}$ in complete agreement to the curved space-time analogy. For large (comoving) momenta $\boldsymbol{\kappa}$, where the dispersion relation (3.77) changes from linear to quadratic and the curved space-time analogy breaks down, the spectrum of the two-point correlation function approaches a constant value corresponding to a Dirac δ-contribution $C(\boldsymbol{\rho},\boldsymbol{\rho}') \propto \delta(\boldsymbol{\rho}-\boldsymbol{\rho}')+\ldots$. Interestingly, after subtracting this local term, a scale-invariant spectrum $C(\boldsymbol{\kappa}) \propto 1/\boldsymbol{\kappa}^2$ for large $\boldsymbol{\kappa}$ is obtained – in analogy to cosmic inflation, where the spectrum is scale-invariant, too (in 3+1 dimensions it is $1/k^3$; see also Chapter 2). However, one should bear in mind that this scale-invariant spectrum occurs in a region where the curved space-time analogy breaks down.

For addressing the question of whether this effect (amplification of the initial quantum fluctuations of the phonon modes) can be measured or not, the order of magnitude of the relative density-density correlations $C(\boldsymbol{\kappa})$ at different spatial points $\boldsymbol{\rho} \neq \boldsymbol{\rho}'$ can be estimated. Since the two-dimensional coupling constant, $g_{2\mathrm{D}}$, is proportional to the ratio of the scattering length, a_s, and the perpendicular extension of the condensate, a_z, one has typically

$$\frac{\langle \delta\hat{\varrho}(\boldsymbol{\rho})\delta\hat{\varrho}(\boldsymbol{\rho}')\rangle}{\varrho_0^2} = \mathcal{O}\left(\frac{a_s}{a_z}\right) . \tag{3.79}$$

Note, however, that this can only be seen as a rough estimate of the order of magnitude, since the two-point function is logarithmically divergent at small distances (where eventually the employed approximations break down). Remembering the conditions (3.39) in Section 3.3, it becomes obvious that the relative density contrast must be significantly smaller than one – which was to be expected. However, the fluctuations could be on the percent-level (see Section 3.5.4) and thus might well be measurable.

3.5.3 Density-Density Correlations in 3D

For an expanding three-dimensional condensate with quartic coupling, the situation is more complicated, since it does not show the perfect scaling behavior as in two dimensions. Therefore, it is not possible to infer the final (frozen) density (or phase) fluctuations from the initial state exactly as in the previous case. Fortunately, for long wavelengths, we may exploit the effective space-time analogy and derive the evolution using the tools known from cosmology. To this end, the effective Painlevé-Gullstrand-Lemaître metric (3.52) is diagonalized by transforming onto comoving coordinates. Note that, in three (spatial) dimensions, the background density scales as $\rho(t) = \rho(0)/b^3(t)$. Assuming the background density to be smooth (Thomas-Fermi limit), the evolution equation for the scale factor – after switching off the trap – reads, cf. [116]

$$\ddot{b}(t) = \frac{\omega_0^2}{b^4(t)} \,. \tag{3.80}$$

Similar to the previous case, the scale factor accelerates (the interaction energy is transformed into kinetic energy) after switching off the trap, but quickly assumes a linear behavior, $b \propto t$ (for $t \gg 1/\omega_0$).

The following calculations are most conveniently performed using the laboratory time but comoving spatial coordinates. One advantage of the analogy to curved space-times is the inherited freedom of choosing suitable coordinates, where the independence of the final result follows automatically from covariance. The equation of motion of the field modes $\phi_{\boldsymbol{\kappa}}$ with comoving wavenumber $\boldsymbol{\kappa}$ assumes the form

$$\left(\frac{\partial^2}{\partial t^2} + 3\frac{\dot{b}}{b}\frac{\partial}{\partial t} + \frac{c_0^2\boldsymbol{\kappa}^2}{b^5}\right)\phi_{\boldsymbol{\kappa}} = 0 \,. \tag{3.81}$$

Initially, for the trapped condensate, the damping term $3\dot{\phi}_{\boldsymbol{\kappa}}\dot{b}/b$ vanishes and the modes oscillate freely. During the expansion, the third term decreases whilst the second one grows and eventually dominates the latter one – in complete analogy to an over-damped oscillator, the modes freeze in. Because most phonon modes have frequencies much larger than the trapping frequency (e.g., [118,119]), this horizon crossing and freezing process happens during the period of linear expansion $b(t) = \alpha t$ (with $\alpha \approx 0.82\omega_0$). In view of the adiabatic theorem (see, e.g., [120] and also Appendix A), the initial vacuum state for these (initially) rapidly oscillating modes is preserved (adiabatic vacuum) during the initial nonlinear expansion. Thus the equation of motion describing the freezing of modes can be simplified considerably by inserting $b(t) = \alpha t$

$$\left(\frac{\partial^2}{\partial t^2} + 3\frac{1}{t}\frac{\partial}{\partial t} + \frac{c_0^2\boldsymbol{\kappa}^2}{\alpha^5 t^5}\right)\phi_{\boldsymbol{\kappa}} = 0 \tag{3.82}$$

and solved analytically in terms of Bessel functions [121]

$$\phi_{\boldsymbol{\kappa}} = C_{\boldsymbol{\kappa}}^{(1)}\frac{1}{t}H_{2/3}^{(1)}\left(\frac{2}{3}\frac{c_0\kappa}{\alpha^{5/2}}t^{-3/2}\right) + C_{\boldsymbol{\kappa}}^{(2)}\frac{1}{t}H_{2/3}^{(2)}\left(\frac{2}{3}\frac{c_0\kappa}{\alpha^{5/2}}t^{-3/2}\right) , \tag{3.83}$$

where $H_{2/3}^{(1,2)}$ denote the Hankel functions with the index $\nu = 2/3$ and $C_{\boldsymbol{\kappa}}^{(1,2)}$ are the corresponding integration constants. As one would expect, for early times, the modes $\phi_{\boldsymbol{\kappa}}$ oscillate $\dot{\phi}_{\boldsymbol{\kappa}}^{(1,2)} = \pm i\omega_{\rm ad}\phi_{\boldsymbol{\kappa}}^{(1,2)}$. It turns out that the Hankel functions $H_{2/3}^{(1,2)}$ have the proper asymptotic behavior for early times such that the integration constants $C_{\boldsymbol{\kappa}}^{(1,2)}$ can be replaced by the (time-independent) creation and annihilation operators (in analogy to the previous Section) associated to the initial adiabatic vacuum state for the quantized phonon modes $\hat{\phi}_{\boldsymbol{\kappa}}$ in the Heisenberg picture

$$C^{(1)}_{\boldsymbol{\kappa}} \to \sqrt{\frac{\pi}{6}\frac{g}{\alpha^3}\frac{2}{\mathcal{V}_{\mathrm{Q}}}}\,\hat{a}_{\boldsymbol{\kappa}}\,, \tag{3.84}$$

where the prefactor can be derived by imposing the canonical commutation relations for the conjugate variables ϕ and $\delta\varrho = \dot{\phi}/g$ obtained from the Lagrangian (3.50) for comoving coordinates. Note that the argument of the Hankel functions coincides (up to a constant) with the proper time, $\tau \propto \frac{2}{3}\alpha^{-5/2}t^{-3/2}$, during the phase of linear expansion.

For late times $t \uparrow \infty$, the modes $\phi_{\boldsymbol{\kappa}}$ approach a constant value (due to horizon crossing and freezing) which can be derived by inserting the asymptotic behavior of the Hankel functions $H^{(1,2)}_{2/3}$ [121]. The frozen late-time $t \uparrow \infty$ expectation value for phase-phase correlations reads

$$\langle\hat{\phi}^2_{\boldsymbol{\kappa}}\rangle = \int d^3\rho\,\cos(\boldsymbol{\kappa}\cdot\boldsymbol{\rho})\langle\hat{\phi}(\boldsymbol{\rho})\hat{\phi}(\mathbf{0})\rangle = \frac{g}{6\pi}\,[\Gamma\,(2/3)]^2\,\frac{\alpha^{1/3}3^{4/3}}{c_0^{4/3}}\kappa^{-4/3}\,. \tag{3.85}$$

Employing Eq. (3.49), we can calculate the density fluctuations, $\delta\varrho = -\dot{\phi}/g$ (in comoving coordinates, where $\boldsymbol{v}_0$ vanishes), and obtain the spectrum of the relative density-density correlation function at late times

$$C_{3\mathrm{D}}(\boldsymbol{\kappa}) = \int d^3\rho\cos(\boldsymbol{\kappa}\cdot\boldsymbol{\rho})\frac{\langle\delta\hat{\varrho}(\boldsymbol{\rho})\delta\hat{\varrho}(\mathbf{0})\rangle}{\varrho_0^2} = \frac{[\Gamma(1/3)]^2 3^{2/3}}{6\pi}\frac{\xi c_0^{1/3}}{\varrho_0\alpha^{1/3}}\,\kappa^{4/3}\,, \tag{3.86}$$

where everything on the right-hand side (healing length etc.) refers to the initial state. Interestingly, one obtains the same spectra ($k^{-4/3}$ for the phase and $k^{+4/3}$ for the density fluctuations) for a condensate at rest after sweeping through the phase transition at $g = 0$ by means of a time-dependent coupling $g(t)$ [37].

In contrast to the quasi-two-dimensional case with perfect scaling, the above results rely on the curved space-time analogy and thus are only valid for wavelengths far above the healing length. Furthermore, in three dimensions, the healing length scales like $\xi(t) = \xi(0)b^{3/2}(t)$ and grows faster (again in contrast to the quasi-two-dimensional case) than the wavelengths $\lambda(t) = \lambda(0)b(t)$ in laboratory coordinates. A rough estimate of the maximal amplification effect can be obtained by inserting the maximum comoving wavenumber $\kappa = 1/\xi(\alpha/\omega_\xi)^{1/4}$ (with ξ the initial healing length and $\omega_\xi = c_0/\xi$) of the phonon modes whose wavelength exceeds the healing length during the relevant period of their evolutions (i.e., until horizon-crossing and freezing)

$$\kappa^3 C_{3\mathrm{D}}(\kappa) = \frac{4\sqrt{\pi}[\Gamma(1/3)]^2(\tilde{\alpha})^{3/4}}{3^{1/3}}\sqrt{a_s^3\varrho_0}\left(\frac{\omega_\xi}{\omega_0}\right)^{-3/4} \approx 30.3\sqrt{a_s^3\varrho_0}\left(\frac{\omega_\xi}{\omega_0}\right)^{-3/4}\,. \tag{3.87}$$

Here $\omega_\xi = c_0/\xi$ denotes the (initial) frequency of the phonons with the (comoving) wavenumber $1/\xi$, and $\alpha = \tilde{\alpha}\omega_0$, where $\tilde{\alpha} \approx 0.82$, is a dimensionless constant. In contrast to the quasi-two-dimensional case, the size of the fluctuations now depends on the diluteness parameter $\sqrt{a_s^3\varrho_0}$ (instead of the ratio a_s/a_z), which must be small for the employed approximations to apply, i.e., $\sqrt{a_s^3\varrho_0} \ll 1$. Furthermore, the ratio $\omega_\kappa/\omega_0 = c_0\kappa/\omega_0$ must be large $\omega_\kappa/\omega_0 \gg 1$ if the period of linear expansion $b(t) = \alpha t$ should be sufficiently long. However, the smallness of these parameters can partly be compensated by the numerical prefactor 30.3 such that the final effect can be on the percent-level (see the next subsection).

The spectrum and size of the frozen-in correlations $C_{3\mathrm{D}}$ could be measured by obtaining a density map of a slice of the condensate (tomographic imaging). By making a projective (e.g., absorption) image instead, one would average over the fluctuations in the (spatial) direction of projection. While the spectrum remains unchanged, this averaging yields an additional suppression by a factor of order ξ/l_z with l_z denoting the transversal (i.e., in direction of projection) extension of the condensate.

3.5.4 Comparison with experiments

By assuming realistic experimental values, an explicit estimate for the size of the correlations (3.78) and (3.86) can be obtained. Inspired by the experiment [91], let us consider a quasi-two-dimensional Bose-Einstein condensate of 10^5 sodium atoms confined in a highly-anisotropic trap with frequencies $\omega_\perp/2\pi = 790\,\mathrm{Hz}$ and $\omega_\parallel/2\pi = 10\,\mathrm{Hz}$. The thickness $a_z = 0.746\,\mu\mathrm{m}$ is much smaller than the healing length $\xi = 1.34\,\mu\mathrm{m}$ but still much larger than the scattering length $a_s = 2.8\,\mathrm{nm}$, and thus complying with the hierarchy of scales discussed in Section 3.3. In view of the perfect scaling of the field operator (see Sec. 3.4.2), the mode with comoving wavenumber $\kappa = 2\pi/\xi$ will be considered. The relative density contrast for this mode inside a volume ξ^2

$$C(\kappa)/\xi^2 = 1.79\% \tag{3.88}$$

follows from Eq. (3.78). For the modes in the linear regime of the spectrum, horizon crossing and thus freezing occur shortly after the trap is switched off. Initially the horizon is at infinity, but very quickly settles at $r_{\mathrm{horizon}}(t \uparrow \infty) = 3.28\,\mu\mathrm{m}$. Hence already after one e-folding of expansion, when the radius of the atom cloud has increased by a factor $e^1 \approx 2.7$, all modes with wavelength larger than ξ are frozen and the fluctuations are transformed into a density contrast. With the correlation function depending on the ratio a_s/a_z, the effect can be enhanced by confining the condensate more tightly in the perpendicular direction. However, if a_s/a_z is not small, the condensate is no longer described by the usual Gross-Pitaevskii Lagrangian (3.32) with quartic coupling and the presented analysis (including the perfect scaling for quasi two dimensions) does not apply anymore in this form. For such a case, the (initial) correlation spectrum with appropriate non-quartic coupling, cf. [110,122], was calculated in Ref. [122] and differs from Eq. (3.78). (Since the condensate does not obey the perfect scaling anymore, it would be necessary to calculate the evolution of the quantum fluctuations during the expansion of the gas cloud explicitly.)

As an example for the three-dimensional case, 10^7 atoms of ^{87}Rb shall be placed inside a spherically-symmetric trap with frequency $\omega_0/2\pi = 200\,\text{Hz}$. According to Ref. [75], these are (potentially) realizable parameters. With a Thomas-Fermi radius of $R = 12.2\,\mu\text{m}$, the frequency of the lowest excitations can be estimated as $\omega_{\text{min}} = \pi c_s/R = 5582\,\text{Hz}$ – a value well above the trap frequency ω_0. Hence all phonon modes evolve adiabatically during the period of nonlinear expansion (which lasts roughly $1/\omega_0$) and the horizon crossing happens during the phase of linear expansion, i.e., the approximations leading to Eq. (3.87) are justified. A rough estimate of the maximum effect yields

$$\kappa^3 C_{3\text{D}}(\kappa) \;=\; \mathcal{O}(2\,\%)\,, \tag{3.89}$$

i.e., a potentially measurable effect, which can be enhanced by increasing the diluteness parameter.

Note that the calculation for the three-dimensional case relies on the effective space-time analogy (hydrodynamics), i.e., the neglect of the quantum pressure term, and therefore applies only to modes with comoving wavelength larger than the growing comoving healing length during all relevant phases of evolution (until horizon crossing). The fluctuations of the remaining modes might well exceed the value given in Eq. (3.89), because Eq. (3.86) gives the low-energy part of the spectrum only.

3.6 On the backreaction problem

Many phenomena in physics can be described, to a sufficient degree of accuracy, by means of the background-field method, wherein one considers linearized quantum fluctuations on top of an approximately classical background. For a scalar gapless (e.g., Goldstone) mode ϕ, propagating in an arbitrary background (e.g., zeroth sound in inhomogeneous superfluids), the low-energy effective action can be cast into the pseudo-covariant form (cf. Sec. 3.4)

$$\mathcal{L}_{\text{eff}} \;=\; \frac{1}{2}\,(\partial_\mu\phi)G^{\mu\nu}(\partial_\nu\phi)\,, \tag{3.90}$$

with $\partial_\mu = (\partial/\partial t, \boldsymbol{\nabla})$ denoting the space-time derivatives (the summation convention is employed), and the space-time dependent tensor $G^{\mu\nu}$ characterizing the background [27, 123–126]. Hence the propagation of ϕ is completely analogous to that of a scalar field in a curved space-time with the effective metric $g^{\mu\nu}_{\text{eff}}$ depending on the background tensor via $G^{\mu\nu} = |g_{\text{eff}}|^{1/2} g^{\mu\nu}_{\text{eff}}$, where $g_{\text{eff}} = \det[g^{\text{eff}}_{\mu\nu}]$ (with possibly an additional dilaton factor). This striking analogy now offers the possibility to apply many tools and methods developed for quantum fields in curves space-time [10], and associated phenomena like Hawking radiation [27, 123], super-radiance etc., may occur. Since the equation of motion for the scalar mode, $\Box_{\rm eff}\phi = \nabla^{\rm eff}_\mu g^{\mu\nu}_{\rm eff}\nabla^{\rm eff}_\nu\phi = 0$, is equivalent to covariant energy-momentum balance, $\nabla^{\rm eff}_\mu T^{\mu\nu} = 0$, one such tool is the pseudo-energy-momentum tensor, cf. [31, 114]

$$T_{\mu\nu} = (\partial_\mu\phi)(\partial_\nu\phi) - \frac{1}{2}\, g^{\rm eff}_{\mu\nu}(\partial_\rho\phi)(\partial_\sigma\phi)g^{\rho\sigma}_{\rm eff}\,. \tag{3.91}$$

The identification of effects by analogy, described above (including the existence of a pseudo-energy-momentum tensor), is of a kinematical nature. An important question concerns the dynamics, that is, the *backreaction* of these quantum fluctuations onto the classical background. Extending the analogy to curved space-times a bit further, one is tempted to apply the effective-action method (see, e.g., [10] and [127, 128]), and, since the dependence of the effective action $\mathcal{A}_{\rm eff}$ on the degrees of freedom of the background η enters via the effective metric $g^{\mu\nu}_{\rm eff} = g^{\mu\nu}_{\rm eff}(\eta)$, to determine the backreaction contribution to their equation of motion by

$$\frac{\delta\mathcal{A}_{\rm eff}}{\delta\eta} = \frac{\delta\mathcal{A}_{\rm eff}}{\delta g^{\mu\nu}_{\rm eff}}\frac{\delta g^{\mu\nu}_{\rm eff}}{\delta\eta} = \frac{1}{2}\sqrt{|g_{\rm eff}|}\left\langle\hat{T}_{\mu\nu}\right\rangle\frac{\partial g^{\mu\nu}_{\rm eff}}{\partial\eta}\,. \tag{3.92}$$

The precise meaning of the expectation value of the pseudo-energy-momentum tensor, $\langle\hat{T}_{\mu\nu}\rangle$, is difficult to grasp in general, due to the non-uniqueness of the vacuum state in a complicated curved space-time background and the ultraviolet renormalization procedure. Adopting a covariant renormalization scheme, the results for $\langle\hat{T}_{\mu\nu}\rangle$ can be classified in terms of geometrical quantities (cf. the trace anomaly [10]).

However, in calculating the quantum backreaction in that way, one is implicitly making two essential assumptions: firstly, that the leading contributions to the backreaction are completely determined by the effective action in Eq. (3.90), and, secondly, that deviations from the low-energy effective action at high energies do not affect the (renormalized) expectation value of the pseudo-energy-momentum tensor, $\langle\hat{T}_{\mu\nu}\rangle$. Since the effective covariance in Eq. (3.90) is only a low-energy property, the applicability of a covariant renormalization scheme is not obvious in general.

In order to address the question of whether the two assumptions mentioned above are justified, e.g., whether $\langle\hat{T}_{\mu\nu}\rangle$ completely determines the backreaction of the linearized quantum fluctuations, the phonon modes in a well understood superfluid, a dilute Bose-Einstein condensate, will be considered. Dynamics of its field operator $\hat{\Psi}$ is described by the Heisenberg equation of motion (3.8) which reads in s-wave scattering approximation (cf. Sec. 3.4.2)

$$i\frac{\partial}{\partial t}\hat{\Psi} = \left(-\frac{1}{2m}\boldsymbol{\nabla}^2 + V_{\rm ext} + g\hat{\Psi}^\dagger\hat{\Psi}\right)\hat{\Psi}\,. \tag{3.93}$$

In the limit of many particles $N \gg 1$, in a finite trap at zero temperature with almost complete condensation, the full field operator $\hat{\Psi}$ can be represented in terms of the particle-number-conserving mean-field ansatz (3.10). Insertion of Eq. (3.10) into (3.93) yields the (modified) Gross-Pitaevskii equation for the order parameter ψ_0 [see also Eqs. (3.11)–(3.13) and (3.22) in Sec. 3.2]

$$i\frac{\partial\psi_0}{\partial t} = \left(-\frac{\boldsymbol{\nabla}^2}{2m} + V_{\rm ext} + g|\psi_0|^2 + 2g\langle\hat{\chi}^\dagger\hat{\chi}\rangle\right)\psi_0 + g\langle\hat{\chi}^2\rangle\psi_0^2\,, \tag{3.94}$$

the Bogoliubov-de Gennes equation [90, 98] for $\hat{\chi}$

$$i\frac{\partial}{\partial t}\hat{\chi} = \left(-\frac{\boldsymbol{\nabla}^2}{2m} + V_{\rm ext} + 2g|\psi_0|^2\right)\hat{\chi} + g\psi_0^2\hat{\chi}^\dagger\,, \tag{3.95}$$

and, neglecting $\mathcal{O}(1/N)$ terms, for the remaining higher-order corrections $\hat{\zeta} = \mathcal{O}(1/\sqrt{N})$ follows

$$i\frac{\partial}{\partial t}\hat{\zeta} \approx \left(-\frac{\boldsymbol{\nabla}^2}{2m} + V_{\rm ext} + 2g|\psi_0|^2\right)\hat{\zeta} + g\psi_0^2\,\hat{\zeta}^\dagger + 2g(\hat{\chi}^\dagger\hat{\chi} - \langle\hat{\chi}^\dagger\hat{\chi}\rangle)\psi_0 + g(\hat{\chi}^2 - \langle\hat{\chi}^2\rangle)\psi_0^*\,. \tag{3.96}$$

3.6.1 Backreaction

The observation that the Gross-Pitaevskii equation (3.94) yields an equation correct to leading order $\mathcal{O}(\sqrt{N})$, using either $|\psi_0|^2$ or $|\psi_0|^2 + 2\left\langle\hat{\chi}^\dagger\hat{\chi}\right\rangle$ in the round brackets of (3.94), hints at the fact that quantum backreaction effects correspond to next-to-leading order terms and cannot be derived *ab initio* in the above manner without additional assumptions. Therefore, an alternative method shall be employed here. In terms of the exact density and current given by

$$\varrho = \left\langle\hat{\Psi}^\dagger\hat{\Psi}\right\rangle\,, \quad \boldsymbol{j} = \frac{1}{2mi}\left\langle\hat{\Psi}^\dagger\boldsymbol{\nabla}\hat{\Psi} - \text{H.c.}\right\rangle\,, \tag{3.97}$$

the time-evolution is governed by the equation of continuity for ϱ and an Euler type equation for the current $\boldsymbol{j}$, cf. Eqs. (3.45) and (3.46) in Sec. 3.4.1. After insertion of the Heisenberg equation (3.93), one finds that the equation of continuity is not modified by the quantum fluctuations but satisfied exactly (i.e., to all orders in $1/N$ or $\hbar$)

$$\dot{\varrho} + \boldsymbol{\nabla}\cdot\boldsymbol{j} = 0\,, \tag{3.98}$$

in accordance with the Noether theorem and the $U(1)$ invariance of the Hamiltonian, cf. [127, 128]. However, if one inserts the mean-field expansion (3.10) and writes the full density as a sum of condensed and non-condensed parts

$$\varrho = \varrho_0 + \langle\hat{\chi}^\dagger\hat{\chi}\rangle + \mathcal{O}(1/\sqrt{N})\,, \tag{3.99}$$

with $\varrho_0 = |\psi_0|^2$, one finds that neither part is conserved separately in general. Note that this split requires $\langle\hat{\zeta}\rangle = \mathcal{O}(1/N)$, i.e., the modifications to the Gross-Pitaevskii equation (3.11) discussed in Sec. 3.2.2. Similarly, the full current can be split up [with $\varrho_0\boldsymbol{v}_0 = \Im(\psi_0^*\boldsymbol{\nabla}\psi_0)$]

$$\boldsymbol{j} = \varrho_0\boldsymbol{v}_0 + \frac{1}{2mi}\langle\hat{\chi}^\dagger\boldsymbol{\nabla}\hat{\chi} - \text{H.c.}\rangle + \mathcal{O}(1/\sqrt{N})\,, \tag{3.100}$$

and an average velocity $\boldsymbol{v}$ can be introduced via $\boldsymbol{j} = \varrho\boldsymbol{v}$. Thus the quantum backreaction $\boldsymbol{Q}$ can be defined unambiguously as the following additional contribution in an equation of motion for $\boldsymbol{j}$ analogous to the Euler equation

$$\frac{\partial}{\partial t}\boldsymbol{j} \;=\; \boldsymbol{f}(\boldsymbol{j},\varrho) + \boldsymbol{Q} + \mathcal{O}(1/\sqrt{N})\,, \tag{3.101}$$

where ($\boldsymbol{j} = \varrho\boldsymbol{v}$)

$$\boldsymbol{f}(\boldsymbol{j},\varrho) \;=\; -\boldsymbol{\nabla}\cdot(\varrho\boldsymbol{v}\otimes\boldsymbol{v}) + \frac{\varrho}{m}\boldsymbol{\nabla}\left(\frac{1}{2m}\frac{\boldsymbol{\nabla}^2\sqrt{\varrho}}{\sqrt{\varrho}} - V_{\text{ext}} - g\varrho\right) \tag{3.102}$$

denotes the usual classical term [that can be obtained from the classical continuity equation (3.45) and the Bernoulli equation (3.46)]. Formulation in terms of the conventional Euler equation yields

$$\left(\frac{\partial}{\partial t} + \boldsymbol{v}\cdot\boldsymbol{\nabla}\right)\boldsymbol{v} \;=\; -\frac{\boldsymbol{\nabla}}{m}\left(V_{\text{ext}} + g\varrho - \frac{1}{2m}\frac{\boldsymbol{\nabla}^2\sqrt{\varrho}}{\sqrt{\varrho}}\right) + \boldsymbol{Q}/\varrho + \mathcal{O}(1/\sqrt{N^3})\,. \tag{3.103}$$

The quantum backreaction $\boldsymbol{Q}$ can now be calculated by comparing the two equations above and expressing $\partial\boldsymbol{j}/\partial t$ in terms of the field operators via Eqs. (3.93) and (3.97)

$$\frac{\partial}{\partial t}\boldsymbol{j} \;=\; \frac{1}{4m^2}\left\langle\hat{\Psi}^\dagger\boldsymbol{\nabla}^3\hat{\Psi} - (\boldsymbol{\nabla}^2\hat{\Psi}^\dagger)\boldsymbol{\nabla}\hat{\Psi} + \text{H.c.}\right\rangle - \frac{\left\langle\hat{\Psi}^\dagger\hat{\Psi}\right\rangle}{m}\boldsymbol{\nabla}V_{\text{ext}} - \frac{1}{2gm}\boldsymbol{\nabla}\left\langle g^2(\hat{\Psi}^\dagger)^2\hat{\Psi}^2\right\rangle\,. \tag{3.104}$$

After insertion of the mean-field expansion (3.10), the leading contribution is obtained in the Thomas-Fermi limit

$$\begin{aligned}\boldsymbol{Q} \;=\;& \boldsymbol{\nabla}\cdot(\boldsymbol{v}\otimes\boldsymbol{j}_\chi + \boldsymbol{j}_\chi\otimes\boldsymbol{v} - \varrho_\chi\boldsymbol{v}\otimes\boldsymbol{v})\\ &-\frac{1}{2gm}\boldsymbol{\nabla}\left(g^2\left\langle 2|\psi_0^2|\hat{\chi}^\dagger\hat{\chi} + \psi_0^2(\hat{\chi}^\dagger)^2 + (\psi_0^*)^2\hat{\chi}^2\right\rangle\right)\\ &-\frac{1}{2m^2}\boldsymbol{\nabla}\cdot\left\langle(\boldsymbol{\nabla}\hat{\chi}^\dagger)\otimes\boldsymbol{\nabla}\hat{\chi} + \text{H.c.}\right\rangle\,,\end{aligned} \tag{3.105}$$

with $\varrho_\chi = \left\langle\hat{\chi}^\dagger\hat{\chi}\right\rangle$ and $\boldsymbol{j}_\chi = (1/m)\Im\left\langle\hat{\chi}^\dagger\boldsymbol{\nabla}\hat{\chi}\right\rangle$. Under the assumption that the relevant length scales λ for variations of, e.g., ϱ and g, are much larger than the healing length $\xi = (g\varrho_0 m)^{-1/2}$, the quantum pressure contributions $\boldsymbol{\nabla}^2\varrho_0$ and $[\boldsymbol{\nabla}\varrho_0]^2$ are neglected (Thomas-Fermi or local-density approximation). These contributions would, in particular, spoil the effective (local) geometry in Eq. (3.90).

3.6.2 Comparison with effective action technique

In order to compare the expression (3.105) with Eq. (3.92), it is necessary to identify ϕ and $G^{\mu\nu}$, see Sec. 3.4. Phonon modes with wavelength $\lambda \gg \xi$ are described by the action in

Eq. (3.90) in terms of the phase fluctuations ϕ provided that $G^{\mu\nu}$ is given by

$$G^{\mu\nu} = \frac{1}{g}\begin{pmatrix} 1 & \boldsymbol{v} \\ \boldsymbol{v} & \boldsymbol{v}\otimes\boldsymbol{v} - c_s^2\mathbf{1} \end{pmatrix}, \tag{3.106}$$

where $c_s^2 = g\varrho/m$ is the speed of sound, cf. Sec. 3.4.1 and Refs. [123–126, 129]. The density fluctuations $\delta\varrho$ are related to the phase fluctuations $\phi = \delta S$ via Eq. (3.49) with $\mathcal{N} = 2$.

If the quantum corrections to the Bernoulli equation (3.46) are now calculated using the effective-action method in Eq. (3.92) by inserting $\partial G^{\mu\nu}/\partial\varrho$ or $\partial g_{\text{eff}}^{\mu\nu}/\partial\varrho$, one obtains

$$\frac{\delta\mathcal{A}_{\text{eff}}}{\delta\varrho} = -\frac{1}{2}\langle(\boldsymbol{\nabla}\hat{\phi})^2\rangle\,. \tag{3.107}$$

Clearly, this result differs from expression (3.105) derived in the previous subsection. Moreover, it turns out that Eq. (3.105) contains contributions which are not part of the pseudo-energy-momentum tensor $\langle\hat{T}_{\mu\nu}\rangle$: even though the phonon flux $\boldsymbol{j}_\chi$ in the first line of Eq. (3.105) roughly corresponds to $\langle\delta\hat{\varrho}\boldsymbol{\nabla}\hat{\phi} + \text{H.c.}\rangle$, which indeed reproduces the mixed space-time components of the pseudo-energy-momentum tensor $\langle\hat{T}_{\mu\nu}\rangle$, the phonon density ϱ_χ contains $\langle\delta\hat{\varrho}^2\rangle$ which is part of $\langle\hat{T}_{\mu\nu}\rangle$ but also $\langle\hat{\phi}^2\rangle$ which is not. (Note that $\langle\hat{\phi}^2\rangle$ cannot be canceled by the other contributions.) The expectation value in the second line of Eq. (3.105) is basically $\langle\delta\hat{\varrho}^2\rangle_{\text{ren}}$ and thus part of $\langle\hat{T}_{\mu\nu}\rangle_{\text{ren}}$. Finally, the expression $\langle(\boldsymbol{\nabla}\hat{\chi}^\dagger)\otimes\boldsymbol{\nabla}\hat{\chi} + \text{H.c.}\rangle$ in the last line of Eq. (3.105) contains $\langle\boldsymbol{\nabla}\hat{\phi}\otimes\boldsymbol{\nabla}\hat{\phi}\rangle$ which does occur in $\langle\hat{T}_{\mu\nu}\rangle$, but also $\langle\boldsymbol{\nabla}\delta\hat{\varrho}\otimes\boldsymbol{\nabla}\delta\hat{\varrho}\rangle$, which does not. One could argue that the latter term ought to be neglected in the Thomas-Fermi or local-density approximation, since it is on the same footing as the quantum pressure contributions $\boldsymbol{\nabla}^2\varrho$ and $[\boldsymbol{\nabla}\varrho]^2$, but it turns out that this expectation value yields cut-off-dependent contributions of the same order of magnitude as the other terms, see Section 3.6.5 below.

3.6.3 Choice of classical background

In order to understand the disagreement between expressions (3.105) and (3.107) and to demonstrate the possible dependence of the explicit expression for the quantum backreaction on the choice of the classical background, two particular backgrounds will be considered in the following. Firstly, it shall be given by the density and current generated by the condensate fraction ψ_0 of the field operator $\hat{\Psi}$, cf. Eqs. (3.99) and (3.100). And secondly, (the expectation values of) the full density and the velocity potential are considered as (classical) background.

In the first case, the background current is given by

$$\boldsymbol{j}_0 = \varrho_0\boldsymbol{v}_0 = \frac{1}{2mi}\left(\psi_0^*\boldsymbol{\nabla}\psi_0 - \text{C.c.}\right) = \boldsymbol{j} - \boldsymbol{j}_\chi\,, \tag{3.108}$$

where C.c. means complex conjugation. Note that the exact splitting $\boldsymbol{j} = \boldsymbol{j}_0 + \boldsymbol{j}_\chi$ is not unique and thus the classical background $\boldsymbol{j}_0$ and the fluctuation $\boldsymbol{j}_\chi$ are (in contrast to $\boldsymbol{j}$) not directly measurable (for $g > 0$), cf. the remark on the Gross-Pitaevskii equation (3.94). The evolution of the phonon flux can be inferred from the Bogoliubov-de Gennes equation (3.95)

$$\begin{aligned}\frac{\partial}{\partial t}\boldsymbol{j}_\chi &= \frac{1}{4m^2}\boldsymbol{\nabla}^3\varrho_\chi - \frac{1}{2m^2}\boldsymbol{\nabla}\cdot\left\langle(\boldsymbol{\nabla}\hat{\chi}^\dagger)\otimes\boldsymbol{\nabla}\hat{\chi} + \text{H.c.}\right\rangle - \frac{\varrho_\chi}{m}\boldsymbol{\nabla}\left(V_{\text{ext}} + 2\varrho_0 g\right) \\ &\quad - \frac{1}{2m}\left[\left\langle\hat{\chi}^2\right\rangle\boldsymbol{\nabla}\left(g\left(\psi_0^*\right)^2\right) + \text{H.c.}\right], \end{aligned} \tag{3.109}$$

which enables us to derive the evolution equation for the condensate part via the subtraction $\boldsymbol{j}_0 = \boldsymbol{j} - \boldsymbol{j}_\chi$

$$\frac{\partial}{\partial t}\boldsymbol{j}_0 = \boldsymbol{f}(\varrho_0, \boldsymbol{v}_0) - \frac{2\varrho_0}{m}\boldsymbol{\nabla}(g\varrho_\chi) - \frac{1}{2m}\left[\left(\psi_0^*\right)^2\boldsymbol{\nabla}\left(g\left\langle\hat{\chi}^2\right\rangle\right) + \text{H.c.}\right], \tag{3.110}$$

which is the same result as obtained from the modified Gross-Pitaevskii equation (3.94). However, the interpretation of the right hand side of the equation above as a force density is not straight-forward, since the equation of continuity for ϱ_0 and $\boldsymbol{j}_0$ is not satisfied

$$\dot{\varrho}_0 + \boldsymbol{\nabla}\cdot\boldsymbol{j}_0 = \frac{i}{m}\left\langle\psi_0^2\left(\hat{\chi}^\dagger\right)^2 - \left(\psi_0^*\right)^2\hat{\chi}^2\right\rangle. \tag{3.111}$$

This means that an acceleration of the atoms in the condensate caused by a real force could make them leave the condensate or induce a change in $\boldsymbol{j}_0$ and it is hard to disentangle these two effects. Roughly speaking, choosing the condensate part $\boldsymbol{j}_0$ (which is not measurable and not conserved) as the classical background would correspond to the artificial variable Y of the toy model discussed in Appendix B, whereas the full (measurable and conserved) current $\boldsymbol{j}$ corresponds to X.

In the second case, the expectation values of the density and the velocity potential are taken as background

$$\begin{aligned}\hat{\phi} &= \langle\hat{\phi}\rangle + \delta\hat{\phi} = \phi_{\text{b}} + \delta\hat{\phi}, \\ \hat{\varrho} &= \langle\hat{\varrho}\rangle + \delta\hat{\varrho} = \varrho_{\text{b}} + \delta\hat{\varrho}. \end{aligned} \tag{3.112}$$

Note that, in contrast to the full density which is a well-defined and measurable quantity, the velocity potential, $\hat{\phi}$, is not[7]. It can be introduced via the following ansatz for the full field operator [cf. Eq. (3.43)]

$$\hat{\Psi} = e^{i\hat{\phi}}\sqrt{\hat{\varrho}}. \tag{3.113}$$

Since $\hat{\phi}$ and $\hat{\varrho}$ do not commute, other forms such as $\hat{\Psi} = \sqrt{\hat{\varrho}}\,e^{i\hat{\phi}}$ would not generate a self-adjoint phase $\hat{\phi}$ and comply with $\hat{\varrho} = \hat{\Psi}^\dagger\hat{\Psi}$. Insertion of the above ansatz into the expression for the full current (3.97) yields

---

[7] The problem that the commutator between density and phase operators, $[\hat{\varrho}(\boldsymbol{r}), \hat{\phi}(\boldsymbol{r}')] = -i\delta(\boldsymbol{r} - \boldsymbol{r}')$, leads to fundamental inconsistencies if one takes the matrix elements of the space integrals of both sides in the number basis was first pointed out by Fröhlich [130]. The commutator makes proper sense only if coarse-grained over a volume with a large enough number of particles, and not locally, i.e., in arbitrarily small volumina, see also [131].

$$\boldsymbol{j} = \frac{1}{m} \left\langle \sqrt{\hat{\varrho}}\, \boldsymbol{\nabla}\hat{\phi}\, \sqrt{\hat{\varrho}} \right\rangle = \varrho_b \boldsymbol{\nabla}\phi_b + \frac{1}{2} \left\langle \delta\hat{\varrho} \boldsymbol{\nabla} \delta\hat{\phi} + \text{H.c.} \right\rangle , \tag{3.114}$$

where terms of third and higher order are neglected. In order to calculate the quantum backreaction in this formulation, it is convenient to express density and phase in terms of the former split (3.10) defined with respect to the condensate fraction of the field operator [cf. also Eqs. (3.99), (3.100)]

$$\begin{aligned} \phi_b &= \phi_0 + \frac{1}{4}\frac{\langle \delta\hat{\varrho}\delta\hat{\phi}\rangle}{\varrho_0} + \frac{1}{4}\frac{\langle \delta\hat{\phi}\delta\hat{\varrho}\rangle}{\varrho_0} + \mathcal{O}(\delta^3) , \\ \varrho_b &= \varrho_0 + \varrho_0 \langle \delta\hat{\phi}^2\rangle + \frac{1}{4}\frac{\langle \delta\hat{\varrho}^2\rangle}{\varrho_0} + \frac{i}{2}\langle[\delta\hat{\phi}, \delta\hat{\varrho}]\rangle + \mathcal{O}(\delta^3) . \end{aligned} \tag{3.115}$$

where $\varrho_0 = |\psi_0|^2$ and $\phi_0 = \arg\psi_0$. The linearized quantum fluctuations $\delta\hat{\phi}$ and $\delta\hat{\varrho}$ are first-order corrections to the classical backgrounds and thus coincide (to leading order) for both expansions, cf. Appendix C. Note that the last term in the second line of Eqs. (3.115), $\propto \langle[\delta\hat{\phi}, \delta\hat{\varrho}]\rangle$, is the equal-time commutator of two conjugate variables at the same spatial position. Since the background densities ϱ_0 and ϱ_b should be finite, the divergence of the commutator must be canceled by the remaining (second-order) contributions, i.e., by $\langle \delta\hat{\phi}^2\rangle$ and $\langle \delta\hat{\varrho}^2\rangle$. In particular, this also means that the quantum backreaction (3.107), which is proportional to $\langle(\boldsymbol{\nabla}\delta\hat{\phi})^2\rangle$, is presumably ultraviolet divergent and not small *a priori*.

The inconsistencies arising when relating the two mean-field decompositions (3.10) and (3.112) already indicate that the outcome of higher-order expectation values crucially depends on the specific choice of the classical background. Since the quantum backreaction is second order in the fluctuations, special care must be taken.

3.6.4 Problems of Effective-Action Technique

After the demonstration of problems of the effective-action method for deducing the quantum backreaction, the reasons for this will be studied in more detail now. The full action governing the dynamics of the fundamental fields Ψ^* and Ψ reads

$$\mathcal{L}^{\Psi} = i\Psi^*\dot{\Psi} - \Psi^* \left(-\frac{1}{2}\boldsymbol{\nabla}^2 + V_{\text{ext}} + \frac{g}{2}\Psi^*\Psi \right) \Psi . \tag{3.116}$$

Linearization $\Psi = \psi_{\text{c}} + \chi$ yields the effective second-order action generating the Bogoliubov-de Gennes equations (3.95)

$$\mathcal{L}_{\text{eff}}^{\chi} = i\chi^*\dot{\chi} - \chi^* \left(-\frac{1}{2}\boldsymbol{\nabla}^2 + V_{\text{ext}} + 2g\,|\psi_{\text{c}}^2| \right) \chi - \left[\frac{g}{2}\,(\psi_{\text{c}}^*)^2\chi^2 + \text{H.c.} \right] . \tag{3.117}$$

Now $\delta\mathcal{A}_{\text{eff}}^{\chi}/\delta\varrho_0$ indeed yields the correct backreaction (3.110) in the condensate formulation.

However, when starting with the action in terms of the non-fundamental variable ϕ

$$\mathcal{L} = -\varrho\left(\dot{\phi} + \frac{1}{2}(\boldsymbol{\nabla}\phi)^2\right) - \epsilon[\varrho] - V_{\rm ext}\varrho\,, \tag{3.118}$$

with $\epsilon[\varrho]$ denoting the internal energy density, the quantum corrections to the equation of continuity $\delta\mathcal{A}_{\rm eff}/\delta\phi_{\rm b}$ are reproduced correctly, but the derived quantum backreaction contribution to the Bernoulli equation $\delta\mathcal{A}_{\rm eff}/\delta\varrho_{\rm b}$ is problematic.

Why is the effective-action method working for the fundamental field Ψ, but not for the non-fundamental variable ϕ? The quantized fundamental field $\hat{\Psi}$ satisfies the equation of motion (3.93) as derived from the above action and possesses a well-defined linearization via the mean-field expansion (3.10). One of the main assumptions of the effective-action method is a similar procedure for the variable ϕ, i.e., the existence of a well-defined and linearizable full quantum operator $\hat{\phi}$ satisfying the Bernoulli equation (for large length scales)

$$\frac{\partial}{\partial t}\hat{\phi} + \frac{1}{2}(\boldsymbol{\nabla}\hat{\phi})^2 + h[\hat{\varrho}] \overset{?}{=} 0\,, \tag{3.119}$$

where $h = {\rm d}\epsilon/{\rm d}\varrho + V_{\rm ext}$. The problem is that the commutator of $\hat{\varrho}$ and $\hat{\phi}$ at the same position diverges and hence the quantum Madelung ansatz in Eq. (3.113) is singular, see Footnote 7 on Page 66. As a result, the above quantum Bernoulli equation is not well-defined (in contrast to the equation of continuity), i.e., insertion of the quantum Madelung ansatz in Eq. (3.113) into Eq. (3.93) generates divergences [130,131].

In order to study these divergences by means of a simple example, let us consider the generalized Bose-Hubbard Hamiltonian (see also Sec. 4.1)

$$\hat{H} = \alpha\sum_{<ij>}(\hat{\Psi}_i^\dagger\hat{\Psi}_j + \text{H.c.}) + \sum_i(\beta\hat{n}_i + \gamma\hat{n}_i^2)\,, \tag{3.120}$$

where $< ij >$ denote nearest neighbors and $\hat{n}_i = \hat{\Psi}_i^\dagger\hat{\Psi}_i$ the filling factor of one lattice site i. In the usual continuum limit, this Hamiltonian generates Eq. (3.93). Inserting the quantum Madelung ansatz in Eq. (3.113), however, the problem of operator ordering arises and the (for the Bernoulli equation) relevant term reads

$$\hat{H}_\phi = \frac{1}{4}\sum_i\sqrt{\hat{n}_i(\hat{n}_i+1)}\,(\boldsymbol{\nabla}\hat{\phi})_i^2 + \text{H.c.}\,, \tag{3.121}$$

with the replacement $\hat{n}_i + 1$ instead of $\hat{n}_i$ being one effect of the non-commutativity. In the superfluid phase with large filling $n \gg 1$, one obtains the following leading correction to the equation of motion

$$\frac{\partial}{\partial t}\hat{\phi} + \frac{1}{2}(\boldsymbol{\nabla}\hat{\phi})^2 + \mu[\hat{\varrho}] + \frac{1}{\hat{n}}\,\frac{(\boldsymbol{\nabla}\hat{\phi})^2}{16}\,\frac{1}{\hat{n}} = \mathcal{O}\left(\frac{1}{n^3}\right)\,, \tag{3.122}$$

which depends on microscopic details (such as the filling).

By means of this simple example, it already becomes apparent that the various limiting procedures such as the quantization and subsequent mean-field expansion, the variable transformation $(\Psi^*, \Psi) \leftrightarrow (\varrho, \phi)$, and the linearization for small fluctuations, as well as continuum limit do not commute in general – which explains the problems of the effective-action method for deducing the quantum backreaction. The variable transformation $(\Psi^*, \Psi) \leftrightarrow (\varrho, \phi)$ is applicable to the zeroth-order equations of motion for the classical background as well as to the first-order dynamics of the linearized fluctuations – but the quantum backreaction is a second-order effect, where the aforementioned difficulties arise.

3.6.5 Cut-off Dependence

As mentioned in the introduction of this section, another critical issue is the ultraviolet divergence of the pseudo-energy-momentum tensor $\langle \hat{T}_{\mu\nu} \rangle$. Extrapolating the low-energy effective action in Eq. (3.90) to large momenta k, the expectation values $\langle \delta\hat{\varrho}^2 \rangle$ and $\langle \hat{\phi}^2 \rangle$ entering ϱ_χ would diverge. For Bose-Einstein condensates, one may infer the deviations from Eq. (3.90) at large k from the Bogoliubov-de Gennes equation (3.95), see also Sec. 3.2. Assuming a static and homogeneous background (which should be a good approximation for large k), a normal-mode expansion yields [cf. Eq. (3.15)]

$$\hat{\chi}_{\boldsymbol{k}} = \sqrt{\frac{\boldsymbol{k}^2}{2m\omega_{\boldsymbol{k}}}} \left[\left(\frac{1}{2} - \frac{m\omega_{\boldsymbol{k}}}{\boldsymbol{k}^2} \right) \hat{a}^\dagger_{\boldsymbol{k}} + \left(\frac{1}{2} + \frac{m\omega_{\boldsymbol{k}}}{\boldsymbol{k}^2} \right) \hat{a}_{\boldsymbol{k}} \right] , \tag{3.123}$$

where $\hat{a}^\dagger_{\boldsymbol{k}}$ and $\hat{a}_{\boldsymbol{k}}$ are the creation and annihilation operators of the phonons, respectively, and the frequency $\omega_{\boldsymbol{k}}$ is determined by the Bogoliubov dispersion relation, cf. Eq. (3.16).

$$\omega^2_{\boldsymbol{k}} = g\varrho\, \boldsymbol{k}^2 + \frac{\boldsymbol{k}^4}{4} . \tag{3.124}$$

Using a linear dispersion $\omega^2_{\boldsymbol{k}} \propto \boldsymbol{k}^2$ instead, expectation values such as $\langle \hat{\chi}^\dagger \hat{\chi} \rangle$ would be ultraviolet divergent, but the correct dispersion relation implies $\hat{\chi}_{\boldsymbol{k}} \sim \hat{a}^\dagger_{\boldsymbol{k}}\, g\varrho/\boldsymbol{k}^2 + \hat{a}_{\boldsymbol{k}}$ for large $\boldsymbol{k}^2$, and hence $\langle \hat{\chi}^\dagger \hat{\chi} \rangle$ is ultraviolet finite in three and lower spatial dimensions. Thus the healing length ξ acts as an effective cut-off $k^{\rm cut}_\xi$ for high energies.

Unfortunately, the quadratic decrease for large k in Eq. (3.123), $\hat{\chi}_{\boldsymbol{k}} \sim \hat{a}^\dagger_{\boldsymbol{k}}\, g\varrho/\boldsymbol{k}^2 + \hat{a}_{\boldsymbol{k}}$, is not sufficient for rendering the other expectation values (i.e., apart from ϱ_χ and $\boldsymbol{j}_\chi$) in Eq. (3.105) ultraviolet finite in three spatial dimensions. This ultraviolet divergence indicates a failure of the s-wave pseudo-potential (3.3) used in Eq. (3.93) at large wavenumbers $\boldsymbol{k}$ and can be eliminated by a more appropriate two-particle interaction potential $V_{\rm int}(\boldsymbol{r} - \boldsymbol{r}')$, see Sec. 3.2 and Refs. [88, 97, 132, 133]. Introducing another ultraviolet cut-off wavenumber $k^{\rm cut}_s$ related to the breakdown of the s-wave pseudo-potential, we obtain $\langle (\boldsymbol{\nabla}\hat{\chi}^\dagger) \otimes \boldsymbol{\nabla}\hat{\chi} + \text{H.c.} \rangle \sim g^2 \varrho^2\, k^{\rm cut}_s$ and $\langle \hat{\chi}^2 \rangle \sim g\varrho\, k^{\rm cut}_s$.

In summary, there are two different cut-off wavenumbers: the first one, $k_\xi^{\rm cut}$, is associated to the breakdown of the effective Lorentz invariance (change of dispersion relation from linear to quadratic) and renders some – but not all – of the naively divergent expectation values finite. The second wavenumber, $k_s^{\rm cut}$, describes the cut-off for all (remaining) ultraviolet divergences. In dilute Bose-Einstein condensates, these two scales are vastly different by definition (diluteness)

$$k_{\rm UV}^{\rm cut} \,=\, k_s^{\rm cut} \,\gg\, k_\xi^{\rm cut} \,=\, k_{\rm Lorentz}^{\rm cut}\,. \tag{3.125}$$

Note the the opposite relation $k_{\rm Lorentz}^{\rm cut} \gg k_{\rm UV}^{\rm cut}$ is very unnatural since it is known that every quantum field theory which has the usual properties such as locality and Lorentz invariance etc., must have ultraviolet divergences (e.g., in the two-point function).

The renormalization of the cut-off-dependent terms is different for the two cases: the $k_s^{\rm cut}$-contributions can be absorbed by a ϱ-independent renormalization of the coupling g, see Eq. (3.23), whereas the $k_\xi^{\rm cut}$-contributions depend on the density in a non-trivial way and thus lead to a renormalization of the pressure and the chemical potential etc., see the example in the following subsection.

3.6.6 Simple Example

In order to provide an explicit example for the quantum backreaction term in Eq. (3.105), without facing the ultraviolet problem, let us consider a quasi-one-dimensional condensate [91, 134], where all the involved quantities are ultraviolet finite. In accordance with general considerations [135], the phonon density ϱ_χ is infrared divergent in one spatial dimension, therefore inducing finite-size effects. Nevertheless, in certain situations, one is able to derive a closed local expression for the quantum backreaction term Q: assume a completely static condensate, $\boldsymbol{v} = 0$, in effectively one spatial dimension, while the spatial density, ϱ, and possibly also the coupling, g, may vary. Furthermore, since spatial variations of ϱ and g occur on length scales λ much larger than the healing length, only the leading terms in $\xi/\lambda \ll 1$, will be kept, i.e., the variations of ϱ and g will be neglected in the calculation of the expectation values (local-density approximation). In this case, the quantum backreaction term Q simplifies considerably and yields (in effectively one spatial dimension, where $g \equiv g_{\rm 1D}$ and $\varrho \equiv \varrho_{\rm 1D}$ now both refer to the one-dimensional quantities)

$$\begin{aligned} Q \,&=\, -\frac{\nabla}{m^2}\left\langle(\nabla\hat\chi^\dagger)\nabla\hat\chi\right\rangle - \frac{1}{2gm}\nabla\left(g^2\varrho\left\langle 2\hat\chi^\dagger\hat\chi + (\hat\chi^\dagger)^2 + \hat\chi^2\right\rangle\right) \\ &=\, -\frac{\nabla}{m^2}\left(\frac{1}{3\pi}\,(gm\varrho)^{3/2}\right) + \frac{1}{2\pi g m^2}\nabla\left(g^{5/2}(m\varrho)^{3/2}\right) + \mathcal{O}(\xi^2/\lambda^2) \\ &=\, \frac{\varrho}{2\pi m}\,\nabla\sqrt{g^3 m\varrho} + \mathcal{O}(\xi^2/\lambda^2)\,. \end{aligned} \tag{3.126}$$

It turns out that the infrared divergences of $2\langle\hat\chi^\dagger\hat\chi\rangle$ and $\langle(\hat\chi^\dagger)^2 + \hat\chi^2\rangle$ cancel each other such that the resulting expression is not only ultraviolet but also infrared finite. Note that the sign of Q is positive and hence opposite to that of the pure phonon density contribution $\langle\hat{\chi}^\dagger\hat{\chi}\rangle$, which again illustrates the importance of the term $\langle(\hat{\chi}^\dagger)^2+\hat{\chi}^2\rangle$.

A possible experimental signature of the quantum backreaction term Q calculated above, is the change incurred on the static Thomas-Fermi solution of the Euler equation (3.103) for the density distribution (cf. [73, 76, 97, 132, 133, 136–138])

$$\varrho_{\rm 1D} = \frac{\mu - V_{\rm ext}}{g_{\rm 1D}} + \frac{\sqrt{\mu - V_{\rm ext}}}{2\pi} + \mathcal{O}(1/\sqrt{N})\,, \tag{3.127}$$

with μ denoting the (constant) chemical potential. The classical $[\mathcal{O}(N)]$ density profile $\varrho_{\rm cl} = (\mu - V_{\rm ext})/g_{\rm 1D}$ acquires non-trivial quantum $[\mathcal{O}(N^0)]$ corrections $\varrho_Q = \sqrt{\mu - V_{\rm ext}}/2\pi$, where the small parameter is the ratio of the inter-particle distance $1/\varrho = \mathcal{O}(1/N)$ over the healing length $\xi = \mathcal{O}(N^0)$. Note that the quantum backreaction term ϱ_Q in the above split $\varrho = \varrho_{\rm cl} + \varrho_Q$ should neither be confused with the phonon density ϱ_χ in $\varrho = \varrho_0 + \varrho_\chi$ (remember that ϱ_χ is infrared divergent and hence contains finite-size effects) nor with the quantum pressure contribution $\propto \boldsymbol{\nabla}^2\sqrt{\varrho}$ in Eq. (3.103).

An explicit evaluation of the change ΔR of the Thomas-Fermi size (half the full length), where $\mu = V_{\rm ext}$, of a quasi-one-dimensional Bose-Einstein condensate induced by backreaction yields from Eq. (3.127) $\Delta R = -2^{-5/2}(\omega_\perp/\omega_z)a_s$. (The quasi-one-dimensional coupling constant $g_{\rm 1D}$ is related to the three-dimensional s-wave scattering length a_s and the perpendicular harmonic trapping $\omega_\perp$ by $g_{\rm 1D} = 2a_s\omega_\perp$ [134].) In units of the classical size $R_{\rm cl} = (3a_sN\omega_\perp/\omega_z^2)^{1/3}$, one has

$$\frac{\Delta R}{R_{\rm cl}} = -\frac{1}{4\sqrt{2}}\left(\frac{1}{3N}\right)^{1/3}\left(\frac{\omega_\perp}{\omega_z}\frac{a_s}{a_z}\right)^{2/3}, \tag{3.128}$$

where $a_z = 1/\sqrt{\omega_z}$ describes the longitudinal harmonic trapping. In quasi-one-dimensional condensates, backreaction thus leads to a *shrinking* of the cloud relative to the classical expectation – whereas in three spatial dimensions one has the opposite effect [73, 76, 97, 132, 133, 136–138]. For reasonably realistic experimental parameters, the effect of backreaction should be measurable; for $N \simeq 10^3$, $\omega_\perp/\omega_z \simeq 10^3$, and $a_s/a_z \simeq 10^{-3}$, one obtains $|\Delta R/R_{\rm cl}| \simeq 1\%$.

3.7 Discussion

In this Chapter, we discussed several aspects of quantum fluctuations in dilute atomic (or molecular) Bose-Einstein condensates. First of all, we scrutinized two frequently-used approximations (which we also employed in the subsequent sections) in Section 3.2: firstly, the approximation of the two-particle potential by a contact interaction, $V_{\rm int}(\boldsymbol{r}-\boldsymbol{r}') \approx g\delta(\boldsymbol{r}-\boldsymbol{r}')$. This simplification is mainly motivated by the dilute character of the gas cloud, where the typical inter-particle separation is much larger than the effective interaction range.

And secondly, a mean-field ansatz is adopted; the full field operator is split into a classical background (e.g., the condensate fraction) and small quantum fluctuations. It is generally believed that this split becomes more accurate as the particle number is increased.

For a *finite-range two-particle interaction* potential, we were able to derive a mean-field expansion and investigate its accuracy for several scaling behaviors of the potential with particle number in Section 3.2. Starting point for our calculation was the Heisenberg equation of motion (3.8) with arbitrary, weak, finite-range two-particle interaction potentials, $V_{\rm int}(\boldsymbol{r}-\boldsymbol{r}')$, obeying a suitable scaling behavior in the large-N limit. Employing the particle-number-conserving mean-field expansion (3.10), we derived the Gross-Pitaevskii equation (3.11) for the classical background ψ_0, the Bogoliubov-de Gennes equation (3.12) for the linear fluctuations $\hat{\chi}$ and the corresponding equation of motion (3.13) for the higher-order corrections $\hat{\zeta}$. It turns out that, although the gas rapidly becomes more dilute in the large $N\uparrow\infty$ limit (the gas parameter scales as $\sqrt{g^3\varrho}\propto 1/N$), the validity of the mean-field approximation strongly depends on the detailed scaling behavior of the particle interaction potential. Therefore, care needs to be exercised in applying the mean-field approximation – if one does not take the detailed structure of the bare interaction potential into account, one possibly encounters inconsistencies with the basic assumptions the mean-field expansion is built on.

Apart from exploring limits of the mean-field approximation, the presented derivation facilitates the calculation of the impact of microscopic details of the interaction beyond the s-wave scattering approximation[8]. Another advantage of the presented approach is the natural emergence and *ab initio* derivation of the cut-off $k_{\rm cut}$ as a microscopic property of the interaction potential – instead of a cut-off $k_{\rm cut}$ introduced *ad hoc* for the regularization of pseudo-potentials $\propto\delta^3(\boldsymbol{r}-\boldsymbol{r}')$, see, e.g., [140]. However, one should bear in mind that the presented method requires weak potentials – if non-perturbative effects such as bound states or total reflection at a finite radius become important, the direct mean-field ansatz (3.10) cannot be applied in this way. Instead of homogeneous plane waves, one has to start from atomic/molecular eigenfunctions in this case and the ansatz (3.10) can only work as a low-energy effective description. Nevertheless, if it is possible to divide a non-perturbative $V_{\rm int}(\boldsymbol{r}-\boldsymbol{r}')$ into a strong ultra-short-range part and a comparably weak remaining contribution, which is more spread out, the presented analysis should be applicable to the latter part, provided the ultra-short-range part can be replaced in an adequate manner by an integrable (pseudo-)potential. As an example for the application to the non-local interactions, a dipole-dipole potential was considered in 3.2.3.

By placing a Bose-Einstein condensate in a highly-anisotropic trap, effectively *lower-dimensional geometries* can be realized. If the trap frequency in the strongly-confined directions is much larger than all internal (mesoscopic) scales of the condensate, such as the inverse healing length $1/\xi$, the motion will be frozen to the ground state in those directions, cf. Sec. 3.3. On the other hand, for the Gross-Pitaevskii Hamiltonian with its quartic coupling (two-body interactions) to apply, the extend of the condensate in all directions must be much larger than the (microscopic) s-wave scattering length, such that the interactions can still be described as three-dimensional scattering.

---

[8] The inadequacy of a_s as the sole parameter to describe Bose-Einstein condensates has also been discussed by S. Geltman and A. Bambini [139]. However, they do not address the actual applicability of the mean-field approach.

In Section 3.4, a more general power-law interaction term $\propto g|\Psi|^{2\mathcal{N}}$ was considered, where we performed a canonic transformation to density and phase for general D-dimensional setups. An *effective space-time metric* for the low-energy phase fluctuations emerges from the linearized equations of motion. The field equations can be formulated covariantly and the methods and tools known from general relativity can be employed. In particular, we diagonalized the effective metric by transforming from laboratory to comoving coordinates. For certain combinations of dimension D and coupling power $\mathcal{N}$, the effective metric becomes flat. It turns out that the full field operator (in a harmonic trapping potential) possesses perfectly-scaling solutions exactly if the effective metric is flat in terms of the comoving coordinates.

Employing this effective space-time metric, we can adopt methods and concepts known from general relativity. In particular, we discussed the evolution of the phonons during the *free expansion of Bose-Einstein condensates* in Section 3.5. This process is interesting for two reasons: firstly, it is exactly the situation occurring in time-of-flight imaging, where the expansion is used to amplify any spatial details of the condensate. And secondly, it bears strong analogies to cosmic inflation, cf. Chapter 2. Similarly to the expanding universe, an effective sonic horizon forms in the expanding gas cloud of a Bose-Einstein condensate; two points at fixed (comoving) spatial positions whose distance exceeds the horizon size cannot be connected anymore by (low-energy) phonons, cf. Section 3.5.1. The formation of this effective horizon implies the amplification of the quantum fluctuations (horizon-crossing and freezing) already known from cosmology, which has been calculated explicitly for quasi-two-dimensional and three-dimensional condensates with quartic coupling. For some realistic experimental values of Bose-Einstein condensate, the density contrast generated by the (zero-temperature) vacuum effect turns out to be on the percent level, see Subsection 3.5.4.

Of course, initial thermal fluctuations would – provided that there is no thermalization during the expansion of the condensate – also be amplified by basically the same mechanism as the quantum fluctuations. In order to ensure that the quantum fluctuations are larger than the (initial) thermal fluctuations, the temperature must be small enough such that the thermal occupation of the phonon modes under consideration is negligible. For the parameters used in Sec. 3.5.4, the relevant temperature scales are $T(1/\xi) = 0.1\,\mathrm{nK}$ for the quasi-two-dimensional case and $T(\kappa) = 3.9\,\mathrm{nK}$ for the three-dimensional condensate, respectively. By increasing the particle number and/or the trapping frequency, the requirements regarding the experimental temperature can be relieved. (Another way to discriminate between thermal and quantum fluctuations is the spectrum; the different frequency dependences of the thermal occupation numbers and the amplified fluctuations should allow to disentangle these two effects.)

In summary, expanding Bose-Einstein condensates facilitate the experimental simulation of exotic effects of quantum fields in curved space-times. On the other hand, the amplification mechanism under consideration sets the ultimate quantum limit of accuracy for time-of-flight experiments: no matter how smooth the initial cloud can be prepared, the frozen and amplified quantum ground-state fluctuations will always generate noticeable density perturbations.

The analogy between phonons in a superfluid (e.g., a Bose-Einstein condensate) and photons in a curved space-time is only of kinematical nature; the impact of the quantum fluctuations onto the dynamics of the classical background is not included [not even if the modified Gross-Pitaevskii equation (3.22) was employed]. In view of the (linear) covariant, effective space-time formulation, introduced in Sec. 3.4, one is tempted to use methods of general relativity, such as the effective-action technique, in order to obtain the *quantum backreaction*. On the other hand, we know the full microscopic action for Bose-Einstein condensates. This action extends beyond the linearized description underlying the effective space-time approach.

In Section 3.6, we calculated the quantum backreaction *ab initio* from the Heisenberg equations for the full field operator $\hat{\Psi}$. We compared our findings with the result obtained using the effective action method. Even though the explicit form of the quantum backreaction terms depends on the definition of the classical background, the effective-action method is not sufficient for deriving the correct result in the general case (i.e., independent of the choice of variables etc.). The knowledge of the classical (macroscopic) equation of motion – such as the Bernoulli equation – may be sufficient for deriving the first-order dynamics of the linearized quantum fluctuations (phonons), but the quantum backreaction as a second-order effect cannot be obtained without further knowledge of the microscopic structure (e.g., operator ordering).

It is tempting to compare these findings to gravity, where we also know the classical equations of motion only

$$R_{\mu\nu} - \frac{1}{2} g_{\mu\nu} R = \kappa T_{\mu\nu} , \tag{3.129}$$

which – in analogy to the Bernoulli equation – might yield the correct first-order equations of motion for the linearized gravitons, but perhaps not their (second-order) quantum backreaction. Another potentially interesting point of comparison is the existence of two different high-energy scales – one associated to the breakdown of Lorentz invariance $k_\xi^{\rm cut} = k_{\rm Lorentz}^{\rm cut}$ and the other $k_{\rm UV}^{\rm cut} = k_s^{\rm cut}$ to the ultraviolet cut-off – as well as the question of whether one of the two (or both) correspond to the Planck scale in gravity.

The dominant $\mathcal{O}(\xi/\lambda)$ quantum backreaction contributions, like those in Eq. (3.127) depend on the healing length as the lower ultraviolet cut-off and hence cannot be derived from the low-energy effective action in Eq. (3.90) using a covariant (i.e., cut-off independent) regularization scheme, which does not take into account details of microscopic physics [represented, for example, in the quasi-particle dispersion relation (3.77)]. Note that the leading $\mathcal{O}(\xi/\lambda)$ quantum correction to the pressure could be identified with a cosmological term, $\langle\hat{T}_{\mu\nu}\rangle = \Lambda\, g_{\mu\nu}$ in Eq. (3.92), provided that Λ is not constant but depends on g and ϱ. (In general relativity, the Einstein equations demand Λ to be constant.)

As became evident from the remarks after Eq. (3.106), the knowledge of the expectation value of the pseudo-energy-momentum tensor $\langle\hat{T}_{\mu\nu}\rangle$ is not sufficient for determining the quantum backreaction effects in general. Even though $\langle\hat{T}_{\mu\nu}\rangle$ is a useful concept for describing the phonon kinematics (at low energies), and one may identify certain contributions in the quantum backreaction (3.105) with terms occurring in $\langle\hat{T}_{\mu\nu}\rangle$ in curved space-times (e.g., next-to-leading-order terms in ξ/λ in the gradient expansion), we have seen that it does not represent the full dynamics. Related limitations of the classical pseudo-energy-momentum tensor have been discussed in [114].

In general, the quantum backreaction corrections Q to the Euler equation in Eq. (3.103) cannot be represented as the gradient of some local potential, cf. Eq. (3.105). Hence they may effectively generate vorticity and might serve as the seeds for vortex nucleation. Note that this effect cannot be observed in the "force" density in the condensate formulation (3.110), i.e., vorticity seeds can only be generated by extracting atoms from the condensate.

In contrast to the three-dimensional case (see, e.g., [73, 76, 97, 132, 133, 136–138]), the quantum backreaction corrections given by Eq. (3.126) *diminish* the pressure in condensates that can be described by Eq. (3.93) in (quasi) one spatial dimension. This is a direct consequence of the so-called "anomalous" term $\langle(\hat{\chi}^\dagger)^2 + \hat{\chi}^2\rangle$ in Eq. (3.126), which – together with the cancellation of the infrared divergence – clearly demonstrates that it cannot be neglected in general. We emphasize that even though Eqs. (3.126)-(3.128) describe the *static* quantum backreaction corrections to the ground state, which can be calculated by an alternative method [97, 132, 133] as well, the expression in Eq. (3.105) is valid for more general dynamical situations, such as expanding condensates.

4 On quantum phase transitions

Fostered by the tremendous progress in the experimental capabilities, there has been increasing interest in quantum phenomena at low temperatures in general and quantum criticality in particular. In view of the creation of entanglement [141, 142], quantum phase transitions are also relevant for quantum information (the continuum limit of an adiabatic quantum algorithm represents just a sweep through a quantum phase transition [143]).

Typically, quantum phase transition can be described by a Hamiltonian consisting of two competing contributions [13, 14]

$$\hat{H} = \hat{H}_0 + g\hat{H}_1 \,, \tag{4.1}$$

where $g \in [0, \infty)$ is an external parameter, e.g., the modulus of the magnetic field. For $g = 0$, the properties of the system are solely determined by the unperturbed part $\hat{H}_0$. Hence, the ground state of the system is given that of $\hat{H}_0$. With increasing g, the influence of $\hat{H}_1$ grows and the eigenfunctions and -values of the Hamiltonian $\hat{H}$ will be altered correspondingly. At a critical value g_c, the (equilibrium) excitation spectrum changes drastically. The system assumes a different ground state and thus develops a new phase. At very large $g \gg g_\mathrm{c}$, the influence of $\hat{H}_0$ becomes negligible and the vacuum state of $\hat{H}$ and $\hat{H}_1$ coincide.

As an illustrative example of the interplay between the two competing contributions of the Hamiltonian (4.1), let us consider a simple example for a first-order transition, where either parts of $\hat{H}$ commute, i.e., $[\hat{H}_0, \hat{H}_1] = 0$. The eigenfunctions of $\hat{H}$ are independent of the external parameter, whereas the eigenvalues do depend on g. The two competing ground states $|\Psi_<\rangle$ and $|\Psi_>\rangle$ (which are the vacua of $\hat{H}_0$ and $\hat{H}_1$, respectively) develop a level crossing[1] at the critical point g_c, cf. Fig. 4.1. In this point, the vacuum energy of the Hamiltonian (4.1) is non-analytical in g.

Characteristic for quantum phase transitions [13,14] (of all orders) is the vanishing of the typical energy gap ΔE of the excitation spectrum (e.g., the energy difference between $|\Psi_<\rangle$ and $|\Psi_>\rangle$, or the energy gap of some excitations) when approaching the phase separating point g_c

---

[1] In finite-sized systems, one typically has $[\hat{H}_0, \hat{H}_1] \neq 0$ and these two modes would form an avoided crossing. Since (quantum) phase transitions are defined in the (thermodynamic) limit of infinite system size (e.g., $N \uparrow \infty$), we will consider these systems from now on only.

$$\Delta E \propto |g - g_\mathrm{c}|^{z\nu}\,, \tag{4.2}$$

where $z\nu$ is some characteristic exponent. (For $[\hat{H}_0, \hat{H}_1] = 0$, we have $z\nu = 1$.) Hence, the response time of the quantum fluctuations $t_\mathrm{resp} \propto 1/\Delta E$ diverges as $g \to g_\mathrm{c}$. When sweeping through the phase transition with a finite velocity $|\mathrm{d}g/\mathrm{d}t| > 0$, the fluctuations cannot follow the changes induced by the sweep and hence adiabaticity will be violated. Non-equilibrium effects, like the amplification of vacuum fluctuations, will occur.

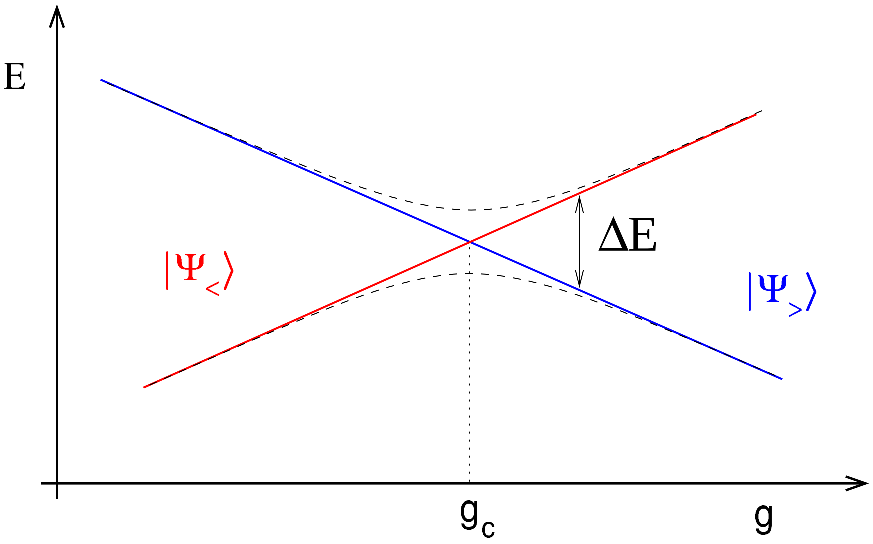

Figure 4.1: Schematic plot of the level structure near the critical point g_c in a first-order quantum phase transition (not to scale). At the critical value g_c of the external parameter, the two competing ground states, $|\Psi_<\rangle$ (red) and $|\Psi_>\rangle$ (blue), respectively, form a level crossing. The energy gap ΔE vanishes and the response time $t_\mathrm{resp} \propto 1/\Delta E$ of the quantum fluctuations diverges as $g \to g_\mathrm{c}$, cf. Eq. (4.2). In systems with finite size, an avoided crossing of these two modes might develop (dashed black line). The vacuum structure still changes, but the gap is, albeit small, non-zero.

Furthermore, the two competing ground states might possess different symmetries, which will be broken or restored when sweeping through the transition. If the stable phase permits topological defects (symmetry-breaking transition), a quantum version of the Kibble-Zurek mechanism may create those defects [38, 39, 144–148]. Both phenomena, the amplification of the vacuum fluctuations as well as the defect creation, can be understood in terms of the emergence of an effective cosmic horizon which corresponds to the loss of causal connection and indicates the breakdown of adiabaticity near the critical point.

In the following Section 4.1, we consider the Bose-Hubbard model: bosons are placed on discrete lattice sites with a certain tunneling probability to neighboring sites, cf. Fig. 4.2. This situation can be realized in experiments by placing a quantum gas in an optical lattice [42, 149]. We discuss the sweep from the superfluid to the Mott-insulator phase when increasing the lattice potential (i.e., diminishing the tunneling rate between adjacent sites). After crossing the critical point, the gapless excitations of the superfluid become unstable and decay into the gapped excitations of the Mott insulator. The initial evolution of number and phase variations (on-site) and correlations (off-site) in dependence of the sweep rate will be calculated. The off-diagonal long-range order, which is characteristic for a condensed phase, decays and adjacent sites become uncorrelated (for vanishing tunnel rates). For the experimental investigation of the diminishing correlations, we propose a persistent ring-current setup, where the decaying phase coherence manifests in a temporal shrinkage of the superfluid fraction.

Motivated by a recent experiment [43], we address in Section 4.2 the rapid quench of a spin-one Bose gas from the (polar) paramagnetic to the (planar) ferromagnetic phase by reducing the external magnetic field applied in the z-direction. In this direction (z), the system shall be strongly confined and thus becomes effectively two-dimensional. After crossing the critical point, ferromagnetic domains of different orientations form. (A uniform magnetization is prohibited by total angular momentum conservation.) The rotational symmetry around the z-axis is broken and stable vortices might occur. We derive the typical domain structure and deduce a scaling law for the standard deviation of the winding number, i.e., the excess vortex number, with the system size. (Since positive and negative defects are equally likely, the expectation value of the winding number is zero.) A generalization to higher dimensions is straightforward and will be discussed in Sec. 4.2 as well.

4.1 Superfluid to Mott transition in the Bose-Hubbard model

4.1.1 Bose-Hubbard model

Besides the Ising model (which can be solved analytically [13, 146]), another archetypical example of a quantum phase transition occurs between the superfluid and the Mott insulator state in the Bose-Hubbard model (where no closed solution has been found). This model provides a simplified description for the problem of interacting bosons hopping on a lattice [150]; its implementation with atoms/molecules in optical lattices [151], and the subsequent experimental realization of the Mott-Hubbard transition [42,149] has recently caused a large amount of research activity [152].

The superfluid phase possesses a rich spectrum ranging from topological defects (e.g.,

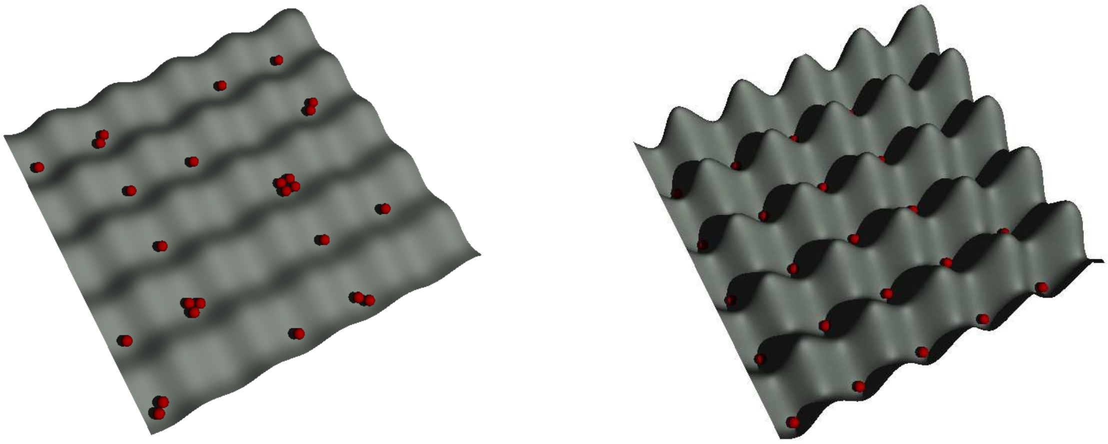

Figure 4.2: Illustration of the different ground states of the Bose-Hubbard model, see also Fig. 1.5: for small lattice potentials and thus high tunneling rates, $J \gg U$, the system is superfluid (left). The bosons (red) can hop to different sites and are thus delocalized. In contrast, by increasing the lattice potential, the tunneling between different sites is suppressed and the system assumes a Mott-insulator state (right) for $J \ll U$ and commensurable filling $\langle \hat{n}_a \rangle \in \mathbb{N}$. The bosons are pinned to the lattice sites and are almost uncorrelated.

kinks in one dimension) to gapless quasi-particle excitations (phonons) but the Mott state does not. Hence, the (quantum version of the) Kibble-Zurek mechanism requires the dynamical transition from the Mott to the superfluid state (quantum melting) whereas the amplification of the quantum fluctuations of the phonon modes occurs in the opposite direction (quantum freezing). The (mostly numerical) studies thus far [148, 153–156] have been devoted to the first case (quantum melting). In this Section, the dynamical behavior of the superfluid to Mott quantum phase transition is studied starting, in contrast to previous investigations, from the superfluid side of the transition. We thus investigate the quantum freezing of number fluctuations[2] [157] and predict their dependence on the sweep rate γ. The thereby created number-squeezed state and its number fluctuations can be studied experimentally, for example by the interference of condensates released from different optical lattice wells [158]. As further observables representing the actual quantum state $|\Psi(t)\rangle$, to bring out the difference to either the superfluid or Mott states (cf. Fig. 4.3), we derive the temporal evolution of the off-diagonal long-range order and the superfluid fraction.

The Bose-Hubbard model with local contact interactions is, on a rather general type of

---

[2] In the superfluid phase, the phase fluctuations are small and the number fluctuations are large [for $J \gg U$ in Eq. (4.3), one approximately has a coherent state with Poissonian number statistics], whereas the Mott phase shows the opposite behavior.

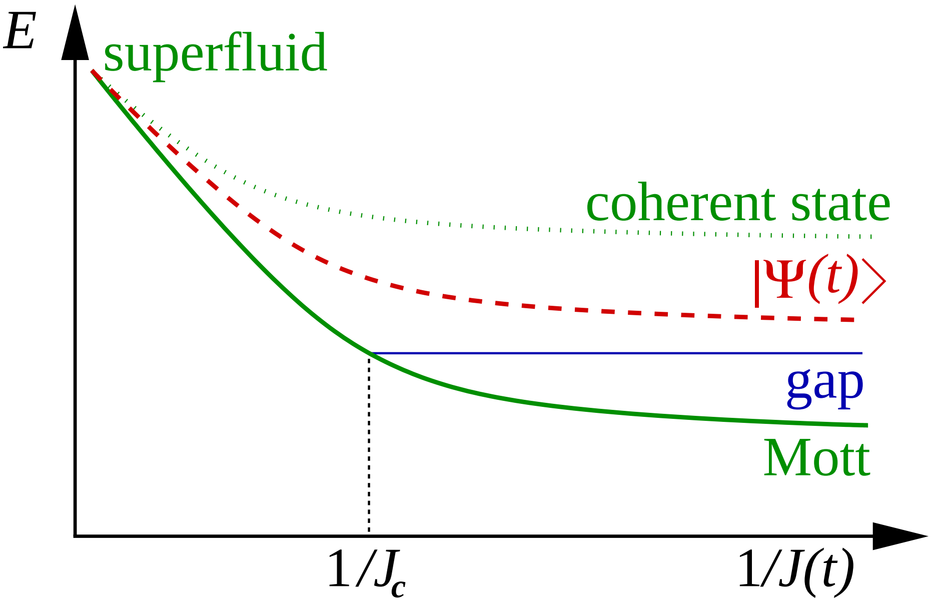

Figure 4.3: Sketch (not to scale) of the level structure near the critical point, i.e., plot of the ground state energy (green solid line) and the energy gap (thin blue line) as a function of the external parameter $1/J(t)$. Since the response time diverges at the critical point $J = J_{\rm c}$, adiabaticity breaks down near the transition for any finite sweep velocity $\mathrm{d}J/\mathrm{d}t$. Hence the actual state $|\Psi(t)\rangle$ (red dashed line) slightly deviates from the exact ground state already before the critical point $J = J_{\rm c}$ is reached and finally lies energetically somewhere between the coherent state (dotted green line) and the Mott state.

lattice, described by the Hamiltonian, cf. Eq. (3.120)

$$\hat{H} \,=\, J(t)\sum_{ab} M_{ab}\hat{\Psi}_a^\dagger\hat{\Psi}_b + \frac{U}{2}\sum_a (\hat{\Psi}_a^\dagger)^2\hat{\Psi}_a^2\,. \tag{4.3}$$

Here $\hat{\Psi}_a^\dagger$ and $\hat{\Psi}_a$ denote the bosonic creation and annihilation operators at the lattice site a. [Similarly, for a Bose-Einstein condensate described the Hamiltonian (3.1), i.e., in the continuum limit of Eq. (4.3), the operators $\hat{\Psi}(\boldsymbol{r})$ annihilate a particle at spatial position $\boldsymbol{r}$.] The energy scale is set by the on-site repulsion $U > 0$ and the time-dependent tunneling rate $J(t) \geq 0$. The structure of the lattice is encoded in the matrix M_{ab}, which is supposed to obey the same (translational) symmetry group, e.g., for a one-dimensional chain with nearest-neighbor hopping, we have $M_{ab} = \delta_{a,b} - \frac{1}{2}(\delta_{a,b+1} + \delta_{a,b-1})$.

4.1.2 Linearization and effective horizon

The initial state is the homogeneous superfluid phase, $J \gg J_{\rm c} = \mathcal{O}(U/n)$, see [159], with a large integer filling $n = \langle\hat{n}_a\rangle \gg 1$ (where $\hat{n}_a = \hat{\Psi}_a^\dagger\hat{\Psi}_a$), which facilitates a particle-number conserving mean-field expansion [92,93,95] in analogy to Eq. (3.10) in Sec. 3.2

$$\hat{\Psi}_a = \left(\psi_0 + \hat{\chi}_a + \hat{\zeta}_a\right) \hat{A}/\sqrt{\hat{N}}\,, \tag{4.4}$$

with $\hat{A} = \hat{\Psi}_\Sigma(\hat{\Psi}_\Sigma^\dagger\hat{\Psi}_\Sigma)^{-1/2}\hat{N}^{1/2}$ and $\hat{A}^\dagger\hat{A} = \hat{N} = \sum_a \hat{n}_a$, where $\hat{\Psi}_\Sigma = \sum_a \hat{\Psi}_a$. Similarly to the treatment of the quantum fluctuations in Bose-Einstein condensates, cf. Chapter 3, the main idea here is to expand the original operator $\hat{\Psi}_a$ into powers of the filling number $n \gg 1$. Formally, we consider the limit $n \uparrow \infty$ with the chemical potential $\mu = Un$ remaining finite, i.e., $U = \mathcal{O}(1/n)$. The leading term is the order parameter $\psi_0 = \mathcal{O}(\sqrt{n})$ and the quantum corrections $\hat{\chi}_a = \mathcal{O}(n^0)$ correspond to quasi-particle excitations. For the validity of this expansion, the remaining higher-order corrections $\hat{\zeta}_a$ must be small $\hat{\zeta}_a \ll \mathcal{O}(n^0)$. Inserting the above expansion (4.4) into the equation of motion

$$i\frac{\partial}{\partial t}\hat{\Psi}_a = J(t)\sum_b M_{ab}\hat{\Psi}_b + U\hat{n}_a\hat{\Psi}_a \tag{4.5}$$

obtained from (4.3) and sorting into powers of n yields the analogue of the Bogoliubov-de Gennes equations for the excitations at site a, cf. Eq. (3.12)

$$i\partial_t\hat{\chi}_a = J(t)\sum_b M_{ab}\hat{\chi}_b + 2U|\psi_0^2|\hat{\chi}_a + U\psi_0^2\hat{\chi}_a^\dagger\,, \tag{4.6}$$

and for the remaining higher-order corrections

$$\begin{aligned} i\partial_t\hat{\zeta}_a = {} & J(t)\sum_b M_{ab}\hat{\zeta}_b + 2U|\psi_0^2|\hat{\zeta}_a + U\psi_0^2\hat{\zeta}_a^\dagger \\ & + 2U\psi_0\hat{\chi}_a^\dagger\hat{\chi}_a + U\psi_0^*\hat{\chi}_a^2 + U\hat{\chi}_a^\dagger\hat{\chi}_a^2 + \mathcal{O}(U\hat{\zeta}_a)\,, \end{aligned} \tag{4.7}$$

cf. Eq. (3.13). Deep in the superfluid phase (our initial state), the higher-order corrections $\hat{\zeta}_a$ are small and the mean-field expansion (4.4) works very well. If we approach the Mott phase, however, these corrections start to grow according to Eq. (4.7) and, at some point, the mean-field expansion (4.4) breaks down. The characteristic time-scale of this breakdown can be estimated from the nonlinear source terms in Eq. (4.7) which are suppressed to $\mathcal{O}(1/\sqrt{n})$ in view of $U = \mathcal{O}(1/n)$, $\psi_0 = \mathcal{O}(\sqrt{n})$ and $\hat{\chi}_a = \mathcal{O}(n^0)$. Hence (starting in the superfluid phase), the higher-order corrections remain small as long as $Ut\sqrt{n} \ll 1$, i.e., for evolution times of order $t = \mathcal{O}(\sqrt{n})$. Thus we can extrapolate the mean-field expansion even into the Mott phase for some time $t = \mathcal{O}(\sqrt{n})$, and follow the evolution of the instabilities which develop because the superfluid state is no longer the ground state of the system.

The polar decomposition $\hat{\Psi}_a = \exp\{i\hat{\phi}_a\}\sqrt{\hat{n}_a}$ [cf. the hydrodynamic formulation for Bose-Einstein condensates in 3.4.1, in particular Eq. (3.43), and also Eq. (3.113)] yields the linearized number fluctuations $\delta\hat{n}_a$ via $\hat{n}_a = n + \delta\hat{n}_a$ and accordingly the conjugate phase fluctuations $\delta\hat{\phi}_a$, where $\hat{\chi}_a = \psi_0[\delta\hat{n}_a/(2n) + i\delta\hat{\phi}_a] + \mathcal{O}(1/\sqrt{n})$. After a normal-mode expansion of these fluctuations

$$\delta\hat{n}_\kappa = v_\kappa^a\delta\hat{n}_a\,, \tag{4.8}$$

where κ are generalized momenta and v_κ^a are the corresponding eigenvectors of the matrix M_{ab} with eigenvalue λ_κ

$$M_{ab} v_\kappa^b \;=\; \lambda_\kappa v_\kappa^a \,, \tag{4.9}$$

we can diagonalize the evolution equation (4.6)

$$\left(\frac{\partial}{\partial t} \frac{1}{J(t)} \frac{\partial}{\partial t} + 8\lambda_\kappa \left[Un + 2J(t)\lambda_\kappa \right] \right) \delta\hat{n}_\kappa \;=\; 0 \,. \tag{4.10}$$

For small $\lambda_\kappa \ll Un/2J(t)$, the above evolution equation is analogous to the modes of a quantum field within an expanding universe with the wavenumber $k \propto \sqrt{\lambda_\kappa}$. Pursuing the similarity a bit further, we get the analogue of a cosmic horizon with the horizon size [see also Eqs. (2.4) and (3.68) in Sections 2.1.2 and 3.5.1, respectively]

$$\Delta_\mathrm{h}(t) \;=\; \int\limits_t^\infty \mathrm{d}t' \, \sqrt{J(t')Un} \,, \tag{4.11}$$

if $J(t)$ changes fast enough [37, 86]. Note that the upper integral limit should not be taken literally, since it must still be within the region of validity of the mean-field expansion. In case an effective horizon occurs, its size constantly decreases. Hence all modes (with small λ_κ) will qualitatively follow the same evolution – but at different times: initially, the wavelength of the modes is well inside the horizon, $\lambda_\kappa \Delta_\mathrm{h}^2 \gg 1$, and the modes oscillate almost freely. At some point of time, however, the constantly shrinking horizon closes in, $\lambda_\kappa \Delta_\mathrm{h}^2 = \mathcal{O}(1)$, and thus the causal connection across a wavelength is lost. After that, the modes cannot oscillate anymore and freeze. This process leads to the amplification of the initial quantum fluctuations via squeezing in analogy to the inflationary epoch in the early universe, cf. Chapter 2 and Refs. [15–18, 37, 86]. We note that these considerations show a major weakness of the adiabatic–impulse approximation used in [147], since modes with different λ_κ become non-adiabatic at different times.

4.1.3 Exponential sweep

Since the tunneling rate J depends exponentially on the amplitude of the laser which generates the optical lattice[3], we shall consider in the following an exponential time-dependence $J(t) = J_0 \exp\{-\gamma t\}$, which is implying the emergence of a quasi-particle horizon according to Eq. (4.11).. Furthermore, Eq. (4.10) reveals that λ_κ can be absorbed by a suitable redefinition of the time coordinate in this case, $\tau_\kappa = -4\lambda_\kappa J(t)/\gamma$, leading to

$$\left(\frac{\partial^2}{\partial \tau_\kappa^2} + \left[1 - \frac{2}{\tau_\kappa} \frac{Un}{\gamma} \right] \right) \delta\hat{n}_\kappa \;=\; 0 \,. \tag{4.12}$$

---

[3] In sufficiently deep D-dimensional simple cubic lattices, $J \propto (V_0/E_\mathrm{R})^{3/4} \exp\{-2\sqrt{V_0/E_\mathrm{R}}\}$ and $U \propto (V_0/E_\mathrm{R})^{D/4}$ hold, where V_0 is the lattice depth given by the laser intensity and E_R is the recoil energy, cf. [160].

The universal scaling solution resulting from the above equation confirms that modes with different λ_κ display the same behavior, but at different times. The only remaining dimensionless parameter is the ratio $\nu = Un/\gamma$, which is a measure of the sweep velocity: $\nu \gg 1$ implies a slow and $\nu \ll 1$ a fast (non-adiabatic) sweep. The differential equation (4.12) has a universal scaling solution in terms of Whittaker functions [121, 161]

$$\delta\hat{n}_\kappa \;=\; \sqrt{n}\, e^{-\pi\nu/2}\, W_{i\nu,1/2}(2i\tau_\kappa)\, \hat{a}_\kappa + \text{H.c.} \tag{4.13}$$

The quasi-particle operator $\hat{a}_\kappa$ annihilates the adiabatic ground state $\hat{a}_\kappa|\text{in}\rangle = 0$ at early times $\tau_\kappa \downarrow -\infty$, where the modes oscillate like $e^{\pm i\tau_\kappa}$ (which can also be obtained from the asymptotic behavior of the Whittaker functions). According to the arguments presented after Eq. (4.7), the mean-field expansion remains valid for intermediate times with $Ut\sqrt{n} \ll 1$ but $\gamma t \gg 1$, and hence can be extrapolated to the “late-time” regime $\tau_\kappa \uparrow 0$, where the functions $W_{i\nu,1/2}(2i\tau_\kappa)$ approach a constant value, i.e., the number fluctuations freeze. Due to the perfect scaling solution, the frozen value is independent of κ, but the decaying corrections do depend on λ_κ:

$$\langle\delta\hat{n}_\kappa^2\rangle \;\equiv\; \langle\text{in}|\delta\hat{n}_\kappa^2|\text{in}\rangle \;=\; n\frac{1-e^{-2\pi\nu}}{2\pi\nu} + \mathcal{O}(t\lambda_\kappa e^{-\gamma t})\,. \tag{4.14}$$

Since the leading term is independent of κ, it just yields a local ($\propto \delta_{a,b}$) contribution after the mode sum ($\kappa \to a$) and thus leads to frozen on-site number variations

$$\Delta^2(n_a) \;=\; \langle\hat{n}_a^2\rangle - \langle\hat{n}_a\rangle^2 \;=\; \langle\delta\hat{n}_a^2\rangle \;=\; n\frac{1-e^{-2\pi\nu}}{2\pi\nu}\,. \tag{4.15}$$

For a rapid sweep $\nu \ll 1$, this variation $\Delta^2(n_a)$ approaches a constant value n, which is characteristic of a superfluid phase with Poissonian number statistics [162]. For a slow sweep $\nu \gg 1$, the variation $\Delta^2(n_a)$ becomes small, $\propto n/\nu$, and so approaches the behavior deep into the Mott phase (with $J \downarrow 0$), where $\Delta^2(n_a) = 0$, cf. [163]. For $J \downarrow 0$, the energy $\langle\hat{H}\rangle$ is basically determined by the variation $\Delta^2(n_a)$ and hence this quantity describes the location of the final state in comparison to the coherent state and the Mott state, see Fig. 4.3.

The sub-leading corrections in $\langle\delta\hat{n}_\kappa^2\rangle$ depend on κ and hence determine the off-site ($a \neq b$) number correlations, which decay exponentially for large times

$$\langle\hat{n}_a\hat{n}_b\rangle - \langle\hat{n}_a\rangle\langle\hat{n}_b\rangle \;=\; \langle\delta\hat{n}_a\delta\hat{n}_b\rangle \;=\; \mathcal{O}(\gamma t\, e^{-\gamma t})\,, \tag{4.16}$$

where we have omitted finite-size effects (which scale with the inverse number of lattice sites), since, strictly speaking, the mode sum does not include the zero-mode $\kappa = 0$.

The conjugate phase fluctuations can be derived in an analogous manner and are determined by the derivatives of the Whittaker functions $\mathrm{d}W_{i\nu,1/2}/\mathrm{d}\tau_\kappa$. As one would expect, they do not freeze – but increase:

$$\langle\delta\hat{\phi}_\kappa^2\rangle \;=\; \nu\frac{1-e^{-2\pi\nu}}{2\pi n}\,\gamma^2 t^2 + \mathcal{O}(\gamma t \ln\lambda_\kappa)\,. \tag{4.17}$$

Again the leading (first) term is independent of κ and thus yields the on-site fluctuations $\langle\delta\hat{\phi}_a^2\rangle$ only (which generate the quadratically growing quantum depletion $\langle\hat{\chi}_a^\dagger\hat{\chi}_a\rangle$ and anomalous term $\langle\hat{\chi}_a^2\rangle$). The second term is the leading κ-dependent contribution and determines the off-site phase correlations $\langle\delta\hat{\phi}_a\delta\hat{\phi}_b\rangle$.

The ascent of the phase fluctuations can be understood as a consequence of the emergence of an effective horizon which entails the loss of causal connection between different sites and thus the decay of the phase coherence across the lattice. As one interesting observable, let us discuss the evolution of the off-diagonal long-range order between sites a and b defined by the correlator $\langle\hat{\Psi}_a^\dagger(t)\hat{\Psi}_b(t)\rangle$. Using the mean-field results valid at intermediate times with $\gamma t \gg 1$ but $Ut\sqrt{n} \ll 1$ as the initial conditions, we may derive the ensuing stages of the quantum evolution, where the tunneling rate $J(t \gg 1/\gamma) \lll 1$ is exponentially small and can be neglected. In this limit, the evolution of the operators can be approximated by $\mathrm{d}\hat{\Psi}_a/\mathrm{d}t = -iU\hat{n}_a\hat{\Psi}_a$ which possesses the simple solution $\hat{\Psi}_a(t) = \exp\{-iU\hat{n}_a^0 t\}\hat{\Psi}_a^0$. Consequently, we obtain $\langle\hat{\Psi}_a^\dagger(t)\hat{\Psi}_b(t)\rangle = n\langle\exp\{iU(\hat{n}_a - \hat{n}_b)t\}\rangle + \mathcal{O}(\sqrt{n})$. The frozen first-order number fluctuations $\delta\hat{n}_a$ are in a squeezed state, which can be approximated by a (continuous) Gaussian distribution (for $n \gg 1$). For a Gaussian variable $\hat{X}$ with $\langle\hat{X}\rangle = 0$, the exponential average yields $\langle\exp\{i\hat{X}\}\rangle = \exp\{-\langle\hat{X}^2\rangle/2\}$ and hence we get

$$\langle\hat{\Psi}_a^\dagger(t)\hat{\Psi}_b(t)\rangle \approx n\exp\{-U^2t^2\Delta^2(n_a)\}\,. \tag{4.18}$$

Note that this expression is only valid for time scales $1/\gamma \ll t \ll 1/U$; for $Ut \in 2\pi\mathbb{N}$ all the exponential factors equal unity again and we have a revival of the phase coherence and thus long-range order similar to a spin echo (assuming that the coupling to the environment is small enough, of course). Furthermore, the above Gaussian decay is independent of the distance between the sites a and b. Since the Fourier transform of $\langle\hat{\Psi}_a^\dagger(t)\hat{\Psi}_b(t)\rangle$ determines the structure factor $S(\boldsymbol{k})$, the decay of the long-range order (4.18) directly corresponds to the temporal decrease of the peak in $S(\boldsymbol{k})$ at $\boldsymbol{k} = 0$. This dependence on time and sweep rate could be observed with time-of-flight measurements [164] (which basically map out $|S(\boldsymbol{k})|$) by varying γ and the time delay between the phase transition and the release of the condensate.

4.1.4 Ring lattice

Let us calculate another simple experimental signature, which involves just neighboring sites, namely the superfluid fraction n_{sf}/n. To this end, we specify our lattice and choose a one-dimensional ring-geometry[4] $a \to \ell$ with the circumference coordinate ℓ. In order to generate a persistent current, we impose a small phase gradient externally by trapping a flux quantum on the ring: $\psi_0 = \sqrt{n}\exp\{-i\mu t + 2\pi i\ell/L\}$, where $L \gg 1$ denotes the number of sites. Naturally, for a decreasing tunneling rate $J(t)$, the induced current diminishes also. In addition, the number of particles contributing to this flux goes down – which will be used as a measure for the superfluid fraction. The flux can be determined by the usual Noether current corresponding to the $U(1)$ invariance and is related to the nearest neighbor correlation function $\langle\hat{\Psi}_\ell^\dagger\hat{\Psi}_{\ell+1}\rangle$. Hence, the shrinkage of the superfluid fraction is given by the same[5] expression as in Eq. (4.18)

---

[4] The experimental implementation of a ring-shaped lattices has been discussed in [165]. The persistent ring currents show up in characteristic interference patterns of the density after time of flight.

$$\frac{n_{\rm sf}}{n} \approx \exp\left\{-U^2t^2n\frac{1-e^{-2\pi\nu}}{2\pi\nu}\right\}\,. \tag{4.19}$$

In the case of a very rapid (impulse) sweep, $\nu \ll 1$, the superfluid fraction decays with $\exp\{-nU^2t^2\}$, i.e., independent of γ. Conversely, for a slow sweep $\nu \gg 1$, the decay takes much longer: $\exp\{-nU^2t^2/(2\pi\nu)\}$.

4.2 Vortex creation and winding number scaling in quenched spinor Bose gas

4.2.1 Introduction

A rapid sweep through a symmetry-breaking zero-temperature phase transition, cf. Sec. 4.1, is the most direct way of amplifying and observing quantum fluctuations. The quench generates causally disconnected spatial domains of different order parameters (positions in the new ground-state manifold), which may ultimately form topological defects in a quantum version of the Kibble-Zurek mechanism [38–40, 145, 166], and constitute a direct evidence of the initial quantum fluctuations. Because of their comparably long response times, dilute atomic gases provide a unique opportunity for exploring these fundamental quantum many-body phenomena far from equilibrium in the laboratory.

In what follows, we derive the spectrum of fluctuations induced by a rapid quench to the ferromagnetic state of a spinor Bose gas, cf. Figure 4.4, and establish a general sample-size dependent scaling law for the resulting variance of the net number of spin vortices (winding number). Besides the total defect density, the winding number within a given area determines the spectrum of the created magnetization fluctuations. Both quantities have implications, *inter alia*, for the scattering of quasi-particles (e.g., ferromagnetic magnons) at the defects, affecting measurable transport properties like conductivity and susceptibility. Therefore, spinor Bose gases (apart from being interesting in their own right) serve as a useful and experimentally accessible toy model for the general case.

---

[5] Note that the coincidence between the long- and short-range behavior in Eqs. (4.18) and (4.19) is a consequence of the exponential time-dependence of $J(t)$, which allows for a scaling solution. The freezing of the number fluctuations and the growth of the phase fluctuations are general phenomena, but the dependence on κ is different for other sweep dynamics; e.g., for a linear sweep $\mathrm{d}J/\mathrm{d}t = \mathrm{const}$, the leading contributions to (4.17) would scale as $\lambda_\kappa^{-1/3}$ for small λ_κ [37].

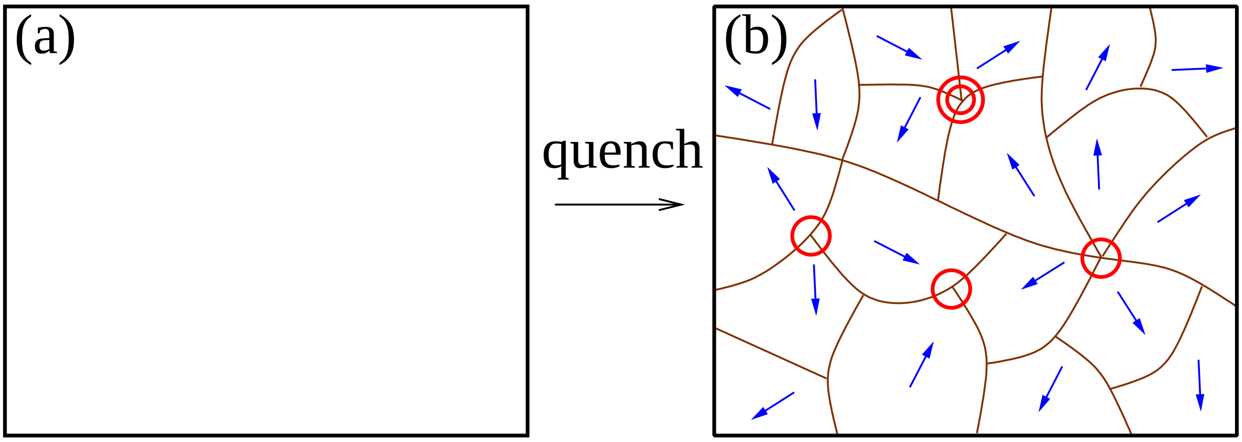

Figure 4.4: Initially, when a high magnetic field is applied in the z-direction, the quasi-two-dimensional (in x/y-plane) spinor condensate is prepared in the polar paramagnetic state (a), which is stable due to the quadratic Zeeman shift. By rapidly lowering the external magnetic field, the homogeneous paramagnetic phase becomes unstable and decays into a ferromagnetic state (b). The ferromagnetic domains have a distinct magnetization (blue arrows) and are separated by domain walls (brown lines). Stable vortices (red circles) may form, where, typically, the magnetization of all neighboring domains points either away from or towards to an unmagnetized vortex core.

Spinor Bose-Einstein condensates are created by trapping different hyperfine states of a particular atomic species by optical means [167], which enables, *inter alia*, the investigation of coherent spin-exchange dynamics [168], and the formation of spin domains by a dynamical instability [169]. Genuine non-equilibrium phenomena in a spinor Bose gas were realized in a recent experiment [43], where an initially polar (paramagnetic) state was rapidly quenched through a quantum phase transition to a final ferromagnetic state. Such a quench results in spin vortices (imaged *in situ* by phase contrast techniques [170]), which are topological defects in the magnetization with a paramagnetic core [171, 172].

4.2.2 Hamiltonian and ground state properties

The dilute spinor Bose gas can be described in terms of multi-component field operators $\hat{\psi}_a$ whose dynamics is governed by the Hamiltonian density

$$\begin{aligned}\hat{\mathcal{H}} = {} & \frac{1}{2m}(\boldsymbol{\nabla}\hat{\psi}_a^\dagger)\cdot\boldsymbol{\nabla}\hat{\psi}_a + V_{\text{trap}}\hat{\psi}_a^\dagger\hat{\psi}_a + \frac{c_0}{2}\hat{\psi}_a^\dagger\hat{\psi}_b^\dagger\hat{\psi}_b\hat{\psi}_a \\ & + \frac{c_2}{2}\boldsymbol{F}_{ab}\cdot\boldsymbol{F}_{cd}\,\hat{\psi}_a^\dagger\hat{\psi}_b\hat{\psi}_c^\dagger\hat{\psi}_d + q\hat{\psi}_{+1}^\dagger\hat{\psi}_{+1} + q\hat{\psi}_{-1}^\dagger\hat{\psi}_{-1}\end{aligned} \tag{4.20}$$

where m denotes the mass of the atoms. The vector $\boldsymbol{F}_{ab}$ contains the spin matrices [173, 174] (see also Appendix D) and determines the effective magnetization $\hat{\boldsymbol{F}} = \boldsymbol{F}_{ab}\hat{\psi}_a^\dagger\hat{\psi}_b/\varrho$, where a summation over component indices a, b, c, d is implied and $\varrho = \langle \hat{\psi}_a^\dagger \psi_a \rangle$ is the total (conserved) density. For spin-one systems, the sum runs over $a = 0, \pm 1$ or, alternatively, over $a = x, y, z$ with $\psi_0 = \psi_z$ and $\psi_\pm = (\psi_x \pm i\psi_y)/\sqrt{2}$. The coupling constants

$$c_0 \;=\; 4\pi(a_0 + 2a_2)/(3m)\,, \qquad c_2 \;=\; 4\pi(a_2 - a_0)/(3m) \tag{4.21}$$

are determined by scattering lengths a_S for the scattering channel with total spin S. For $c_0 \gg |c_2|$, density fluctuations are energetically suppressed in comparison with the spin modes. Since we are interested in the effects of the phase transition (which is, strictly speaking, only well-defined for infinite systems) and not in the impact of inhomogeneities, we assume $\varrho \approx$ const., and hence omit the scalar trapping potential V_{trap}. Finally, q denotes the strength of the quadratic Zeeman shift $q\langle \hat{F}_z^2 \rangle$ [43], where an external magnetic field is oriented along the z-direction (the linear Zeeman shift can be eliminated by transforming to the co-rotating frame, because the Larmor precession is much faster than all other frequency scales [171]).

Assuming $c_2 < 0$, the system is ferromagnetic for vanishing Zeeman shift $q = 0$, i.e., the magnetization $\hat{\boldsymbol{F}}$ assumes a maximum value $\langle \hat{\boldsymbol{F}} \rangle^2 = 1$ in some given but arbitrary direction (broken-symmetry phase). For small but non-zero q, the magnetization $\langle \hat{\boldsymbol{F}} \rangle$ lies in x, y-plane due to the term $q\langle \hat{F}_z^2 \rangle$ but is still maximal, $\langle \hat{\boldsymbol{F}} \rangle^2 = 1$. For large q, however, the ground state corresponds to a condensate in the $\psi_0 = \psi_z$ component only and the symmetry is restored, i.e., the magnetization $\langle \hat{\boldsymbol{F}} \rangle$ vanishes (paramagnetic phase). Hence, by rapidly lowering q, one may quench the system from an initially paramagnetic to the ferromagnetic phase.

In order to study the evolution of the quantum field during the quench, a number-conserving mean-field ansatz[6]

$$\hat{\psi}_z \;=\; (\psi_{\text{co}} + \delta\hat{\psi}_z)\frac{\hat{A}}{\sqrt{\hat{N}}} \tag{4.22}$$

will be employed. It is adapted to the initial paramagnetic phase but can be extrapolated for some finite time after the quench, as long as $\delta\psi_x, \delta\psi_y, \delta\psi_z \ll \psi_{\text{co}}$ (cf. Sec. 4.1). This ansatz allows for a linearized expression for the magnetization (which assumes in Cartesian coordinates the simple form $\hat{F}_a = -i\varepsilon_{abc}\hat{\psi}_b^\dagger \hat{\psi}_c/\varrho$) and to derive an effective mean-field Hamiltonian for the transverse magnetization $\hat{\boldsymbol{F}} = (\hat{F}_x, \hat{F}_y)$ from the full Hamiltonian (4.20), see Appendix D for more details

$$\frac{\hat{\mathcal{H}}_{\text{eff}}}{\varrho} \;=\; \frac{\hat{\boldsymbol{\Pi}}}{\varrho}\left(q - \frac{\boldsymbol{\nabla}^2}{2m}\right)\frac{\hat{\boldsymbol{\Pi}}}{\varrho} + \hat{\boldsymbol{F}}\left(\frac{q + 2c_2\varrho}{4} - \frac{\boldsymbol{\nabla}^2}{8m}\right)\hat{\boldsymbol{F}}\,, \tag{4.23}$$

with the (transverse) canonical momentum operator for spin-one bosons

$$\hat{\boldsymbol{\Pi}} \;=\; \frac{\sqrt{\varrho}}{2}\left(\begin{array}{c} \hat{\psi}_y^\dagger + \hat{\psi}_y \\ -\hat{\psi}_x^\dagger - \hat{\psi}_x \end{array}\right). \tag{4.24}$$

---

[6] Here $\hat{N} = \hat{A}^\dagger \hat{A}$ counts the total number of particles, see the remarks after Eq. (4.4) and Refs. [92–95].

The experiment [43] is described by a two-dimensional transverse magnetization $\hat{\boldsymbol{F}} = (\hat{F}_x, \hat{F}_y)$. It obeys the $SO(2)$-symmetry of rotations around the z-axis in effectively two spatial dimensions $\boldsymbol{\nabla} = (\partial_x, \partial_y)$ and thus permits topological defects in the form of spin vortices. However, the above expressions for the Hamiltonian are completely analogous for a $SO(D)$-symmetry[7] of the order parameter $\langle \hat{\boldsymbol{F}} \rangle$ in $D > 2$ spatial dimensions, where the analogous topological defects are generically called "hedgehogs", see Figure 4.2.2 and, e.g., Refs. [33, 175–178]. Therefore, the general $SO(D)$ situation shall be discussed in the following and the experimentally realized example $D = 2$ of [43] will be treated in Subsection 4.2.5.

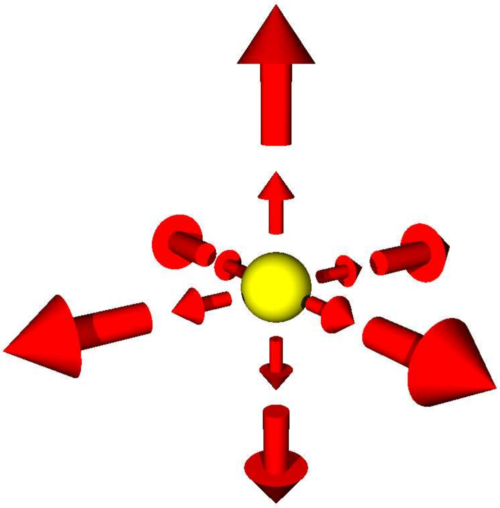

Figure 4.5: Typical field distribution of a three-dimensional hedgehog. The field lines (red arrows) point away from the unmagnetized hedgehog core (yellow ball) and the field strength increases with the distance from the core, $\boldsymbol{F}(\boldsymbol{r}) = \boldsymbol{e}_r f(r)$.

4.2.3 Domain formation in a $SO(D)$-symmetry breaking quench

The simple expression (4.23) allows us to directly read off the critical value $q_{\mathrm{cr}} = 2|c_2|\varrho$ of the phase transition, where the paramagnetic state becomes unstable. After a quench from $q_{\mathrm{in}} > q_{\mathrm{cr}}$ to $q_{\mathrm{out}} < q_{\mathrm{cr}}$, and using a normal-mode expansion, we obtain exponentially growing modes corresponding to imaginary frequencies

$$\omega_k^q = \sqrt{(\epsilon_k + q)(\epsilon_k + q + 2c_2\varrho_0)}\,, \tag{4.25}$$

where $\epsilon_k = k^2/(2m)$, cf. Fig. 4.6. There are two regimes: for $q_{\mathrm{cr}} > q_{\mathrm{out}} > q_{\mathrm{cr}}/2$, the exponential growth rate $\Im(\omega_k^q)$ of the normal modes increases with their wavelength, but

---

[7] Although it is custom to denote the argument of the symmetry group by a capital N, we will abandon this customary convention in order to avoid confusion, because N and $\hat{N}$ denote the total particle number (of bosons in the trap) and the corresponding operator throughout this Thesis.

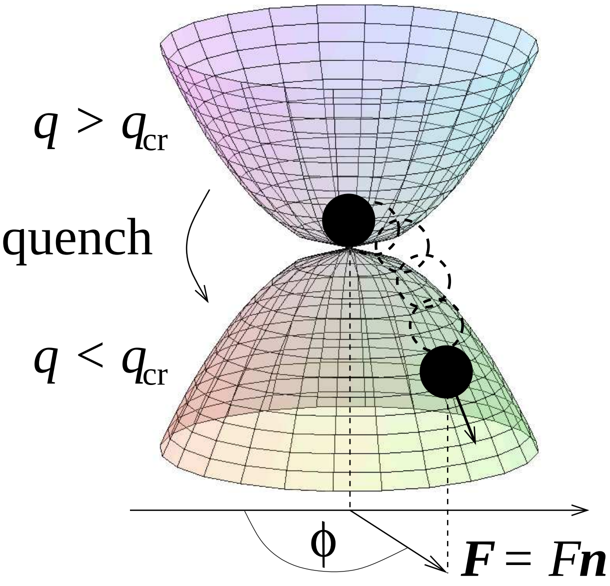

Figure 4.6: Inversion behavior of the effective potential from (4.23). After crossing the critical point, the direction $\boldsymbol{n}$ of the effective magnetization $\boldsymbol{F}$ in the plane, at any given point in space, gets frozen at a particular angle Φ, while its modulus F continues to grow exponentially in time ("rolls down" the potential hill).

for $q_{\rm out} < q_{\rm cr}/2$, the growth rate assumes its maximum at a given wavenumber

$$k_{\rm max} = \sqrt{m(q_{\rm cr} - 2q_{\rm out})}\,. \tag{4.26}$$

In view of the experimental parameters [43], we shall focus on the second scenario. Assuming the Bose gas to be sufficiently dilute, we may extrapolate our linearized (mean-field) description (4.23) to intermediate times t. At those times, the unstable modes have already grown by many e-foldings $\Im(\omega^q_{k_{\rm max}})t \gg 1$, whereas the magnetization is still small enough, $\boldsymbol{F}^2 \ll 1$, to be in the linear regime. In this limit, expectation values containing the magnetization are dominated by the fastest-growing modes with $|\boldsymbol{k}| = k_{\rm max}$, and thus can be calculated by approximating the $\mathrm{d}^D k$-integrals via the saddle-point method. For example, if the initial state (paramagnetic phase) is isotropic such as the ground state of (4.23) or the thermal ensemble, the dominant contribution to the two-point magnetization correlation function is calculated to be (see Appendix D for more details)

$$\langle \hat{F}_a(\boldsymbol{r})\hat{F}_b(\boldsymbol{r}')\rangle = C_\nu^{\rm max}\delta_{ab}\frac{\exp\{q_{\rm cr}t\}}{\sqrt{t}}\frac{J_\nu(k_{\rm max}|\boldsymbol{r}-\boldsymbol{r}'|)}{(k_{\rm max}|\boldsymbol{r}-\boldsymbol{r}'|)^\nu}\,, \tag{4.27}$$

where J_ν is the Bessel function of the first kind with the index $\nu = D/2 - 1$. Note that the above result is universal: apart from ν, $g_{\rm cr}$ and $k_{\rm max}$, all information enters the prefactor $C_\nu^{\rm max}$ only, which depends on $q_{\rm out}$, sweep rate, temperature etc.

4.2.4 Defect creation in a $SO(D)$-symmetry breaking quench

Now let us study the creation of topological defects, i.e., $SO(D)$-hedgehogs, by the symmetry-breaking quench. Their characteristic size, i.e., the extent of the paramagnetic core, can be determined by comparing the kinetic term $\propto \boldsymbol{\nabla}^2$ with the c_2-contribution in the Hamiltonian (4.20), which yields

$$\xi_s = \frac{1}{\sqrt{2|c_2|\varrho m}} = \frac{1}{\sqrt{m q_{\rm cr}}}\,, \tag{4.28}$$

i.e., the spin healing length. In order to deal with well-separated and therefore well-defined topological defects, the dominant wave-length $\lambda_{\rm max} = 2\pi/k_{\rm max}$ (which determines their typical distance, see below) can be assumed to be much larger than the spin healing length ξ, which amounts to requiring $0 < q_{\rm cr} - 2q_{\rm out} \ll q_{\rm cr}$. This condition is reasonably well satisfied in the experiment [43] where $\xi_s \approx 2.4\,\mu$m and $\lambda_{\rm max} \approx 16\,\mu$m.

Within the saddle-point approximation (i.e., focusing on the dominant modes), the term $-\boldsymbol{\nabla}^2 \to k^2_{\rm max}$ in the equations of motion resulting from (4.23) can be neglected compared to $q_{\rm cr}$ and we may approximate $\ddot{\boldsymbol{F}} \approx q^2_{\rm cr}\boldsymbol{F}/4$. Consequently, at each spatial position, the magnetization $\boldsymbol{F}$ behaves as the coordinate of a harmonic oscillator (in D dimensions), becoming inverted upon crossing the transition, cf. Fig. 4.6. Splitting $\boldsymbol{F}$ up into its modulus F and a unit vector of direction $\boldsymbol{n}$ via

$$\boldsymbol{F} = F\boldsymbol{n}\,, \tag{4.29}$$

we find that F grows exponentially whereas the dynamics of $\boldsymbol{n}$ freezes: in view of the conserved "angular momentum" $\boldsymbol{L} = \boldsymbol{F} \times \dot{\boldsymbol{F}}$, we find that $|\dot{\boldsymbol{n}}| = |\boldsymbol{L}|/F^2 \propto F_0^2/F^2(t)$ decreases rapidly. Ergo, after a short time (of order $1/q_{\rm cr}$), the magnetization $\boldsymbol{F}$ at each spatial position $\boldsymbol{r}$ grows exponentially in some given direction $\boldsymbol{n}(\boldsymbol{r})$, i.e., the system rolls down the parabolic potential hill whereby the direction of descent does not change anymore, cf. Fig. 4.6. The correlations between the frozen directions $\boldsymbol{n}$ at different spatial positions are governed by the initial state and determine the seeds for the creation of topological defects – objects which cannot be deformed to a constant $\boldsymbol{n}$ in a smooth way [175].

The topological defects considered here are $SO(D)$ (anti-)hedgehogs in D spatial dimensions with the typical order parameter distribution $\boldsymbol{n} = \pm\boldsymbol{r}/r$, cf. Fig. 4.2.2, and can be characterized by a non-vanishing winding number, i.e., a topological invariant belonging to the homotopy group $\pi_{D-1}(S_{D-1}) = \mathbb{Z}$ (with S_{D-1} being the unit sphere in $D-1$ dimensions). The winding number is calculated by an integral over a $D-1$-dimensional hypersurface enclosing a D-dimensional volume [177]:

$$\hat{\mathfrak{N}} = \oint dS_a\,\frac{\varepsilon_{abc\ldots}\varepsilon^{ab\gamma\ldots}}{\Gamma(N)\,\mathcal{S}_{N-1}}\,\hat{n}^a(\partial_b\hat{n}^b)(\partial_\gamma\hat{n}^c)\ldots\,. \tag{4.30}$$

Here $\mathcal{S}_{D-1} = 2\pi^{D/2}/\Gamma(D/2)$ denotes the surface of the unit sphere embedded in D dimensions, and ε are the D-dimensional Levi-Civita symbols. Since the winding number counts the difference between hedgehogs and anti-hedgehogs, its expectation value vanishes, $\langle\hat{\mathfrak{N}}\rangle = 0$ (conservation of magnetization), but its variance $\langle\hat{\mathfrak{N}}^2\rangle$ as a function of the enclosed volume yields the desired spectrum of net magnetization fluctuations.

In order to calculate the variance $\langle\hat{\mathfrak{N}}^2\rangle$ of the winding number, we make an additional approximation: for a D-dimensional harmonic oscillator $\ddot{\boldsymbol{F}} \approx q_{\rm cr}^2\boldsymbol{F}/4$, the ground-state probability distribution $p(F) \propto F^{D-1}\exp\{-F^2\}$ of the amplitude F is peaked around a (for $D > 1$) non-zero value and the relative width of this peak decreases with increasing D. Therefore, we approximate the operator $\hat{F}$ by an exponentially growing classical value $\hat{F} \to F(t)$ in all expectation values. This semiclassical approximation will become asymptotically exact in the limit $D \uparrow \infty$, but we expect it to yield qualitatively correct results also in lower dimensions down to $D = 2$, since $p(F)$ is discernibly peaked even for $D = 2$ and the topological defects are mainly determined by the (quantum) fluctuations of $\hat{\boldsymbol{n}}$ (and not by those of $\hat{F}$).

For example, calculating [in analogy to (4.27)] the contribution of the fastest growing modes to the correlator $\langle\hat{\boldsymbol{F}}^2(t,\boldsymbol{r})\hat{\boldsymbol{F}}^2(t,\boldsymbol{r}')\rangle = F^4(t)+2\langle\hat{\boldsymbol{F}}(t,\boldsymbol{r})\cdot\hat{\boldsymbol{F}}(t,\boldsymbol{r}')\rangle^2/D$, we see that the accuracy of the semiclassical approximation $\hat{F} \to F(t)$ increases for large distances $|\boldsymbol{r}-\boldsymbol{r}'|$ and/or for large D, see Appendix D. Note that all the linearized $\hat{F}_a$ possess independent initial ground states and commute with each other. Therefore, the $\hat{n}_a$ do also commute with each other [so that operator ordering in (4.30) is not an issue] and with $\hat{F}$, which ultimately makes possible the semiclassical approximation of $\hat{F} \to F$.

4.2.5 Vortex number scaling in two spatial dimensions

The above approach enables us to calculate $\langle\hat{\mathfrak{N}}^2\rangle$ in arbitrary dimensions $D \geq 2$. After inserting (4.30) and using the semiclassical approximation $\hat{\boldsymbol{F}}(t,\boldsymbol{r}) \approx F(t)\,\hat{\boldsymbol{n}}(\boldsymbol{r})$, the expectation value can be decomposed into a product of D two-point correlators (4.27). Let us exemplify this procedure for two spatial dimensions: the transverse magnetization can be decomposed via

$$\hat{F}_\perp = \hat{F}_x + i\hat{F}_y = \hat{F}e^{i\hat{\Phi}} \tag{4.31}$$

into its modulus $\hat{F}$ and phase $\hat{\Phi}$ which commute and are both self-adjoint[8]. The winding number (4.30) reads[9]

$$\hat{\mathfrak{N}} = \frac{1}{2\pi}\oint\limits_{\mathfrak{C}} d\boldsymbol{l}\cdot\boldsymbol{\nabla}\hat{\Phi} = \oint\limits_{\mathfrak{C}} d\boldsymbol{l}\cdot\frac{\hat{F}_x\boldsymbol{\nabla}\hat{F}_y - \hat{F}_y\boldsymbol{\nabla}\hat{F}_x}{2\pi\hat{F}^2}\,. \tag{4.32}$$

---

[8] Note that this is distinct from the non-vanishing commutator of density and phase operators resulting from the analogous decomposition of the single-component field operator $\hat{\Psi} = e^{i\hat{\Phi}}\sqrt{\hat{\varrho}}$, cf. Eqs. (3.43) and (3.113), which underlies the definition of conventional momentum/velocity vortices in a fluid. Roughly speaking, the components $\hat{F}_a$ of the magnetization $\hat{\boldsymbol{F}}$ are independent variables, whereas real and imaginary parts of the field operator $\hat{\Psi}$ of Bose-Einstein condensates are not.

[9] In contrast to spin vortices, domain walls (lines with vanishing F) are not topologically stable for the order parameter considered here. Thus, the domain-boundaries observed in the experiment are line-like regions with small but not vanishing F and do not enter Eqs. (4.30) and (4.32).

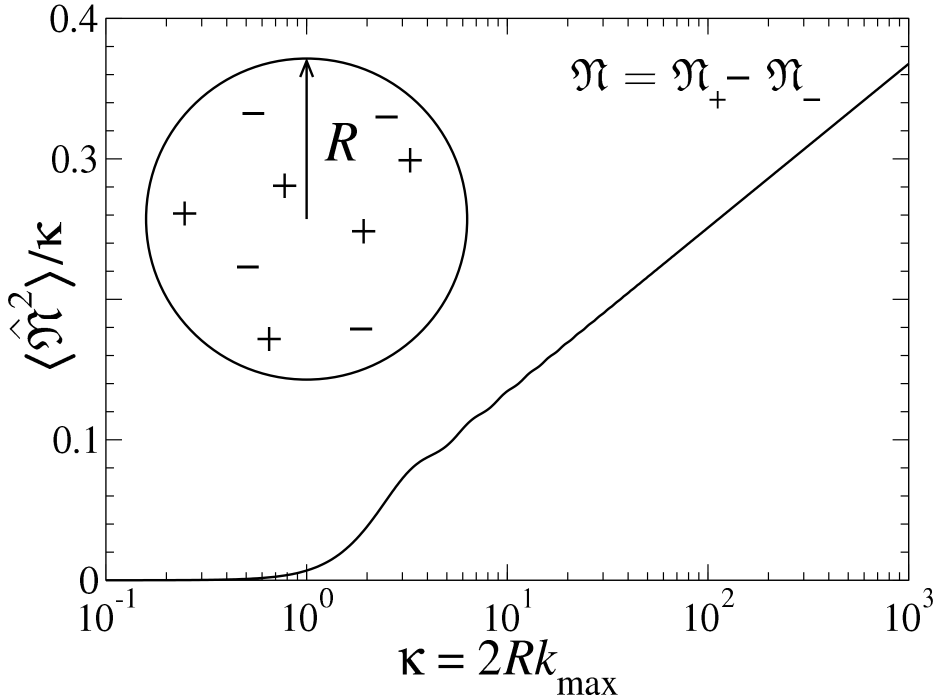

Figure 4.7: Scaling of the variance of the winding number $\langle\hat{\mathfrak{N}}^2\rangle$ with the sample size R. A logarithmic plot of $\langle\hat{\mathfrak{N}}^2\rangle/\kappa$ is used in order to visualize the asymptotic $\kappa\ln\kappa$ scaling.

Using Eq. (4.27), replacing $\hat{F} \to F$, and choosing the contour $\mathfrak{C}$ as a circle with radius R, we get

$$\langle\hat{\mathfrak{N}}^2(R)\rangle = \frac{\kappa^2}{2\pi}\int_0^1 \mathrm{d}x\sqrt{1-x^2}\,J_1^2(\kappa x)\,, \tag{4.33}$$

with $\kappa = 2k_{\max}R$, cf. Fig. 4.7. As anticipated, the characteristic length scale (e.g., typical distance between vortices) is set by the dominant wavelength $\lambda_{\max}$ (instead of the spin healing length ξ_s, for example).

The analytic expression (4.33) enables us to study the large-scale spectrum of the winding number, i.e., the difference between the number of vortices and anti-vortices $\mathfrak{N} = \mathfrak{N}_+ - \mathfrak{N}_-$. Typically, two popular models for its scaling behavior are discussed in the literature [33, 40, 166]. Assuming a random distribution of vortices and anti-vortices (*random vortex gas* model), the typical difference $|\mathfrak{N}|$ scales with $\sqrt{\mathfrak{N}_\pm}$. Because the total number $\mathfrak{N}_+ + \mathfrak{N}_-$ increases proportional to the area R^2, this model predicts a scaling of $\langle\hat{\mathfrak{N}}^2\rangle \sim R^2$ ($D = 2$). Alternatively, the *random phase walk* model assumes a random walk of the phase Φ along the circumference of the circle. The accumulated winding number $|\mathfrak{N}|$ scales with $\sqrt{R}$ in this situation, implying a scaling of $\langle\hat{\mathfrak{N}}^2\rangle \sim R$. Of course, both models cannot be the final truth (consider the deformation of the circle to a slim ellipse, for example), and it is not obvious how to generalize the random phase walk model to higher dimensions – but one can compare the different predictions with the presented approach. For large κ, the asymptotic expansion $J_1(\kappa x \uparrow \infty) \propto \cos(\kappa x - 3\pi/4)/\sqrt{\kappa x}$ yields (cf. Fig. 4.7)

$$\langle \hat{\mathfrak{N}}^2(\kappa \gg 1) \rangle \sim \kappa \ln \kappa \,, \tag{4.34}$$

which is close to the scaling predicted by the random phase walk model – but still not quite in agreement due to the additional factor of $\ln \kappa$. This extra factor only occurs for $D = 2$ and arises from the slow decay of the two-point correlator (4.27) at large distances $|\boldsymbol{r} - \boldsymbol{r}'|^{-1/2}$, which deviates from a local random phase walk[10]. Although the sample size in [43] is probably not sufficient for extracting the factor $\ln \kappa$, this prediction could be tested in future experiments.

Finally, let us study intermediate κ values: in Ref. [179], the defect density is calculated to be $k_{\max}^2/(4\pi)$ treating the magnetization as a Gaussian stochastic field. Hence, a circle with a radius of $R = 2/k_{\max}$ should typically contain one (anti-)vortex. However, if we calculate $\langle \hat{\mathfrak{N}}^2 \rangle$ at $\kappa = 4$, we obtain around $1/3$ instead of one, cf. Figure 4.7 Although the discrepancy is not huge, it already suggests that our results are not quite compatible with Ref. [179], and thus experiment should judge which approach yields the better description. Alternatively, numerical simulations (supplemented by suitable assumptions about the initial noise spectrum) provide a complementary approach [180].

4.3 Conclusions

In conclusion, an adapted mean-field expansion enabled us to analytically calculate the freezing of number fluctuations and the growth of phase fluctuations during an (exponential) sweep through the superfluid to Mott insulator quantum phase transition in the Bose-Hubbard model for large fillings. As further experimental signatures, we predict the temporal decay of the superfluid fraction $n_{\rm sf}/n$ and of the central $\boldsymbol{k} = 0$ peak in the structure factor $S(\boldsymbol{k})$.

As second example, we studied the creation of topological defects during the quench of a spinor Bose gas from the (polar) paramagnetic to the (planar) ferromagnetic phase with broken $SO(D)$-symmetry. By extrapolating the mean-field ansatz[11], we found that the direction $\boldsymbol{n}$ of the effective magnetization $\boldsymbol{F}$ freezes shortly after the quench while its magnitude F grows exponentially. Hence, we were able to derive the (frozen) winding number $\hat{\mathfrak{N}}$ of the seeds for $SO(D)$ topological defects and to predict its scaling behavior which is universal in the sense that it does not depend on temperature and sweep rate etc. For $D = 2$, the obtained variance of the winding number (i.e., the difference between the number of vortices and anti-vortices within a given area) is not compatible with the random vortex gas model, but favors the random phase walk model instead, although an additional logarithmic factor $\ln \kappa$ occurs in Eq. (4.34) (which might be an artifact of the employed saddle-point approximation, which but might also have a physical origin).

---

[10] Observe that the extra factor of $\ln \kappa$ in Eq. (4.34) in only valid within the saddle-point approximation, i.e., for large times t (but still in the linear regime). Keeping the time t fixed to a large value and considering the limit of ultra-large distances R (where the saddle point approximation breaks down), on the other hand, the scaling levels off to κ.

[11] Note that our results do only describe the initial stage, and are, strictly speaking, only valid in the linear regime, i.e., as long as the directions $\boldsymbol{n}(\boldsymbol{r})$ are frozen. The subsequent nonlinear dynamics, including annihilation of vortex–anti-vortex pairs, for example, is not taken into account.

5 Conclusions

The focus of this Thesis lay on effects associated with quantum vacuum fluctuations. Although these fluctuations are small and almost not perceivable in the everyday world, they might generate macroscopic effects in certain situations, some of which we studied. We were particularly interested in dynamical systems, where the quantum fluctuations are subject to time-dependent external influences. If the typical variation time of these external influences is shorter than the response time of the fluctuations, they cannot follow and will evolve non-adiabatically (i.e., they effectively freeze and get amplified).

As an example of such a quantum effect at high energies, cosmic inflation was considered in Chapter 2. During inflation, the quantum vacuum fluctuations of the inflaton field were stretched by the expanding space-time background and thus froze and got amplified when neighboring nodes lost causal contact (i.e., were separated by a horizon). We calculated the three-point correlation function of the frozen vacuum fluctuations – a signal which may be still observable in the cosmic microwave background radiation. By tracing the observed anisotropies of the microwave radiation back in time, they originate from quantum fluctuations at very high energies and thus might give access to new physics beyond the standard model at high (e.g., Planck-scale) energies.

An analogous process occurs in expanding Bose-Einstein condensates, see Sec. 3.5. Adopting an effective space-time description for the phonon modes (cf. Sec. 3.4), we were able to identify several aspects of cosmic inflation in this laboratory system. In particular, the stretching, freezing, and amplification of the phonon fluctuations can be understood in terms of an emerging effective sound horizon. It becomes thus possible to study quantum aspects of cosmic inflation in the laboratory by means of this analogue system.

On the other hand, this “cosmic effect” marks the ultimate quantum limit of time-of-flight imaging: the noise generated by the frozen and amplified quantum fluctuations is always present and thus poses a limit on the achievable resolution; no matter how careful the condensate is prepared in an experiment, details smaller than this pure quantum vacuum effect cannot be resolved. The strong similarities between these two effects, cosmic inflation and expanding Bose-Einstein condensate, which correspond to vastly different energy scales, reveal the universal character of quantum fluctuations.

In the former examples (inflation and expanding condensate), adiabaticity was violated due to rapid changes of some external conditions, e.g., the rapid expansion of the background. If the changes were sufficiently slow, the system would stay in its ground state. On the other hand, adiabaticity will also be violated if the response time becomes too long. This is the case in dynamic quantum phase transitions, where the response time of the quantum fluctuations diverges at the critical point.

We addressed two particular scenarios of quantum phase transitions in this Thesis: in Sec. 4.1, we studied the superfluid to Mott insulator transition in the Bose-Hubbard model and calculated the decaying long-range order of the superfluid phase. Again, the loss of phase coherence can be understood through the emergence of an effective horizon. And, secondly, we discussed in Sec. 4.2 a quasi-two-dimensional spin-one Bose gas, which is quenched from a (polar) paramagnetic initial state into a (planar) ferromagnetic phase. We deduced a scaling law for the excess vortex number within a given area generated by the sweep.

Both quantum phase transitions studied in this Thesis can be realized in experiments using ultracold quantum gases. But they might also serve as toy models for studying similar processes, in solid state physics, for example: firstly, a metal-insulator transition (Mott transition) can, in the simplest models, be described by the (fermionic) Hubbard model. A similar transition might also occur in superconductors, which are insulating above the critical temperature. (In these superconductors, an effective interaction binds to fermionic electrons to bosonic Cooper pairs, which then condense and form a superfluid.) And secondly, the defects created during the paramagnetic to ferromagnetic quench in spinor Bose gases might serve as toy models for the flux lines in superconductors. Superconductivity breaks down in these flux lines and hence, transport properties (conductivity, susceptibility etc.) will depend on the number of lines, i.e., defects.

6 Outlook

We have seen that certain aspects of quantum field theory in curved space-times can be modeled by means of analogue laboratory systems. These parallels are founded on the linearized low-energy action, which can be cast into an (effectively) covariant form. It is thus possible to study quantum effects known from cosmology in the laboratory. On the other hand, the full action (i.e., beyond first order) of the laboratory analogues enables us to investigate the influence of the full microscopic physics onto the quantum effects.

With the lessons learned from these "toy" systems, several questions of quantum gravity might be investigated by means of the analogues. For instance, there are two scales in Bose-Einstein condensates, where the fluctuation spectrum changes: firstly, the healing length ξ, at which the dispersion relation becomes nonlinear and the effective Lorentz symmetry is broken. And secondly, a cut-off wavenumber k_{cut}, which emerges naturally due to the finite range of the two-particle interaction potential. The change in the dispersion relation at the healing lengths ξ suffices to render some, but not all, expectation values ultraviolet finite (without *ad hoc* renormalization). The remaining divergences will be removed by the cut-off wavenumber, which is in general much larger than the inverse healing length $k_{\text{cut}} \gg 1/\xi$. Both scales might have counterparts in quantum gravity. For instance, the Planck scale might correspond to the scale where the Lorentz symmetry is broken, or a where coarse-graining of the space-time becomes important.

Another interesting issue of quantum field theory in curved space-times regards the quantum backreaction. In Sec. 3.6, we calculated it *ab initio* from the full action. This finding was compared to results obtained using the effective action technique, which is based on the linearized action. Since the explicit expression for the backreaction crucially depends on the choice of the classical background, the applicability of the effective action technique is problematic. The difficulties associated with the effective action technique might also have a severe impact on cosmology: for instance, the actual value of the cosmological constant, which is believed to be the vacuum pressure of the universe, probably differs from a naive calculation, where the low-energy effective action is extrapolated to arbitrarily high energies.

When considering quantum phase transitions in Chapter 4, we restricted ourselves to homogeneous condensates, i.e., infinite systems. In experiments, the atoms are usually confined in an additional harmonic potential, which implies a spatially-varying atom density.

Bearing in mind that the value of the critical J in the Bose-Hubbard model, for example, depends on the filling per lattice site, the critical point will be crossed at different times throughout the lattice, when sweeping through the phase transition with a finite velocity. If we started with the superfluid phase and increased the lattice potential, the Mott phase will first develop at the rim of the gas cloud, where the filling is small. By further increasing the lattice potential, the phase transition in the inner parts of the trap could be triggered by two effects: firstly, by the quantum vacuum fluctuations as in a homogeneous transition. And secondly, by the moving phase boundary (similar to shock-waves) originating from the Mott rim. In order to describe realistic experiments of atoms in optical lattices, the interplay between these two competing effects requires further investigations.

Appendix A Adiabatic expansion

In order to derive adiabatic corrections to a given state vector $|\Psi(t)\rangle$, one most conveniently starts with the time-dependent Schrödinger equation

$$\hat{H}|\Psi(t)\rangle \;=\; i|\dot{\Psi}(t)\rangle\,. \tag{A.1}$$

An expansion of $|\Psi(t)\rangle$ into instantaneous eigenstates $|n(t)\rangle$ of the Hamilton operator, $\hat{H}|n(t)\rangle = E_n(t)|n(t)\rangle$

$$|\Psi(t)\rangle \;=\; \sum_n a_n(t)\exp\left\{-i\int^t E_n(t')\mathrm{d}t'\right\}|n(t)\rangle \tag{A.2}$$

can be inserted into Schrödinger's equation (A.1), yielding for the coefficients $a_n(t)$

$$\sum_n \dot{a}_n(t)e^{-i\int^t E_n}|n(t)\rangle + \sum_n a_n(t)e^{-i\int^t E_n}|\dot{n}(t)\rangle \;=\; 0\,. \tag{A.3}$$

In view of the orthonormality of the states $|n(t)\rangle$, the derivatives $\dot{a}_n(t)$ can be obtained by projection. Using $\langle k|\dot{n}\rangle = \langle k|\dot{H}|n\rangle/(E_n - E_k)$ for $n \neq k$, it follows

$$\dot{a}_k + a_k\langle k|\dot{k}\rangle \;=\; e^{i\gamma_k}\frac{\partial}{\partial t}a_k e^{-i\gamma_k} \;=\; -\sum_{n\neq k} a_n e^{-i\int g_{nk}(t')\mathrm{d}t'}\frac{\langle k|\dot{H}|n\rangle}{g_{nk}}\,, \tag{A.4}$$

where $g_{nk}(t) = E_n(t) - E_k(t)$ denotes the energy gap of two modes and $\gamma_k = i\int_{t_0}^t \mathrm{d}t'\langle k(t)|\dot{k}(t)\rangle$ is Berry's phase. Defining

$$F_{nk}(t) \;=\; a_n(t)\langle k(t)|\dot{\hat{H}}(t)|n(t)\rangle e^{-i\gamma_k(t)}\,, \tag{A.5}$$

the integration of Eq. (A.4) yields

$$a_k(t)e^{-i\gamma_k(t)} \;=\; a_k(t_0) - \sum_{n\neq k}\int\limits_{t_0}^{t}\mathrm{d}t'\frac{F_{nk}(t')}{g_{nk}(t')}e^{-i\int^{t'} g_{nk}}\,. \tag{A.6}$$

The integral on the right-hand side can be evaluated by subsequently using

$$e^{-i\int^t g_{nk}} \;=\; \frac{i}{g_{nk}}\frac{\mathrm{d}}{\mathrm{d}t}e^{-i\int^t g_{nk}}\,, \tag{A.7}$$

and performing an integration by parts, yielding an additional differentiation under the integral for each sequence. For instance, the next order reads

$$\begin{aligned} a_k(t)e^{-i\gamma_k(t)} &= a_k(t_0) - i\sum_{n\neq k}\frac{F_{nk}(t)}{g_{nk}^2(t)}e^{-i\int^t g_{nk(t')}} + i\sum_{n\neq k}\frac{F_{nk}(t_0)}{g_{nk}^2(t_0)} \\ &\quad + i\sum_{n\neq k}\int\limits_{t_0}^{t}\mathrm{d}t' e^{-i\int^{t'} g_{nk}(t')}\frac{\mathrm{d}}{\mathrm{d}t'}\frac{F_{nk}(t')}{g_{nk}^2(t')}\,. \end{aligned} \tag{A.8}$$

Often, the corrections are expressed as a series expansion in a small parameter and each differentiation yields one additional power (e.g., $1/g_{nk}$). When the desired accuracy is reached, the higher-order version of Eq. (A.6) can be solved iteratively since $F_{nk}(t) \propto a_n(t)$ [i.e., the right hand side of Eq. (A.6) depends on the left hand side].

The Hamiltonian (2.12) contains two small parameters, the Hubble constant $\mathfrak{H}$ and the coupling constant g. We need an expansion to first order in g and second order in $\mathfrak{H}$ (because they are the leading order of the adiabatic corrections). Note that the calculations in Chapter 2 are performed in the conformal time τ. Hence, each differentiation with respect to τ yields a factor $\mathfrak{H}$. Omitting the terms with τ_0 as argument (they correspond to the adiabatic corrections at time τ_0), the coefficients are given by

$$\begin{aligned} a_k(\tau)e^{-i\gamma_k(\tau)} &= a_k(\tau_0) - i\sum_{n\neq k}\frac{F_{nk}(\tau)}{g_{nk}^2(\tau)}e^{-i\int^\tau g_{nk}(\tau')} \\ &\quad - e^{-i\int^\tau g_{nk}(\tau')}\frac{1}{g_{nk}(\tau)}\frac{\mathrm{d}}{\mathrm{d}\tau}\frac{F_{nk}(\tau)}{g_{nk}^2(\tau)} + \mathcal{O}(\mathfrak{H}^3) + \mathcal{O}(g^2)\,. \end{aligned} \tag{A.9}$$

As next step, this equation is solved iteratively. Since $F_{nm} \propto \partial_\tau\hat{H} = \mathcal{O}(\mathfrak{H}^2) + \mathcal{O}(g\mathfrak{H})$, Eq. (A.5) can be approximated by $F_{nm} = a_k(\tau_0)\langle k(\tau)|(\partial_\tau\hat{H})|n(\tau)\rangle e^{-i\gamma_k(\tau)}$. For the initial ground state, we have $a_k(\tau\downarrow 0) = \delta_{k0}$. Noting that the exponential factors $\exp\{-i\int g_{nk}\}$ and $\exp\{-i\gamma_k\}$ yield a contribution of order $1 + \mathcal{O}(\mathfrak{H}^3) + \mathcal{O}(g^2)$, we obtain Eq. (2.13).

Appendix B Backreaction for a Toy Model

To given a simple illustration of the influence of the choice of coordinates, let us consider a very simple quantum system, the one-dimensional harmonic oscillator with the frequency Ω. The equation of motion for the position operator $\hat{X}$ reads

$$\frac{\partial^2}{\partial t^2}\hat{X} + \Omega^2 \hat{X} \,=\, 0\,. \tag{B.1}$$

Of course (as it is well known from the theory of coherent states), splitting up this position operator $\hat{X}$ into a classical (background) part $X_\mathrm{b} = \langle\hat{X}\rangle$ and a quantum fluctuation part $\delta\hat{X}$ with $\langle\delta\hat{X}\rangle = 0$ via $\hat{X} = X_\mathrm{b} + \delta\hat{X}$ yields the same equation of motion for both parts separately, i.e., there is no backreaction at all.

However, if we artificially introduce another variable Y via $X = Y^2/2$, its (classical) equation of motion reads

$$\ddot{Y} + \frac{\dot{Y}^2}{Y} + \frac{\Omega^2}{2}Y \,=\, 0\,. \tag{B.2}$$

Now the same procedure $\hat{Y} = Y_\mathrm{b} + \delta\hat{Y}$ would yield a non-vanishing quantum backreaction term. Therefore, one must be careful when comparing different expressions for the quantum backreaction, since the explicit form may depend on the choice of splitting the system into a classical background and quantum fluctuations (e.g., $\hat{X} = X_\mathrm{b} + \delta\hat{X}$ versus $\hat{Y} = Y_\mathrm{b} + \delta\hat{Y}$). This illustrates the importance of working with measurable quantities such as $\hat{X}$ or $\boldsymbol{j}$ and ϱ. Exploiting the simple example a bit further, an an-harmonic oscillator $\partial_t^2\hat{X} + \Omega^2\hat{X} = g\hat{X}^2$ yields

$$\frac{\partial^2}{\partial t^2}\langle\hat{X}\rangle + \Omega^2\langle\hat{X}\rangle - g\langle\hat{X}\rangle^2 \,=\, g\langle\delta\hat{X}^2\rangle\,, \tag{B.3}$$

i.e., a real quantum backreaction term.

Appendix C On mean-field splits

In this Appendix, we will derive the relation between two different mean-field expansions for density $\hat{\varrho}$ and phase operators $\hat{\phi}$. On one hand, we can adopt the mean-field expansion (3.10), where the classical background is defined with respect to the field operator $\hat{\Psi}$

$$\hat{\Psi} \,=\, \left(\psi_0 + \hat{\chi} + \hat{\zeta}\right) \frac{\hat{A}}{\sqrt{\hat{N}}}\,, \tag{C.1}$$

whereas we might also adopt a polar decomposition (3.113) of the field operator and expand density and phase around their expectation values, cf. Eq. (3.112)

$$\begin{aligned} \hat{\varrho} \,&=\, \langle \hat{\varrho} \rangle + \delta\hat{\varrho} \,=\, \varrho_b + \delta\hat{\varrho}\,, \\ \hat{\phi} \,&=\, \langle \hat{\phi} \rangle + \delta\hat{\phi} \,=\, \phi_b + \delta\hat{\phi}\,. \end{aligned} \tag{C.2}$$

Insertion of this split into Eq. (3.113) yields (to second order)

$$\hat{\Psi} \,=\, e^{i\phi_b}\sqrt{\varrho_b}\left(1 - \frac{1}{8}\frac{\delta\hat{\varrho}^2}{\varrho_b^2} - \frac{\delta\hat{\phi}^2}{2} - \frac{i}{2}\frac{\delta\hat{\phi}\delta\hat{\varrho}}{\varrho_b} + i\delta\hat{\phi} - \frac{1}{2}\frac{\delta\hat{\varrho}}{\varrho_b}\right) + \mathcal{O}(\delta^3)\,. \tag{C.3}$$

The expectation value of this expression can be compared to Eq. (C.1), it follows

$$\hat{\chi} \,=\, e^{i\phi_b}\sqrt{\varrho_b}\left(i\delta\hat{\phi} - \frac{1}{2}\frac{\delta\hat{\varrho}}{\varrho_b}\right) + \mathcal{O}(\delta^2)\,, \tag{C.4}$$

for the fluctuations and

$$\langle \hat{\Psi} \rangle \,=\, \psi_0 \,=\, e^{i\phi_0}\sqrt{\varrho_0} = e^{i\phi_b}\sqrt{\varrho_b}\left(1 - \frac{1}{8}\frac{\langle\delta\hat{\varrho}^2\rangle}{\varrho_b^2} - \frac{\langle\delta\hat{\phi}^2\rangle}{2} - \frac{i}{2}\frac{\langle\delta\hat{\phi}\delta\hat{\varrho}\rangle}{\varrho_b}\right) + \mathcal{O}(\delta^3) \tag{C.5}$$

for the background. (Note that $\langle \hat{\Psi} \rangle \sim \psi_0$ only holds in the limit of large $N \uparrow \infty$, where $\langle \hat{A}/\sqrt{\hat{N}} \rangle \sim 1$. Since this additional term does not affect our argumentation, we will omit it.) Bearing in mind that $\hat{\varrho} = \hat{\Psi}^\dagger\hat{\Psi}$, the hydrodynamic background variables ϱ_b and ϕ_b can be expressed in terms of ϱ_0 and ϕ_0

$$\begin{aligned} \phi_b \,&=\, \phi_0 + \frac{1}{4}\frac{\langle\delta\hat{\varrho}\delta\hat{\phi}\rangle}{\varrho_0} + \frac{1}{4}\frac{\langle\delta\hat{\phi}\delta\hat{\varrho}\rangle}{\varrho_0}\,, \\ \varrho_b \,&=\, \varrho_0 + \varrho_0\langle\delta\hat{\phi}^2\rangle + \frac{1}{4}\frac{\langle\delta\hat{\varrho}^2\rangle}{\varrho_0} + \frac{i}{2}\langle[\delta\hat{\phi}, \delta\hat{\varrho}]\rangle\,. \end{aligned} \tag{C.6}$$

Appendix D Effective Hamiltonian for magnetization operator

In this Appendix, the derivation of the effective Hamiltonian (4.23) will be sketched and we will also deduce the correlation function (4.27). We start with the Hamiltonian (4.20)

$$\begin{aligned} \hat{\mathcal{H}} &= \frac{1}{2m}(\boldsymbol{\nabla}\hat{\psi}_a^\dagger)\cdot\boldsymbol{\nabla}\hat{\psi}_a + V_{\text{trap}}\hat{\psi}_a^\dagger\hat{\psi}_a + \frac{c_0}{2}\hat{\psi}_a^\dagger\hat{\psi}_b^\dagger\hat{\psi}_b\hat{\psi}_a \\ &\quad + \frac{c_2}{2}\boldsymbol{F}_{ab}\cdot\boldsymbol{F}_{cd}\,\hat{\psi}_a^\dagger\hat{\psi}_b\hat{\psi}_c^\dagger\hat{\psi}_d + q\hat{\psi}_1^\dagger\hat{\psi}_1 + q\hat{\psi}^\dagger_{-1}\hat{\psi}_{-1}\,, \end{aligned} \tag{D.1}$$

with the indices $a = 0, \pm 1$ and the spin-one matrices F^i_{ab} given by

$$F^x_{ab} = \frac{1}{\sqrt{2}}\begin{pmatrix} 0 & 1 & 0 \\ 1 & 0 & 1 \\ 0 & 1 & 0 \end{pmatrix}\,,\; F^y_{ab} = \frac{i}{\sqrt{2}}\begin{pmatrix} 0 & 1 & 0 \\ -1 & 0 & 1 \\ 0 & -1 & 0 \end{pmatrix}\,,\; F^z_{ab} = \begin{pmatrix} 1 & 0 & 0 \\ 0 & 0 & 0 \\ 0 & 0 & -1 \end{pmatrix}\,. \tag{D.2}$$

The spin-spin part reads *in extenso*

$$\begin{aligned} \hat{\mathcal{H}}_{ss} &= \frac{c_2}{2}\boldsymbol{F}_{ab}\cdot\boldsymbol{F}_{cd}\hat{\Psi}_a^\dagger\hat{\Psi}_b\hat{\Psi}_c^\dagger\hat{\Psi}_d \\ &= \frac{c_2}{2}\Big(\hat{\Psi}_1^\dagger\hat{\Psi}_1^\dagger\hat{\Psi}_1\hat{\Psi}_1 + \hat{\Psi}^\dagger_{-1}\hat{\Psi}^\dagger_{-1}\hat{\Psi}_{-1}\hat{\Psi}_{-1} - 2\hat{\Psi}_1^\dagger\hat{\Psi}^\dagger_{-1}\hat{\Psi}_1\hat{\Psi}_{-1} + 2\hat{\Psi}_1^\dagger\hat{\Psi}_0^\dagger\hat{\Psi}_1\hat{\Psi}_0 \\ &\qquad + 2\hat{\Psi}^\dagger_{-1}\hat{\Psi}_0^\dagger\hat{\Psi}_{-1}\hat{\Psi}_0 + 2\hat{\Psi}_0^\dagger\hat{\Psi}_0^\dagger\hat{\Psi}_1\hat{\Psi}_{-1} + 2\hat{\Psi}_1^\dagger\hat{\Psi}^\dagger_{-1}\hat{\Psi}_0\hat{\Psi}_0\Big)\,. \end{aligned} \tag{D.3}$$

Starting from the (homogeneous) paramagnetic ground state, we adopt a mean-field expansion

$$\hat{\Psi}_a = e^{-i\mu t}(\Psi_a + \delta\hat{\Psi}_a)\,, \qquad \Psi_a = \sqrt{\varrho_0}\delta_{a,z} \tag{D.4}$$

where $\mu = V_{\text{trap}} + c_0\varrho_0$ is the chemical potential (in Thomas-Fermi approximation). By setting $\mu = 0$ (shifting the potential), the global oscillating prefactor $e^{-i\mu t}$ becomes unity. Omitting the unmagnetized component $\hat{\Psi}_z = \hat{\Psi}_0$ (because the linearized field equations for this component are independent of the external magnetic field $q \propto B^2$), we obtain the effectively two-dimensional linearized Hamiltonian

$$\hat{\mathcal{H}}^{(2)} = \delta\hat{\Psi}_a^\dagger\left(\frac{-\boldsymbol{\nabla}^2}{2m} + \mu + q + c_2\varrho_0\right)\delta\hat{\Psi}_a + c_2\varrho_0\left(\delta\hat{\Psi}_1\delta\hat{\Psi}_{-1} + \delta\hat{\Psi}_1^\dagger\delta\hat{\Psi}^\dagger_{-1}\right)\,. \tag{D.5}$$

with the index $a = \pm 1$. The Hamiltonian (4.23) can be obtained from the expression above after a series of canonic transformations. First, in order to decouple the equations for the two quasi-particle $a = \pm 1$ excitations, we introduce the components of the Cartesian spinor

$$\hat{\Psi}_x = \frac{1}{\sqrt{2}}\left(\hat{\Psi}_1 - \hat{\Psi}_{-1}\right), \qquad \hat{\Psi}_y = \frac{i}{\sqrt{2}}\left(\hat{\Psi}_1 + \hat{\Psi}_{-1}\right), \qquad \hat{\Psi}_z = \hat{\Psi}_0 . \tag{D.6}$$

And secondly, we map them onto the magnetization operator $\hat{\mathcal{F}}_i = -\varepsilon_{ijk}\hat{\Psi}_j^\dagger\hat{\Psi}_k$. This mapping, however, is not yet canonic (as can be easily checked, $\hat{\mathcal{F}}_i$ are self-adjoint). We therefore need to introduce the momentum conjugate to the magnetization. For the linearized fields, the transformations [only x and y components, since $\hat{\mathcal{F}}_z = \mathcal{O}(\delta^2)$] are given by

$$\begin{aligned} \hat{\mathcal{F}}_x &= i\sqrt{\varrho_0}(\delta\hat{\Psi}_y - \delta\hat{\Psi}_y^\dagger), & \hat{\mathcal{F}}_y &= -i\sqrt{\varrho_0}(\delta\hat{\Psi}_x - \delta\hat{\Psi}_x^\dagger), \\ \hat{P}_x &= \frac{1}{2\sqrt{\varrho_0}}(\delta\hat{\Psi}_y^\dagger + \delta\hat{\Psi}_y), & \hat{P}_y &= -\frac{1}{2\sqrt{\varrho_0}}(\delta\hat{\Psi}_x^\dagger + \delta\hat{\Psi}_x) . \end{aligned} \tag{D.7}$$

The Hamiltonian density becomes

$$\begin{aligned} \hat{\mathcal{H}}^{(2)} = \frac{1}{2}\sum_{a=x,y} \Bigg[& 2\varrho_0\hat{P}_a\left(-\frac{\boldsymbol{\nabla}^2}{2m} + V_{\text{trap}} + \mu + q\right)\hat{P}_a \\ & + \frac{1}{2\varrho_0}\hat{\mathcal{F}}_a\left(-\frac{\boldsymbol{\nabla}^2}{2m} + V_{\text{trap}} + \mu + q + 2c_2\varrho_0\right)\hat{\mathcal{F}}_a \\ & + \frac{i}{2}\left[\hat{\mathcal{F}}_a, \hat{P}_a\right](V_{\text{trap}} + \mu + q + c_2\varrho_0) - \frac{i}{4m}\left(\hat{\mathcal{F}}_a\boldsymbol{\nabla}^2\hat{P}_a - \hat{P}_a\boldsymbol{\nabla}^2\hat{\mathcal{F}}_a\right)\Bigg] . \end{aligned} \tag{D.8}$$

The terms in the last line are merely commutators of the conjugate variables and do not affect the field equation for the magnetization. (Note that the $\boldsymbol{\nabla}^2$ can be shifted under the integration in the Hamiltonian from $\hat{\mathcal{F}}_a$ to $\hat{P}_a$ and *vice versa.*) Neglecting the last line of Eq. (D.8), the effective Hamiltonian follows

$$\hat{\mathcal{H}}^{(2)}_{\text{eff}} = \frac{1}{2}\sum_{a=x,y}\left[2\varrho_0\hat{P}_a\left(-\frac{\boldsymbol{\nabla}^2}{2m} + q\right)\hat{P}_a + \frac{1}{2\varrho_0}\hat{\mathcal{F}}_a\left(-\frac{\boldsymbol{\nabla}^2}{2m} + q - q_{\text{cr}}\right)\hat{\mathcal{F}}_a\right] , \tag{D.9}$$

where we set $\mu = -V_{\text{trap}}$ and introduced the critical value of the external parameter $q_{\text{cr}} = -2c_2\varrho_0 = 2|c_2|\varrho_0$. The Hamiltonian can easily be generalized to D dimensions. After a further canonical transformation to the normalized magnetization operator

$$\hat{F}_a = \frac{\hat{\mathcal{F}}_a}{\varrho}, \qquad \hat{\Pi}_a = \varrho\hat{P}_a , \tag{D.10}$$

the effective Hamiltonian (4.23) will be obtained.

$$\frac{\hat{\mathcal{H}}_{\text{eff}}}{\varrho} = \frac{\hat{\boldsymbol{\Pi}}}{\varrho}\left(q - \frac{\boldsymbol{\nabla}^2}{2m}\right)\frac{\hat{\boldsymbol{\Pi}}}{\varrho} + \hat{\boldsymbol{F}}\left(\frac{q + 2c_2\varrho}{4} - \frac{\boldsymbol{\nabla}^2}{8m}\right)\hat{\boldsymbol{F}} , \tag{D.11}$$

where the self-adjoint normalized magnetization operators $\hat{\boldsymbol{F}}$ and $\hat{\boldsymbol{\Pi}}$ obey the canonic equal-time commutation relation $[\hat{F}_a(\boldsymbol{r}), \hat{\Pi}_b(\boldsymbol{r}')] = i\delta_{ab}\delta(\boldsymbol{r}-\boldsymbol{r}')$. It is now straight-forward to deduce the Heisenberg equations of motion for the (normalized) magnetization operator

$$\dot{\hat{F}}_a = \frac{2}{\varrho}\left(-\frac{\boldsymbol{\nabla}^2}{2m}+q\right)\hat{\Pi}_a\,, \qquad \dot{\hat{\Pi}}_a = -\frac{\varrho}{2}\left(-\frac{\boldsymbol{\nabla}^2}{2m}+q-q_{\mathrm{cr}}\right)\hat{F}_a\,, \tag{D.12}$$

which can be solved for a given quench $q(t)$. In view of the kinetic term $\propto \boldsymbol{\nabla}^2$, it is convenient to adopt a Fourier expansion

$$\hat{F}_a = \int \frac{\mathrm{d}^N k}{(2\pi)^N}\hat{F}_{\boldsymbol{k},a}(t)e^{i\boldsymbol{k}\cdot\boldsymbol{r}}\,, \qquad \hat{\Pi}_a = \int \frac{\mathrm{d}^N k}{(2\pi)^N}\hat{\Pi}_{\boldsymbol{k},a}(t)e^{i\boldsymbol{k}\cdot\boldsymbol{r}}\,, \tag{D.13}$$

where

$$\begin{aligned}\hat{F}_{\boldsymbol{k},a} &= C_{\boldsymbol{k},a}\hat{a}_{\boldsymbol{k},a} + C^*_{-\boldsymbol{k},a}\hat{a}^\dagger_{-\boldsymbol{k},a}\,,\\ \hat{\Pi}_{\boldsymbol{k},a} &= \frac{\varrho}{2}\left[\frac{\boldsymbol{k}^2}{2m}+q(t)\right]^{-1}\left(\dot{C}_{\boldsymbol{k},a}\hat{a}_{\boldsymbol{k},a} + \dot{C}^*_{-\boldsymbol{k},a}\hat{a}^\dagger_{-\boldsymbol{k},a}\right)\,.\end{aligned} \tag{D.14}$$

Since no spatial direction is distinct [and the equations of motion (D.12) are linear], the coefficient functions will be isotropic as well, i.e., $C_{\boldsymbol{k},a}(t) = C_k(t)$. In contrast, the creation and annihilation operators $\hat{a}^\dagger_{\boldsymbol{k},a}$, $\hat{a}_{\boldsymbol{k},a}$ must bear an additional index a to label the (independent) spatial components of $\boldsymbol{F}(\boldsymbol{r})$.

The entire time-dependence of the linearized fluctuations is now contained in the $C_k(t)$. Their equation of motion follows from Eqs. (D.12) and (D.13)

$$\ddot{C}_k - \dot{q}(t)\left[\frac{k^2}{2m}+q(t)\right]^{-1}\dot{C}_k + \omega_k^2(t)C_k = 0\,, \tag{D.15}$$

with $\omega_k^2(t) = [k^2/2m + q(t)][k^2/2m + q(t) - q_{\mathrm{cr}}]$, and can be solved for different shapes $q(t)$ of the quench. The initial values of C_k can be obtained by demanding the bosonic equal-time commutation relation $[\hat{a}_{\boldsymbol{k},a}, \hat{a}^\dagger_{\boldsymbol{k}',b}] = \delta_{ab}\delta_{\boldsymbol{k},\boldsymbol{k}'}$ for the creation and annihilation operators $\hat{a}^\dagger_{\boldsymbol{k},a}$, $\hat{a}_{\boldsymbol{k},a}$. (Note that $\dot{C}_k = -i\omega_k C_k$ before the quench.)

The typical domain structure of the ferromagnetic phase expresses itself in the correlation function of the magnetization, which reads

$$\left\langle \hat{F}_a(\boldsymbol{r})\hat{F}_b(\boldsymbol{r}')\right\rangle = \delta_{ab}\int \frac{\mathrm{d}^D k}{(2\pi)^{2D}}e^{i\boldsymbol{k}(\boldsymbol{r}-\boldsymbol{r}')}|C_k(t)|^2\,. \tag{D.16}$$

The long-wavelength modes successively become unstable during the quench and start growing exponentially $C_k \propto e^{|\omega_k^{\mathrm{f}}|t}$ (there is also an exponentially-decaying term, which becomes negligible at late times). Thus the main contribution to the correlation function arises from these modes

$$\left\langle \hat{F}_a(\boldsymbol{r})\hat{F}_b(\boldsymbol{r}')\right\rangle \approx \delta_{ab}\int\limits_{\{k\,|\,\omega_k^2<0\}} \frac{\mathrm{d}^D k}{(2\pi)^D}e^{i\boldsymbol{k}(\boldsymbol{r}-\boldsymbol{r}')}|\widetilde{C}_k|^2 e^{2|\omega_k|t}\,, \tag{D.17}$$

where $|C_k| \approx (2\pi)^D e^{|\omega_k| t} |\widetilde{C}_k|$ at sufficiently late times after the quench (but also at sufficiently early times such that the mean field approximation is still valid). Observing that $|\omega_k^{\mathrm{f}}|$ possesses a maximum for wavenumbers k_{max}, we can evaluate the integral (D.16) using the saddle-point approximation. (For $q_{\mathrm{f}} < q_{\mathrm{c}}/2$, the maximum will be a local extremum, i.e., it will possess a vanishing derivative $\partial|\omega_k|/\partial k|_{k=k_{\mathrm{max}}} = 0$. In our calculation, we only concentrate on this case.) After some algebra, we obtain Eq. (4.27)

$$\langle \hat{F}_a(\boldsymbol{r}) \hat{F}_b(\boldsymbol{r}') \rangle = C_\nu^{\mathrm{max}} \delta_{ab} \frac{\exp\{q_{\mathrm{cr}} t\}}{\sqrt{t}} \frac{J_\nu(k_{\mathrm{max}}|\boldsymbol{r}-\boldsymbol{r}'|)}{(k_{\mathrm{max}}|\boldsymbol{r}-\boldsymbol{r}'|)^\nu}, \tag{D.18}$$

where $\nu = D/2 - 1$ and

$$C_\nu^{\mathrm{max}} = \frac{\mathcal{S}_{D-1}}{(2\pi)^{D-1}} \frac{|\widetilde{C}_{k_{\mathrm{max}}}|^2 k_{\mathrm{max}}^{D-2}}{\sigma} \tag{D.19}$$

with the surface area $\mathcal{S}_{D-1}$ of the $D-1$-dimensional unity sphere and the width of the unstable peak $\sigma^2 = \partial^2|\omega_k|/\partial k^2|_{k=k_{\mathrm{max}}}$. However, the numerical value of C_ν^{max} is not important, since the correlation function (4.27) describes only the initial domain formation.

In order to calculate the variance of the winding number in Subsection 4.2.5, we firstly factorize the linearized magnetization operator $\hat{\boldsymbol{F}} = \hat{F}\hat{\boldsymbol{n}}$ into its modulus $\hat{F} = \sqrt{\hat{\boldsymbol{F}}^2}$ and a unit-vector operator $\hat{\boldsymbol{n}}$ accounting for the direction, i.e., the broken symmetry. Such a factorization is always possible, since it represents just a canonic transformation. The new operators are independent and thus commute $[\hat{F}, \hat{\boldsymbol{n}}] = 0$. Furthermore, we approximate the modulus by its expectation value, i.e., by a c-number. This approximation, however, is only viable if the absolute values of the magnetization, $\hat{F}$, at different points are uncorrelated. Their correlation length can be estimated by calculating the $\hat{\boldsymbol{F}}^2$-$\hat{\boldsymbol{F}}^2$ correlations. After some algebra, it follows

$$\begin{aligned}\left\langle \hat{\boldsymbol{F}}^2(\boldsymbol{r}) \hat{\boldsymbol{F}}^2(\boldsymbol{r}') \right\rangle &= \left\langle \hat{\boldsymbol{F}}^2(\boldsymbol{r}) \right\rangle^2 + \frac{2}{D} \left\langle \hat{\boldsymbol{F}}(\boldsymbol{r}) \cdot \hat{\boldsymbol{F}}(\boldsymbol{r}') \right\rangle^2 \\ &\propto \left(\frac{1}{2^\nu} \frac{1}{\Gamma(\nu+1)} \right)^2 + \frac{2}{D} \left(\frac{J_\nu(k_{\mathrm{max}}|\boldsymbol{r}-\boldsymbol{r}'|)}{(k_{\mathrm{max}}|\boldsymbol{r}-\boldsymbol{r}'|)^\nu} \right)^2 .\end{aligned} \tag{D.20}$$

The first term describes the classical, uncorrelated behavior, whereas the spatial correlations are described by the second term.

For short distances, $k_{\mathrm{max}}|\boldsymbol{r}-\boldsymbol{r}'| \leqq \mathcal{O}(1)$, and in low dimensions, $D = \mathcal{O}(1)$, both contributions to the correlation function (D.20) are of the same order. By increasing either the separation, $k_{\mathrm{max}}|\boldsymbol{r}-\boldsymbol{r}'| \gg 1$, or the dimension, $D \gg 1$, the second term in Eq. (D.20) will be suppressed and the magnetization at different spatial points becomes uncorrelated and can thus be approximated classically. Hence, the winding-number correlations (4.33) calculated in Subsection 4.2.5 should yield the correct result for large radii $Rk_{\mathrm{max}} \gg 1$ but might give a wrong scaling behavior at small distances. At those scales, $Rk_{\mathrm{max}} \ll 1$, it can be expected that the $\hat{F}$-$\hat{F}$ correlations become important.

Bibliography

[1] H B G Casimir, *On the attraction between Two Perfectly Conducting Planes*, Proc. K. Ned. Akad. Wet. **51**, 793 (1948).

[2] M Bordag, editor, *The Casimir Effect 50 Years Later*, World Scientific, Singapore, (1998).

[3] K A Milton, *The Casimir effect: recent controversies and progress*, J. Phys. A **37**, R209 (2004).

[4] S K Lamoreaux, *Demonstration of the Casimir force in the 0.6 to 6 micrometer range*, Phys. Rev. Lett. **78**, 5 (1997).

[5] U Mohideen and A Roy, *Precision measurement of the Casimir force from 0.1 to 0.9* μm, Phys. Rev. Lett. **81**, 4549 (1998).

[6] G Bressi, G Carugno, R Onofrio, and G Ruoso, *Measurement of the Casimir Force between Parallel Metalic Surfaces*, Phys. Rev. Lett. **88**, 041804 (2002).

[7] F Chen, G L Klimchitskaya, U Mohideen, and V M Mostapanenko, *Theory confronts experiment in the Casimir force measurements: Quantification of errors and precision*, Phys. Rev. A **69**, 022117 (2004).

[8] V V Dodonov. *Modern Nonlinear Optics, Part 1, Second Edition, Advances in Chemical Physics, Volume 119*, chapter Nonstationary Casimir Effect and Analytic Solutions for Quantum Fields in a Cavity with Moving Boundaries, page 309. John Wiley & Sons, Inc., New York, (2001).

[9] S A Fulling, *Aspects of quantum field theory in curved space time*, Cambridge University Press, Cambridge (UK), (1991).

[10] N D Birrell and P C W Davies, *Quantum fields in curved space*, Cambridge University Press, Cambridge (UK), (1984).

[11] S. W. Hawking, *Black Hole Expansion*, Nature **248**, 30 (1974).

[12] R M Wald, *Quantum Field Theory in Curved Spacetime and Black Hole Thermodynamics*, University of Chicago Press, Chicago, IL, (1994).

[13] S Sachdev, *Quantum Phase Transitions*, Cambridge University Press, Cambridge, UK, (1999).

[14] M Vojta, *Quantum Phase Transitions*, Rep. Prog. Phys. **66**, 2069 (2003).

[15] A R Liddle and D H Lyth, *Cosmological Inflation and Large-Scale Structure*, Cambridge University Press, Cambridge (UK), (2000).

[16] A R Liddle, *An Introduction to Modern Cosmologoy*, J Wiley & Sons, Chichester (UK), (2003).

[17] P J E Peebles, *Principles of Physical Cosmology*, Princeton University Press, Princeton, New Jersey, (1993).

[18] A Linde, *Particle Physics and Inflationary Cosmology*, Harwood Academic, Chur, Switzerland, (1990).

[19] A H Guth, *Inflationary universe: A possible solution to the horizon and flatness problems*, Phys. Rev. D **23**, 347 (1981).

[20] A H Guth and S-Y Pi, *Fluctuations in the New Inflationary Universe*, Phys. Rev. Lett. **49**, 1110 (1982).

[21] http://map.gsfc.nasa.gov.

[22] H Stephani, *Allgemeine Relativitätstheorie*, VEB Deutscher Verlag der Wissenschaften, Berlin, (1977).

[23] R M Wald, *General Relativity*, University of Chicago Press, Chicago, IL, (1984).

[24] M Visser, *Lorentzian Wormholes: From Einstein to Hawking*, Springer, New York, (1996).

[25] http://planck.esa.int.

[26] http://lhc.web.cern.ch/lhc.

[27] W G Unruh, *Experimental Black Hole Evaporation*, Phys. Rev. Lett. **46**, 1351 (1981).

[28] P Painlevé, C. R. Hebd. Seances Acad. Sci. **173**, 677 (1921).

[29] A Gullstrand, Ark. Matter. Astron. Fys. **16**, 1 (1922).

[30] G Lemaître, Ann. Bull. Soc. Ro. Sci. Med. Nat. Brux. **53**, 51 (1933).

[31] M Novello, M Visser, and G Volovik, editors, *Artificial Black Holes*, World Scientific, Singapore, (2002).

[32] C Barceló, S Liberati, and M Visser, *Analogue Gravity*, Living Rev. Rel. **8**, 12 (2005).

[33] G Volovik, *The Universe in a Helium Droplet*, Oxford University Press, (2003).

[34] G E Volovik, *Superfluid Analogies of Cosmological Phenomena*, Phys. Rep. **351**, 195 (2001).

[35] M H Anderson, J R Ensher, C E Matthews, M R andWieman, and E A Cornell, Science **269**, 198 (1995).

[36] K B Davis, M-O Mewes, M R Andrews, N J van Druten, D S Durfee, Kurn D M, and W Ketterle, *Bose-Einstein Condensation in a Gas of Sodium Atoms*, Phys. Rev. Lett. **75**, 3969 (1995).

[37] R Schützhold, *Dynamical Zero-Temperature Phase Transitions and Cosmic Inflation or Deflation*, Phys. Rev. Lett. **95**, 135703 (2005).

[38] T W B Kibble, *Topology of cosmic domains and strings*, J. Phys. A **9**, 1387 (1976).

[39] W H Zurek, *Cosmological experiments in superfluid helium?*, Nature **317**, 505 (1985).

[40] W H Zurek, *Cosmological Experiments in Condensed Matter Systems*, Phys. Rep. (1996).

[41] I Bloch, J Dalibard, and W Zwerger, *Many-Body Physics with Ultracold Gases*, arXiv:0704.3011 (2007).

[42] I Bloch, *Ultracold quantum gases in optical lattices*, Nature Phys. **1**, 23 (2005).

[43] L E Sadler, J M Higbie, S R Leslie, M Vengalattore, and D M Stamper-Kurn, *Spontaneous symmetry breaking in a quenched ferromagnetic spinor Bose-Einstein condensate*, Nature **443**, 312 (2006).

[44] M Bennett and *et al*, *First-Year Wilkinson Microwave Anisotropy Probe (WMAP) Observations: Preliminary Maps and Basic Results*, Astrophys. J. Supplement **148**, 1 (2003).

[45] S W Hawking and G F R Ellis, *The Large Scale Structure of Space-Time*, Cambridge University Press, Cambridge (UK), (1973).

[46] G F R Ellis and T Rothman, *Lost horizons*, Am. J. Phys. **61**, 10 (1993).

[47] S Shankaranarayanan and Musongela Lubo, *Gauge-invariant perturbation theory for trans-Planckian inflation*, Phys. Rev. D **72**, 123513 (2005).

[48] R H Brandenberger, S E Jorás, and J Martin, *Trans-Planckian physics and the spectrum of fluctuations in a bouncing universe*, Phys. Rev. D **66**, 083514 (2002).

[49] J Martin and R H Brandenberger, *Trans-Planckian problem of inflationary cosmology*, Phys. Rev. D **63**, 123501 (2001).

[50] J Martin and R H Brandenberger, *Corley-Jacobson dispersion relation and trans-Planckian inflation*, Phys. Rev. D **65**, 103514 (2002).

[51] R H Brandenberger and J Martin, *The robustness of inflation to changes in super-Planck-scale physics*, Mod. Phys. Lett. A **16**, 999 (2001).

[52] R H Brandenberger and J Martin, *On Signatures of Short Distance Physics in the Cosmic Microwave Background*, Int. J. Mod. Phys. A **17**, 3663 (2002).

[53] J C Niemeyer and R Parentani, *Trans-Planckian dispersion and scale invariance of inflationary perturbations*, Phys. Rev. D **64**, 101301(R) (2001).

[54] J C Niemeyer, *Inflation with a Planck-scale frequency cutoff*, Phys. Rev. D **63**, 123502 (2001).

[55] R H Brandenberger and J Martin, *Back-reaction and the trans-Planckian problem of inflation reexamined*, Phys. Rev. D **71**, 023504 (2005).

[56] S Shankaranarayanan and L Sriramkumar, *Trans-Planckian corrections to the primordial spectrum in the infrared and the ultraviolet*, Phys. Rev. D **70**, 123520 (2004).

[57] A Ashoorioon, A Kempf, and R B Mann, *Minimum length cutoff in inflation and uniqueness of the action*, Phys. Rev. D **71**, 023503 (2005).

[58] A Ashoorioon, J L Hovdebo, and R B Mann, *Running ot the spectral index and violation of the consistency relation between tensor and scalar spectra from trans-Planckian physics*, Nucl. Phys. B **727**, 63 (2005).

[59] A Ashoorioon and R B Mann, *On the tensor/scalar ratio in inflation with UV cutoff*, Nucl. Phys. B **716**, 261 (2005).

[60] S Alexander, R Brandenberger, and J Magueijo, *Noncommutative inflation*, Phys. Rev. D **67**, 081301(R) (2003).

[61] E Easther, B R Greene, W H Kinney, and G Shiu, *Inflation as a probe of short distance physics*, Phys. Rev. D **64**, 103502 (2001).

[62] A Kempf, *Mode generating mechanism in inflation with a cutoff*, Phys. Rev. D **63**, 083514 (2001).

[63] A Kempf, *Perturbation spectrum in inflation with a cutoff*, Phys. Rev. D **64**, 103501 (2001).

[64] Seoktae Koh, *Squeezed quantum state in inflation with trans-Planckian cutoff*, Mod. Phys. Lett. A **19**, 1223 (2004).

[65] J Martin and R Brandenberger, *Dependence of the spectra of fluctuations in inflationary cosmology on trans-Planckian physics*, Phys. Rev. D **68**, 063513 (2003).

[66] K Goldstein and D A Lowe, *Initial state effects on the cosmic microwave background and trans-Planckian physics*, Phys. Rev. D **67**, 063502 (2003).

[67] J C Niemeyer, R Parentani, and D Campo, *Minimal modifications of the primoridal power spectrum from an adiabatic short distance cutoff*, Phys. Rev. D **66**, 083510 (2002).

[68] U H Danielson, *Note on inflation and trans-Planckian physics*, Phys. Rev. D **66**, 023511 (2002).

[69] D Seery and J E Lidsey, *Primordial non-Gaussianities in single-field inflation*, JCAP **0506**, 003 (2005).

[70] P Creminelli, *On non-Gaussianities in single-field inflation*, JCAP **0310**, 003 (2003).

[71] D Seery and J E Lidset, *Primordial non-Gaussianities from multiple-field inflation*, JCAP **0509**, 011 (2005).

[72] J Maldacena, *Non-gaussian features of primordial fluctuations in single field inflationary models*, JHEP05(2003), 013 (2003).

[73] Franco Dalfovo, Stefano Giorgini, Lev P. Pitaevskii, and Stringari Sandro, *Theory of Bose-Einstein condensation in trapped gases*, Rev. Mod. Phys. **71**, 463 (1999).

[74] L Pitaevskii and S Stringari, *Bose-Einstein Condensation*, Oxford University Press, Oxford (UK), (2004).

[75] Erik W Streed, Ananth P Chikkatur, Todd L Gustavson, Micah Boyd, Yoshia Torii, Dominik Schneble, Gretchen K Campbell, David E Pritchard, and Wolfgang Ketterle, *Large atom number Bose-Einstein Condensate machines*, Rev. Sci. Instrum. **77**, 023106 (2006).

[76] A J Leggett, *Bose-Einstein condensation in the alkali gases: Some fundamental concepts*, Rev. Mod. Phys. **73**, 307 (2001).

[77] D M Stamper-Kurn, M R Andrews, A P Chikkatur, S Inouye, H-J Miesner, J Stenger, and W Ketterle, *Optical Confinement of a Bose-Einstein Condensate*, Phys. Rev. Lett. **80**, 2027 (1998).

[78] C Barceló, S Liberati, and M Visser, *Analogue Models for FRW Cosmologies*, Int. J. Mod. Phys. D **12**, 1641 (2003).

[79] E Tiesinga, B J Verhaar, and Stoof H T C, *Threshold and resonance phenomena in ultracold ground-state collisions*, Phys. Rev. A **47**, 4114 (1993).

[80] S Inouye, M R Andrews, J Stenger, H-J Miesner, D M Stamper-Kurn, and W Ketterle, *Observation of Feshbach resonances in a Bose-Einstein condensate*, Nature **392**, 151 (1998).

[81] Ph Courteille, Freeland R S, and D J Heinzen, *Observation of a Feshbach Resonance in Cold Atom Scattering*, Phys. Rev. Lett. **81**, 69 (1998).

[82] J Stenger, S Inouye, M R Andrews, H-J Miesner, D M Stamper-Kurn, and W Ketterle, *Strongly Enhanced Inelastic Collisions in a Bose-Einstein Condensate near Feshbach Resonances*, Phys. Rev. Lett. **82**, 2422 (1999).

[83] V Vuletić, C Chin, A J Kerman, and S Chu, *Suppresion of Atomic Radiative Collisions by Tuning the Ground State Scattering Length*, Phys. Rev. Lett. **83**, 943 (1999).

[84] C Chin, V Vuletić, A J Kerman, and S Chu, *High Resolution Feshbach Spectroscopy of Cesium*, Phys. Rev. Lett. **85**, 2717 (2000).

[85] P J Leo, C J Williams, and P S Julienne, *Collision Properties of Ultracold* ^{133}*Cs Atoms*, Phys. Rev. Lett. **85**, 2721 (2000).

[86] U R Fischer and R Schützhold, *Quantum simulation of cosmic inflation in two-component Bose-Einstein condensates*, Phys. Rev. A **70**, 063615 (2004).

[87] Matt Visser and Silke Weinfurtner, *Massive Klein-Gordon equation from a Bose-Einstein-condensation-based analogue spacetime*, Phys. Rev. D **72**, 044020 (2005).

[88] D Schumayer, O Melchert, W Scheid, and B Apagyi, *Reconstruction of Rb-Rb inter-atomic potential from ultracold Bose-gas collision*, cond-mat/0702568 (2007).

[89] http://cua.mit.edu/ketterle_group.

[90] N N Bogoliubov, *On the theory of superfluidity*, J. Phys. (USSR) **11**, 23 (1947).

[91] A Görlitz, J M Vogels, A E Leanhardt, Raman C, T L Gustavson, J R Abo-Shaeer, A P Chikkatur, S Gupta, S Inouye, T Rosenband, and W Ketterle, *Realization of Bose-Einstein Codnensates in Lower Dimensions*, Phys. Rev. Lett. **87**, 130402 (2001).

[92] M Girardeau and R Arnowitt, *Theory of Many-Boson Systems: Pair Theory*, Phys. Rev. **113**, 755 (1959).

[93] C W Gardiner, *Particle-number-conserving Bogoliubov method which demonstrates the validity of the time-dependent Gross-Pitaevskii equation for a higly condensed Bose gas*, Phys. Rev. A **56**, 1414 (1997).

[94] M D Girardeau, *Comment on"Particle-number-conserving Bogoliubov method which demonstrates the validity of the time-dependent Gross-Pitaevskii equation for a highly condensaed Bose gas*, Phys. Rev. A **58**, 775 (1998).

[95] Y Castin and R Dum, *Low-temperature Bose-Einstein condensates in time-dependent traps: Beyond the U(1) symmetry-breaking approach*, Phys. Rev. A **57**, 3008 (1998).

[96] E H Lieb, R Seiringer, and J Yngwason, *Bosons in a trap: A rigorous derivation of the Gross-Pitaevskii energy functional*, Phys. Rev. A **61**, 043602 (2000).

[97] T D Lee, K Huang, and C N Yang, *Eigenvalues and Eigenfunctions of a Bose System of Hard Spheres and Its Low-Temperature Properties*, Phys. Rev. **106**, 1135 (1957).

[98] P G de Gennes, *Supercoductivity of Metals and Alloys*, W. A. Benjamin, New York, (1966).

[99] E H Lieb, R Seiringer, and J Yngvason, *One-Dimensional Bosons in Three-Dimensional Traps*, Phys. Rev. Lett. **91**, 150401 (2003).

[100] S Yi and L You, *Trapped atomic condensates with anisotropic interactions*, Phys. Rev. A **61**, 041604(R) (2000).

[101] A Griesmaier, J Werner, S Hensler, Stuhler J, and T Pfau, *Bose-Einstein Condensation of Chromium*, Phys. Rev. Lett. **94**, 160401 (2005).

[102] K Góral, K Rzążewski, and T Pfau, *Bose-Einstein condensation with magnetic diploe-diploe forces*, Phys. Rev. A **61**, 051601(R) (2000).

[103] A M Kamchatnov, *Expansion of Bose-Einstein Condensates Confined in Quasi-One-Dimensional or Quasi-Two-Dimensional Traps*, JETP **98**, 908 (2003).

[104] E Zaremba, *Sound propagation in a cylindrical Bose-condensed gas*, Phys. Rev. A **57**, 518 (1998).

[105] D S Petrov, M Holzmann, and G V Shlyapnikov, *Bose-Einstein Condensation in Quasi-2D Trapped Gases*, Phys. Rev. Lett. **84**, 2551 (2000).

[106] D S Petrov, G V Shlyapnikov, and J T M Walraven, *Regimes of Quantum Degeneracy in Trapped 1D Gases*, Phys. Rev. Lett. **85**, 3745 (2000).

[107] D S Petrov and G V Shlyapnikov, *Interatomic collisions in a tightly confined Bose gas*, Phys. Rev. A **64**, 012706 (2001).

[108] E B Kolomeisky and J P Straley, *Renormalization-group analysis of the ground-state properties of dilute Bose systems in d spatial dimensions*, Phys. Rev. B **46**, 11749 (1992).

[109] E B Kolomeisky, T J Newman, J P Straley, and X Qi, *Low-Dimensional Bose Liquids: Beyond the Gross-Pitaevskii Approximation*, Phys. Rev. Lett. **85**, 1146 (2000).

[110] M D Lee, S A Morgan, M J Davis, and K Burnett, *Energy-dependent scattering and the Gross-Pitaevskii equation in two-dimensional Bose-Einstein condensates*, Phys. Rev. A **65**, 043617 (2002).

[111] U R Fischer, *Quasiparticle universes in Bose-Einstein condensates*, Mod. Phys. Lett. A **19**, 1789 (2004).

[112] C Barceló, S Liberati, and M Visser, *Probing semiclassical analog gravity in Bose-Einstein condensates with widely tunable interactions*, Phys. Rev. A **68**, 053613 (2003).

[113] P O Fedichev and U R Fischer, *"Cosmological" quasiparticle production in harmonically trapped superfluid gases*, Phys. Rev. A **69**, 033602 (2004).

[114] M Stone, *Acoustic energy and momentum in a moving medium*, Phys. Rev. E **62**, 1341 (2000).

[115] Y Castin and R Dum, *Bose-Einstein Condensates in Time-Dependent Traps*, Phys. Rev. Lett. **77**, 5315 (1996).

[116] Yu Kagan, E L Surkov, and G V Shlyapnikov, *Evolution of a Bose-condensed gas under variations of the confining potential*, Phys. Rev. A **54**, R1753 (1996).

[117] G E Volovik, *Induced Gravity in Superfluid* ^{3}*He*, J. Low Temp. Phys. **113**, 667 (1998).

[118] R Ozeri, J Steinhauer, N Katz, and N Davidson, *Direct Observation of the Phonon Energy in a Bose-Einstein Condensate by Tomographic Imaging*, Phys. Rev. Lett. **88**, 220401 (2002).

[119] J Steinhauer, R Ozeri, N Katz, and N Davidson, *Excitation Spectrum of a Bose-Einstein Condensate*, Phys. Rev. Lett. **88**, 120407 (2002).

[120] M S Sarandy, L-A Wu, and D A Lidar, *Consistency of the Adiabatic Theorem*, Quantum Information Processing **3**, 331 (2004).

[121] M Abramowitz and I A Stegun, *Handbook of Mathematical Functions*, Dover Publications, (1972).

[122] C Gies and D A W Hutchinson, *Coherence properties of the two-dimensional Bose-Einstein condensate*, Phys. Rev. A **70**, 043606 (2004).

[123] M Visser, *Acoustic black holes: horizons, ergospheres and Hawking radiation*, Class. Quant. Grav. **15**, 1767 (1998).

[124] C Barceló, S Liberati, and M Visser, *Analog gravity from Bose-Einstein condensates*, Class. Quant. Grav. **18**, 1137 (2001).

[125] C Barceló, S Liberati, and M Visser, *Analog gravity from field theory normal modes?*, Class. Quant. Grav. **18**, 3595 (2001).

[126] L J Garay, J R Anglin, J I Cirac, and P Zoller, *Sonic Analog of Gravitational Black Holes in Bose-Einstein Condensates*, Phys. Rev. Lett. **85**, 4643 (2000).

[127] R Balbinot, S Fagnocchi, A Fabbri, and G P Procopio, *Backreaction in Acoustic Black Holes*, Phys. Rev. Lett. **94**, 161302 (2005).

[128] R Balbinot, S Fagnocchi, and A Fabbri, *Quantum effects in acoustic black holes: The backreaction*, Phys. Rev. D **71**, 064019 (2005).

[129] W G Unruh. *Measurability of Dumb Hole Radiation?* World Scientific, Singapore, (2002).

[130] H Fröhlich, *A contradiction between quantum hydrodynamics and the existence of particles*, Physica **34**, 47 (1967).

[131] Y Castin, *Simple theoretical tools for low dimension Bose gases*, J. Phys IV (France) **116**, 89 (2004).

[132] T D Lee and C N Yang, *Many-Body Problem in Quantum Mechanics and Quantum Statistical Mechanics*, Phys. Rev. **105**, 1119 (1959).

[133] E Timmermans, P Tommasini, and K Huang, *Variational Thomas-Fermi theory of a nonuniform Bose condensate at zero temperature*, Phys. Rev. A **55**, 3645 (1997).

[134] M Olshanii, *Atomic Scattering in the Presence of an External Confinement and a Gas of Impenetrable Bosons*, Phys. Rev. Lett. **81**, 938 (1998).

[135] L Pitaevskiĭ and S Stringari, *Uncertainty principle and off-diagonal long-range order in the fractional quantum Hall effect*, Phys. Rev. B **47**, 10915 (1993).

[136] E P Gross, Nuovo Cimento **20**, 454 (1961).

[137] E P Gross, *Hydrodynamics of a Superfluid Condensate*, J. Math. Phys. **4**, 195 (1963).

[138] L P Pitaevskiĭ, Sov. Phys. JETP **13**, 451 (1961).

[139] S Geltman and A Bambini, *Triplet Scattering Lengths for Rubidium and Their Role in Bose-Einstein Condensation*, Phys. Rev. Lett. **86**, 3276 (2001).

[140] E Braaten and A Nieto, *Quantum corrections to the ground state of a trapped Bose-Einstein condensate*, Phys. Rev. B **56**, 14745 (1997).

[141] G Vidal, J I Latorre, E Rico, and A Kitaev, *Entanglement in Quantum Critical Phenomena*, Phys. Rev. Lett. **90**, 227902 (2003).

[142] U Dorner, P Fedichev, D Jaksch, M Lewenstein, and P Zoller, *Entangling Strings of Neutral Atoms in 1D Atomic Pipeline Structures*, Phys. Rev. Lett. **91**, 073601 (2003).

[143] J I Latorre and R Orús, *Adiabatic quantum computation and quantum phase transition*, Phys. Rev. A **69**, 062302 (2004).

[144] B Damski, *The Simplest Quantum Model Supporting the Kibble-Zurek Mechanism of Topological Defect Production: Landau-Zener Transitions from a New Perspective*, Phys. Rev. Lett. **95**, 035701 (2005).

[145] W H Zurek, U Dorner, and P Zoller, *Dynamics of a Quantum Phase Transition*, Phys. Rev. Lett. **95**, 105701 (2005).

[146] J Dziarmaga, *Dynamics of a Quantum Phase Transition: Exact Solution of the Quantum Ising Model*, Phys. Rev. Lett. **95**, 245701 (2005).

[147] B Damski and W H Zurek, *Adiabatic-impulse approximation for avoided level crossings: From phase-transition dynamics to Landau-Zener evolutions and back again*, Phys. Rev. A **73**, 063405 (2006).

[148] F M Cucchietti, B Damski, J Dziarmaga, and W H Zurek, *Dynamics of the Bose-Hubbard model: transition for Mott insulator to superfluid*, Phys. Rev. A **75**, 023603 (2007).

[149] M Greiner, O Mandel, T Esslinger, T W Hänsch, and I Bloch, *Quantum phase transition from a superfluid to a Mott insulator in a gas of ultracold atoms*, Nature **415**, 39 (2002).

[150] M P A Fisher, P B Weichmann, G Grinstein, and D S Fisher, *Boson localization and the superfluid-insulator transition*, Phys. Rev. B **40**, 546 (1989).

[151] D Jaksch, C Bruder, J I Cirac, C W Gardiner, and P Zoller, *Cold Bosonic Atoms in Optical Lattices*, Phys. Rev. Lett. **81**, 3108 (1998).

[152] D Jaksch and P Zoller, *The cold atom Hubbard toolbox*, Ann. Phys. (N.Y.) **315**, 52 (2005).

[153] A Polkovnikov, S Sachdev, and S M Girvin, *Nonequilibrium Gross-Pitaevskii dynamics of boson lattice models*, Phys. Rev. A **66**, 053607 (2002).

[154] S R Clark and D Jaksch, *Dynamics of the superfluid to Mott-insulator transition in one dimension*, Phys. Rev. A **70**, 043612 (2004).

[155] K Sengupta, S Powell, and S Sachdev, *Quench dynamics across quantum critical points*, Phys. Rev. A **69**, 053616 (2004).

[156] L Isella and Ruostekoski, *Nonadiabatic dynamics of a Bose-Einstein condensate in an optical lattice*, Phys. Rev. A **72**, 011601(R) (2005).

[157] F Gerbier, S Fölling, A Widera, O Mandel, and I Bloch, *Probing Number Squeezing of Ultracold Atoms across the Superfluid-Mott Insulator Transition*, Phys. Rev. Lett. **96**, 090401 (2006).

[158] C Orzel, A K Tuchman, M L Fenselau, M Yasuda, and M A Kasevich, *Squeezed States in a Bose-Einstein Condensate*, Science **291**, 2386 (2001).

[159] L Amico and V Penna, *Dynamical Mean Field Theory of the Bose-Hubbard Model*, Phys. Rev. Lett. **80**, 2189 (1998).

[160] D Boers, C Weiss, and M Holthaus, *Bogoliubov speed of sound for a dilute Bose-Einstein condensate in a 3d optical lattice*, Europhys. Lett. **67**, 887 (2004).

[161] A Erdélyi, W Magnus, F Oberhettinger, and F G Tricomi, editors, *Higher Transcendental Functions*, McGraw-Hill, (1953).

[162] J Javanainen, *Phonon approach to an array of traps containing Bose-Einstein condensates*, Phys. Rev. A **60**, 4902 (1999).

[163] C Schroll, F Marquardt, and C Bruder, *Perturbative corrections to the Gutzwiller mean-field solution for the Mott-Hubbard model*, Phys. Rev. A **70**, 053609 (2004).

[164] F Gerbier, A Widera, S Fölling, O Mandel, T Gericke, and I Block, *Phase Coherence of an Atomic Mott Insulator*, Phys. Rev. Lett. **95**, 050404 (1995).

[165] L Amico, A Osterloh, and F Cataliotti, *Quantum Many Particle Systems in Ring-Shaped Optical Lattices*, Phys. Rev. Lett. **95**, 063201 (2005).

[166] M Hindmarsh and Kibble T W B, *Cosmic strings*, Rep. Prog. Phys. **58**, 477 (1995).

[167] J Stenger, S Inouye, Stampler-Kurn D M, H-J Miesner, A P Chikkatur, and W Ketterle, *Spin domains in ground-state Bose-Einstein condensates*, Nature **396**, 345 (1998).

[168] M-S Chang, Q Qin, W Zhang, L You, and M S Chapman, *Coherent spinor dynamics in a spin-1 Bose condensate*, Nature Phys. **1**, 111 (2005).

[169] W Zhang, D L Zhou, M-S Chang, and M S Champan, *Dynamical Instability and Domain Formation in a Spin-1 Bose-Einstein Condensate*, Phys. Rev. Lett. **95**, 180403 (2005).

[170] J M Higbie, L E Sadler, S Inouye, A P Chikkatur, S R Leslie, K L Moore, V Savalli, and D M Stamper-Kurn, *Direct Nondestructive Imaging of Magnetization in a Spin-1 Bose-Einstein Gas*, Phys. Rev. Lett. **95**, 050401 (2005).

[171] H Saito and M Ueda, *Spontaneous magnetization and structure formation in a spin-1 ferromagnetic Bose-Einstein condensate*, Phys. Rev. A **72**, 023610 (2005).

[172] H Saito, Y Kawaguchi, and M Ueda, *Breaking of Chiral Symmetry and Spontaneous Rotation in a Spinor Bose-Einstein Condensate*, Phys. Rev. Lett. **96**, 064302 (2006).

[173] T Ohmi and Machida K, *Bose-Einstein Condensation with Internal Degrees of Freedom in Alkali Atom Gases*, J. Phys. Soc. Jpn. **67**, 1822 (1998).

[174] T-J Ho, *Spinor Bose Condensates in Optical Traps*, Phys. Rev. Lett. **81**, 742 (1998).

[175] Mermin, *The topological theory of defects in ordered media*, Rev. Mod. Phys. **51**, 591 (1979).

[176] L Michel, *Symmetry defects and brocken symmetry. Configurations hidden symmetry*, Rev. Mod. Phys. **52**, 617 (1979).

[177] A G Abanov and P B Wiegmann, *Theta-terms in nonlinear sigma models*, Nucl. Phys. B **570**, 685 (2000).

[178] C M Savage and Ruostekoski, *Dirac monopoles and dipoles in ferromagnetic spinor Bose-Einstein condensates*, Phys. Rev. A **68**, 043604 (2003).

[179] A Lamacraft, *Quantum quenches in a spinor condensate*, Phys. Rev. Lett. **98**, 160404 (2007).

[180] H Saito, Y Kawaguchi, and M Ueda, *Topological defect formation in quenched ferromagnetic Bose-Einstein condensates*, cond-mat/0610862 (2006).

List of Publications

Scientific journals

[I] M Uhlmann, R Schützhold, and U R Fischer,
Vortex quantum creation and winding number scaling in a quenched spinor Bose gas
Phys. Rev. Lett. **99**, 120407 (2007). [4 pages]

[II] F Queisser, M Uhlmann, and R Schützhold,
Signatures of Planck-scale interactions in the cosmic microwave background?,
Class. Quant. Grav. **24**, 1375 (2007). [9 pages]

[III] R Schützhold, M Uhlmann, Y Xu, and U R Fischer,
Sweeping from the superfluid to Mott phase in the Bose-Hubbard model,
Phys. Rev. Lett. **97**, 200601 (2006). [4 pages]

[IV] R Schützhold, M Uhlmann, Y Xu, and U R Fischer,
Mean-field expansion in Bose-Einstein condensates with finite-range interactions,
Int. J. Mod. Phys. B **20**, 3555 (2006). [11 pages]

[V] M Uhlmann, Y Xu, and R Schützhold,
Aspects of Cosmic Inflation in Expanding Bose-Einstein Condensates,
New J. Phys. **7**, 248 (2005). [17 pages]

[VI] R Schützhold, M Uhlmann, Y Xu, and U R Fischer,
Quantum backreaction in dilute Bose-Einstein condensates,
Phys. Rev. D **72**, 105005 (2005). [8 pages]

[VII] M Uhlmann, G Plunien, R Schützhold, and G Soff,
Resonant-cavity photon creation via the dynamical Casimir effect,
Phys. Rev. Lett. **93**, 193601 (2004). [4 pages]

Proceedings

[VIII] R Schützhold and M Uhlmann,
Horizon Analogues in the Laboratory,
Proceedings of the Memorial Symposium for Gerhard Soff
(April 25 and 26, 2005, Frankfurt, Germany). [10 pages]

[IX] M Uhlmann, G Plunien, G Schaller, R Schützhold, and G Soff,
Resonante Photonenerzeugung in einer Kavität,
EAS Arbeitsbericht 2004 (ISSN 0724-4975). [3 pages]

Danksagung

An dieser Stelle möchte ich mich bei allen bedanken, die auf die eine oder andere Weise zum Entstehen dieser Arbeit beigetragen haben.

Besonderer Dank gebührt Dr. Ralf Schützhold. Er gab mir die Möglichkeit in seiner Emmy-Noether-Nachwuchsgruppe an sehr interessanten Themen zu forschen und diese Dissertation anzufertigen. Mit seinem enormen Wissen hat er mir bei vielen Fragen weiterhelfen können.

Des Weiteren danke ich Priv.-Doz. Dr. Uwe R. Fischer, Dr. Yan Xu und Friedemann Queisser für die fruchtbare Zusammenarbeit während einzelner Teile dieser Arbeit. In zahlreichen Diskussionen haben sie zum Gelingen dieser Dissertation mit beigetragen.

Dr. Gernot Schaller, Dr. Mathias Uhlmann, Priv.-Doz. Dr. Günter Plunien, Dr. Andreas Kreyßig und Enrico Faulhaber haben mir bei verschiedenen Problemen weiterhelfen können und Teile dieser Arbeit Korrektur gelesen.

Bei den Mitgliedern des Instituts für Theoretische Physik, insbesondere bei denen der Nachwuchsgruppe “Quantensimulationen/Quanteninformationstheorie” und den Sekretärinnen Gundula Schädlich, Gudrun Latus und Ute Wächtler, möchte ich mich für die angenehme Atmosphäre bedanken. Im Institut wurde mir die Möglichkeit gegeben, meine Studien nach dem verfrühten Ableben von Prof. Dr. Gerhard Soff fortzusetzen. Insbesondere bin ich Prof. Dr. Jan-Michael Rost dafür dankbar, dass er die Rolle des Doktorvaters übernommen hat.

Meinen Eltern, Ursula Uhlmann und Prof. Dr. Klaus Uhlmann, möchte ich für ihre Unterstützung danken.

Erklärung

Hiermit versichere ich, daß ich die vorliegende Arbeit ohne unzulässige Hilfe Dritter und ohne Benutzung anderer als der angegebenen Hilfsmittel angefertigt habe; die aus fremden Quellen direkt oder indirekt übernommenen Gedanken sind als solche kenntlich gemacht. Diese Arbeit wurde bisher weder im Inland noch im Ausland in gleicher oder ähnlicher Form einer anderen Prüfungsbehörde vorgelegt.

Dresden, den 23. Mai 2007

Michael Uhlmann